

Microsecond reaction kinetics and catalytic mechanism of bacterial cytochrome oxidases

Paulus, Angela

DOI

[10.4233/uuid:28e0dfa-72f2-4feb-9fd0-fcc807bb3593](https://doi.org/10.4233/uuid:28e0dfa-72f2-4feb-9fd0-fcc807bb3593)

Publication date

2017

Document Version

Final published version

Citation (APA)

Paulus, A. (2017). *Microsecond reaction kinetics and catalytic mechanism of bacterial cytochrome oxidases*. [Dissertation (TU Delft), Delft University of Technology]. <https://doi.org/10.4233/uuid:28e0dfa-72f2-4feb-9fd0-fcc807bb3593>

Important note

To cite this publication, please use the final published version (if applicable).
Please check the document version above.

Copyright

Other than for strictly personal use, it is not permitted to download, forward or distribute the text or part of it, without the consent of the author(s) and/or copyright holder(s), unless the work is under an open content license such as Creative Commons.

Takedown policy

Please contact us and provide details if you believe this document breaches copyrights.
We will remove access to the work immediately and investigate your claim.

Microsecond reaction kinetics and catalytic mechanism of bacterial cytochrome oxidases

PROEFSCHRIFT

ter verkrijging van de graad van doctor
aan de Technische Universiteit Delft,
op gezag van de Rector Magnificus prof. ir. K.C.A.M. Luyben,
voorzitter van het College voor Promoties,
in het openbaar te verdedigen op
vrijdag 12 mei 2017 om 12:30 uur

door

Angela PAULUS

Master of Life Science & Technology, Technische Universiteit Delft, Nederland
geboren te Zevenhuizen (Zuid-Holland)

Dit proefschrift is goedgekeurd door de promotoren:
Prof.dr. S. de Vries† en Prof.dr. W.R. Hagen

Samenstelling promotiecommissie:

Rector Magnificus	voorzitter
Prof.dr. S. de Vries†	Technische Universiteit Delft, promotor
Prof.dr. W.R. Hagen	Technische Universiteit Delft, promotor

Onafhankelijke leden:

Prof. dr. A.J. Pierik	Technische Universität Kaiserslautern
Prof. dr. R. Wever	Universiteit van Amsterdam
Prof. dr. ir. A.J.M. Stams	Wageningen Universiteit
Prof. dr. I.W.C.E. Arends	Technische Universiteit Delft
Prof. dr. U. Hanefeld	Technische Universiteit Delft
Dr. ir. P.L. Hagedoorn	Technische Universiteit Delft



The studies presented in this thesis were performed at the Department of Biotechnology, Delft University of Technology, The Netherlands.
This research has been financed by a grant from the Council for Chemical Sciences of the Netherlands Organization for Scientific research (NWO) (700.54.003).

ISBN: 978-94-028-0630-4

Copyright © 2017 Angela Paulus All rights reserved.
Gedrukt door: Ipskamp Printing, Enschede.
Ontwerp omslag: Wieske van der Heijden.



Een digitale versie van dit proefschrift is beschikbaar via de TU Delft Repository.

Contents

Summary		5
Samenvatting		7
Chapter I	Introduction	9
Chapter II	Energy conversion and conservation by cytochrome oxidases	19
Chapter III	Oxoferryl “P” intermediates of cytochrome <i>aa</i> ₃ oxidase	41
Chapter IV	The cytochrome <i>ba</i> ₃ oxidase from <i>Thermus thermophilus</i> does not generate a tryptophan radical during turnover; implications for the mechanism of proton pumping	61
Chapter V	Oxoferryl-porphyrin radical catalytic intermediate in cytochrome <i>bd</i> oxidases protects cells from formation of reactive oxygen species	81
Chapter VI	Conclusions and outlook	107
Curriculum vitae		111
List of publications		111
Dankwoord		113

Summary

Fundamental biochemical research is of crucial importance for a complete and detailed understanding of what drives enzyme activity and how enzyme kinetic properties are optimized towards survival of the host organism. When cells fail to produce a fully functional enzyme, the organism's ability to survive or thrive is impacted. In humans, for example, low levels or absence of lactase causes lactose intolerance, while decreased performance of the proton-pumping enzyme cytochrome *aa*₃ oxidase in the mitochondrial electron transport chain in brain cells is linked to Alzheimer's disease.

Direct observation of all steps of the catalytic cycle of bacterial oxidoreductases is challenging, since a full turnover of these enzymes typically takes only ~1 ms. Through targeted mutagenesis of enzymes it is possible to create variants of an enzyme that can only catalyze part of the reaction, or that will perform the entire reaction, yet with different kinetics of the individual reaction steps, providing clues as to what drives or limits the enzymatic reaction. Hypotheses based on observations with mutated enzyme variants can be proven or disproven by studying the wildtype uncorrupted enzyme under mild conditions, minimizing artefacts introduced by working *in vitro*. The stopped-flow spectrophotometer is a valuable tool for kinetic analysis of enzyme reactions, but does not offer the time resolution required to resolve early pre-steady state kinetics. The microsecond freeze-hyperquenching setup (MHQ), on the other hand, is able to create 'snapshot' samples of enzymes during catalytic turnover at reaction times down to 74 μ s. The quenched samples can be subjected to further analysis by UV-vis or EPR spectroscopy. This thesis describes the kinetic study of three bacterial oxidoreductases and makes the comparison between the catalytic mechanisms of oxygen reduction (and proton pumping) of each of the three enzymes.

Chapter 2 provides a review of the catalytic and proton-pumping activity of the different classes of cytochrome oxidases. The differences and similarities between the mechanisms of cytochrome oxidases from different species are discussed.

Chapter 3 deals specifically with the reaction mechanism of cytochrome *aa*₃ oxidase from *Paracoccus denitrificans*, focusing on the P_M intermediate of the reaction. The validity of using artificially obtained oxoferryl 'P_{CO/O2}' intermediate as a molecular model for P_M is investigated.

The mechanistic details of the reduction of oxygen by cytochrome *ba*₃ oxidase from *Thermus thermophilus* are studied in **Chapter 4**. The observed differences in comparison to the mechanism of cytochrome *aa*₃ oxidase are linked to implications for proton-pumping.

In **Chapter 5** the class of cytochrome *bd* quinol oxidases is compared to the heme-copper oxidases (such as cytochrome *aa*₃ and *ba*₃ oxidase) using the example of the cytochrome *bd*-I oxidase from *Escherichia coli*. Similarities in the mechanism of oxygen reduction are explained as a convergent evolution of both classes of oxidases towards a single four-electron step breaking the O-O double bond, avoiding formation of reactive oxygen species (ROS).

Samenvatting

Fundamenteel biochemisch onderzoek is van cruciaal belang voor een volledig en gedetailleerd begrip van wat enzymactiviteit drijft en hoe enzymkinetische eigenschappen zijn geoptimaliseerd ten behoeve van het overleven van de gastheer. Wanneer cellen er niet in slagen een volledig functioneel enzym te produceren heeft dit invloed op de bekwaamheid van het organisme om te overleven of te floreren. In mensen, bijvoorbeeld, veroorzaakt een lage concentratie lactase, of afwezigheid van lactase, lactose-intolerantie, terwijl verminderd functioneren van het protonenpompende enzym cytochrome *aa*₃ oxidase in de mitochondriale elektron transportketen in hersencellen gerelateerd wordt aan de ziekte van Alzheimer.

Directe observatie van alle stappen van de katalytische cyclus van bacteriële oxidoreductases is uitdagend, aangezien een volledige omzetting van deze enzymen slechts ~1 ms in beslag neemt. Via gerichte mutagenese van enzymen is het mogelijk om varianten van een enzym te creëren die slechts een deel van de reactie katalyseren, of die de volledige reactie uitvoeren, echter met een andere kinetiek van de afzonderlijke reactiestappen, wat informatie verschaft over wat de enzymatische reactie drijft of limiteert. Hypotheses die zijn gebaseerd op observaties met gemuteerde enzymvarianten kunnen worden bewezen of verworpen door het 'wildtype' ongewijzigde enzym te bestuderen onder milde condities, waarbij artefacten als gevolg van het werken *in vitro* worden geminimaliseerd. De stopped-flow spectrofotometer is waardevol gereedschap voor de kinetische analyse van enzymreacties, maar levert niet de tijdsresolutie die nodig is om vroege pre-steady state kinetiek op te lossen. De microsecond freeze-hyperquenching setup (MHQ) daarentegen, is in staat om 'snapshot'-monsters te creëren van enzymen tijdens een katalytische omzetting bij reactietijden vanaf 74 μs. De bevroren samples kunnen verder worden bestudeerd met UV-vis of EPR spectroscopie. Dit proefschrift beschrijft de kinetische studie van drie bacteriële oxidoreductases en maakt het vergelijk tussen de katalytische mechanismen van zuurstofreductie (en het pompen van protonen) van elk van de drie enzymen.

Hoofdstuk 2 geeft een overzicht van het katalytische en protonpomp-activiteit van de verschillende klassen van cytochroom oxidases. De verschillen en overeenkomsten tussen de mechanismen van cytochroom oxidases van verschillende soorten worden besproken.

Hoofdstuk 3 behandelt in het bijzonder het reactiemechanisme van cytochroom *aa*₃ oxidase uit *Paracoccus denitrificans*, met bijzondere aandacht voor de P_M intermediair van de reactie. De geldigheid van het gebruik van een kunstmatig verkregen oxoferryl 'P_{CO/O2}' intermediair wordt onderzocht.

De mechanistische details van de reductie van zuurstof door cytochroom *ba*₃ oxidase uit *Thermus thermophilus* worden bestudeerd in **Hoofdstuk 4**. The gevonden verschillen in vergelijking met het mechanisme van cytochroom *aa*₃ oxidase worden gekoppeld aan de implicaties voor het pompen van protonen.

In **Hoofdstuk 5** wordt de klasse van de cytochroom *bd* oxidases vergeleken met die van de heem-koper oxidases (zoals cytochroom *aa*₃ en *ba*₃ oxidase) aan de hand van het voorbeeld van cytochroom *bd*-I oxidase uit *Escherichia coli*. Overeenkomsten in het mechanisme van zuurstofreductie worden verklaard door convergerende evolutie van beide klassen van oxidases naar een enkele vier-elektron stap om de dubbele O-O binding te breken, zodat vorming van hoogreactieve afbraakproducten van zuurstof (ROS) wordt vermeden.

Chapter I

Introduction

All living entities consist of cells¹. The larger organisms consist of trillions of cells, but there are also many organisms in which all the requirements for life and reproduction are combined in a single cell. The earliest fossils of (developing) multicellular life discovered so far date back 1-2 billion years^{2,3}, but unicellular organisms inhabited the earth even long before that (at least 3.5 billion years ago^{4,5,6}). Although Darwinian evolution of life⁷, based on variation and natural selection can explain many steps in the development of species on earth, it still seems a leap to go from a single-celled organism to a group of living, differentiated cells working together, with a certain degree of intercellular communication. In humans, there are many different cell types with different functionalities and characteristics forming the various tissues of the body (see figure 1).

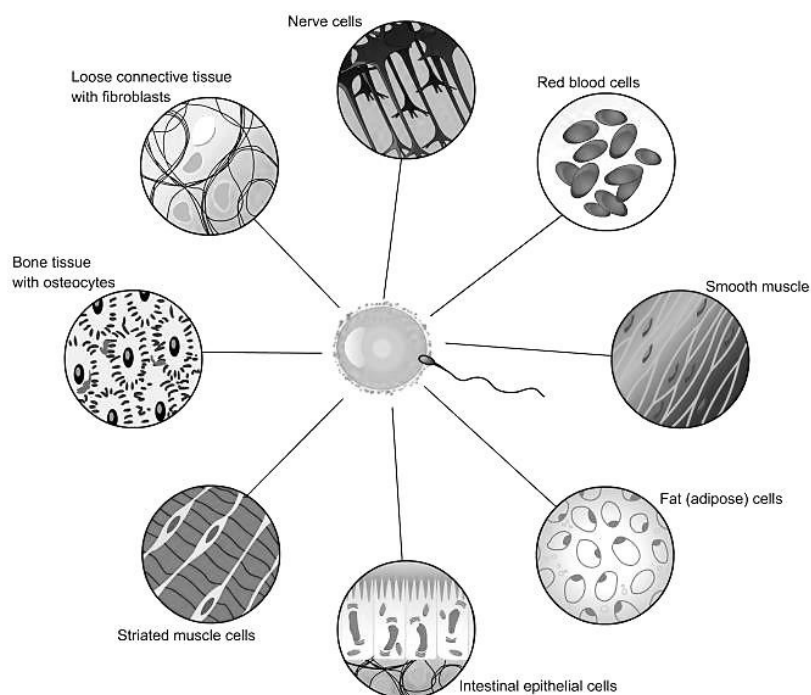


Figure 1: overview of different cell types encountered in multicellular organisms, such as humans (from <http://www.tutorvista.com>)

Many views exist on the evolution of multicellular organisms. The three more widely supported theories are:

1. *Symbiotic Theory*

Symbiotic theory states that the first multicellular organisms arose from symbiosis of *different* species of single celled organisms, each with different functions.

2. *Cellularization Theory*

Cellularization theory states that a unicellular organism would, at some point, have developed membrane boundaries/partitions around each of its nuclei, thus giving rise to multicellularity.

3. *Colonial Theory*

Colonial theory states that the symbiosis of many organisms of the *same* species led to a multicellular organism.

Serial Endosymbiotic Theory

An adjusted form of Symbiotic theory can be applied to the development of the first single-celled eukaryotic organisms and is then usually referred to as Serial Endosymbiotic Theory, or SET (for a comprehensive overview on the topic, see the work of L. Margulis⁸). SET dictates that cellular features such as chloroplasts, mitochondria and even flagella are a result of the fusion of several types of bacterial cells, after which there would have been further optimization of the integration of the cells.

According to SET, it all started with a species of thermoacidophilic archaea that fused with an anaerobic motile bacterium. Their plasmic contents then combined to a single nucleocytoplasm and they evolved as one species up to the first occurrence of a cell nucleus and the process of mitosis. The next step was incorporation of an oxidophilic proteobacterium, which resulted in a symbiotic organism that did well in warm, acidic, oxygen-containing environments. The organism was now much more versatile and started to get used to, and take advantage of, higher oxygen concentrations in its habitat. Finally, a cyanobacterium joined the mix and added the ability to harvest the energy from sunlight to drive intracellular processes. The resulting eukaryotic cell had an amazing complexity compared to the species of thermoacidophilic archaea it originated from, and it was better equipped to cope with changing environmental conditions, which made it thrive. Since then, these simplest eukaryotic cells have continued to develop to the cells of plants we see today and the different cells from which the eukaryotic symbiont originated have integrated further to the point where the green cyanobacterium is simply a chloroplast, the oxidophile has turned into a mitochondrion and nothing is left of the motile bacterium, except the remaining ability of the eukaryotic cell to form flagella, cilia and other cellular protuberances.

The larger part of SET (concerning the origin of chloroplasts and mitochondria) has been accepted by the scientific community. Chloroplasts and mitochondria display many features of single-celled organisms, e.g. having an internal space, bordered by membranes, and with that the ability to maintain an internal environment. In addition, chloroplasts and mitochondria carry their own genetic material^{9,10}, which is not related to the genome of the eukaryotic host. Mitochondria and chloroplasts are known to have the ability to replicate at different moments and in different ways than the rest of the eukaryotic cell they are part of^{11,12}, although in the 'older' single cell eukaryotes the division of the organelles more often coincides with the division of the cell.

With SET in mind, it makes sense to use unicellular organisms as model systems for organelles. Human mitochondria for example (figure 2) resemble the soil bacterium *Paracoccus denitrificans*, also in terms of their appearance and cellular machinery. *P. denitrificans* is therefore widely used as a source of mitochondrial-type enzymes for scientific study.

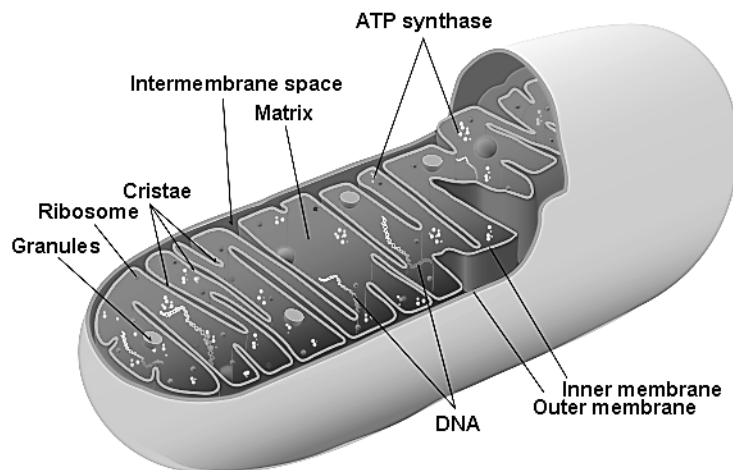


Figure 2: schematic of a human mitochondrion
(from <http://commons.wikimedia.org>)

Respiratory chain in aerobic organisms (e.g. *Paracoccus denitrificans*)

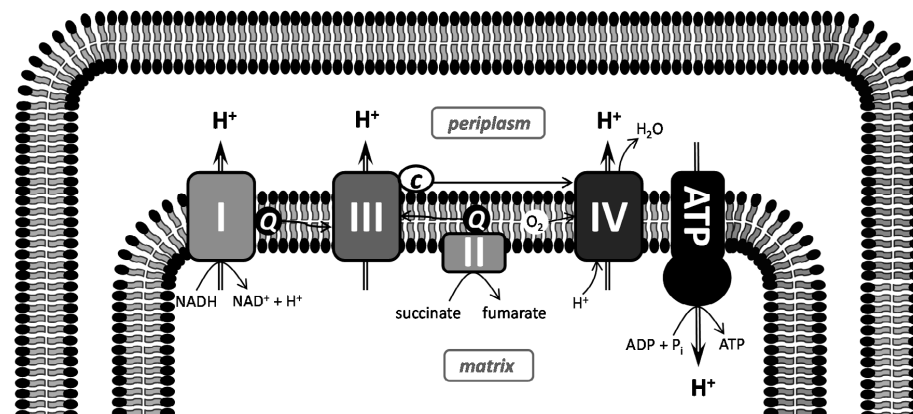


Figure 3: Respiratory chain and ATP synthase

I: Complex I, NADH dehydrogenase; II: Complex II, succinate dehydrogenase; III: Complex III, cytochrome bc_1 ; IV: Complex IV, cytochrome c oxidase, ATP: ATP synthase; Q: quinone/quinol; c: cytochrome c ; O_2 : molecular oxygen; H^+ : proton.

Through the processes of glycolysis and the citric acid cycle *P. denitrificans* is able to catabolize carbohydrates (sugars) to H_2O , CO_2 and succinate to form high-energy compounds

such as ATP, GTP and NADH. Succinate and NADH serve as substrates to the respiratory chain (or electron transport chain) that is present in all aerobic organisms (see figure 3). In this chain of membrane-associated enzymes and transport proteins electrons are taken from succinate (by Complex II) and NADH (by Complex I) and are transported via mobile carriers (ubiquinone and cytochrome *c*) along the chain of enzymes to the final enzyme complex, the terminal oxidase (Complex IV). The electrons are finally used to reduce oxygen to water, which concludes the electron transport chain. The transfer of electrons along the transport chain is thermodynamically downhill and therefore potentially liberates free energy to be used to drive thermodynamically uphill cellular processes such as synthesis of new biomass. The particular way in which free energy is utilized by the different enzymes in the chain is by the net translocation of protons from the mitochondrial matrix to the periplasmic space. In this way a *proton electrochemical gradient* is produced, which is then used by the ATP synthase to generate ATP in the process of oxidative phosphorylation, or which can be used directly to fuel anabolic processes and energy-driven transmembrane transport.

Electrochemical proton gradient

The proton electrochemical gradient across the inner membrane of the bacterial cell is also referred to as the *proton-motive force* (pmf). Peter Mitchell was the first to describe the energy storage capacity of ionic gradients across the cellular membrane in 1961¹³, proposing the redox-loop mechanism for generation of the pmf by the membrane bound redox enzymes and predicting the existence of a reversible ATP synthase to produce ATP or use ATP to drive transport, for which he was awarded the Nobel prize in Chemistry in 1978. The electrochemical proton gradient can be expressed as follows:

$$\Delta\mu_{H^+} = -F \Delta\psi + 2.3 RT \Delta pH \quad (\text{kJ/mol})$$

where *F* is the Faraday constant ($\sim 9.65 \times 10^4 \text{ C mol}^{-1}$), $\Delta\psi$ is the electrical potential difference between the matrix and the intermembrane space due to charge separation, *R* is the gas constant ($\sim 8.31 \text{ J mol}^{-1} \text{ K}^{-1}$), *T* is the temperature and ΔpH is an expression of the concentration gradient of protons across the membrane.

The proton-motive force is expressed as:

$$\Delta p = -\Delta\mu_{H^+} / F = \Delta\psi - 59 \Delta pH \quad (\text{mV})$$

Proton pumping

A part of the proton-motive force generated in *P. denitrificans* comes from consumption of positive charges (protons) from the matrix and the translocation of negative charges (electrons) across the membrane by membrane enzymes through, what Mitchell described as, a redox-loop mechanism. The other process contributing to the pmf is *genuine* proton pumping: the uptake of protons from the matrix and the release of protons to the periplasmic space, by complex I and IV. In order to take up protons to the active site, many enzymes in the respiratory chain are equipped with one to three so-called proton entry pathways that consist of amino acid residues capable of accepting and donating protons. In addition, these pathways are filled with water molecules, which may be functional in transporting protons to the enzyme's active site. Genuine proton pumps also need to be able to release the protons to the periplasmic space, which is why they have a similar pathway, or access to a water-containing compartment, on the periplasmic side of the enzyme. An important feature of genuine proton pumps is that they have found a way to mitigate the risk of futile cycling by

proton backflow from the periplasmic space to the matrix. The mechanism of this proton gating is not fully understood and may not be the same for all genuine proton pumps. Similarly, the exact structure and amount of proton pathways varies between enzymes, even within the same enzyme family and subclass.

Electron transfer

Electrons are transferred within and between proteins, via several mechanisms. Intermolecular electron transfer occurs through docking interactions between molecules, usually of a relatively small and mobile electron carrier onto a larger transmembrane enzyme complex. The mobile electron carriers in the mitochondrial respiratory chain are NADH/ferredoxin, ubiquinone, menaquinone and cytochrome *c*. Ubiquinone and menaquinone can carry up to two electrons at once, whereas cytochrome *c* can transfer only one electron at a time. The strength of docking of the carriers on the membrane-bound respiratory enzyme complexes relies heavily on ionic interaction, yet the rate at which these interactions occur is also dependent on the abundance of the carrier molecules and their diffusion rate in the membrane.

Intramolecular electron transfer, for example between the carrier docking site and the active site of the enzyme, generally occurs via the redox active centers in the molecule. These redox active centers can be e.g. heme irons or copper centers, or in some cases amino acid residues that transiently take a radical form when passing on an electron. The rate of electron transfer is largely dependent on the difference in redox potentials between the donating and the accepting site, as well as the distance between those sites. Intramolecular electron transfer takes place rapidly through covalent bonds, or at a lower rate through vacuum. Since heme irons are covalently bound in larger porphyrin systems, the relevant electron transfer distance between hemes through a vacuum is in fact the shortest distance between the porphyrin edges.

Terminal oxidases

The terminal oxidases can be depicted as black box systems that convert electrons and oxygen to water and a contribution to proton-motive force (figure 4). There is quite some diversity in terminal oxidases across aerobic organisms, but all terminal oxidases can be assigned to one of two enzyme classes: the cytochrome *bd* quinol oxidases and the heme-copper oxidases (which also includes the more distant NO reductases). The cytochrome *bd* quinol oxidases and the heme-copper oxidases differ in a number of aspects, both structural and functional (see table 1 for an overview, or the review in chapter 2 for more details).

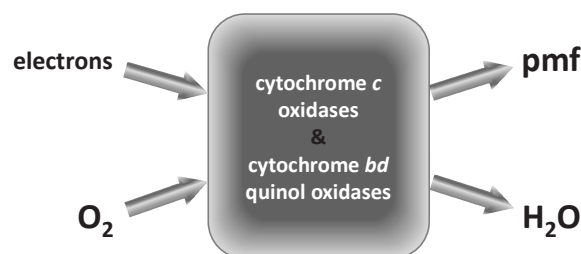


Figure 4: black box representation of terminal oxidases

Table 1: overview of some of the differences between the two subclasses of the terminal oxidase superfamily. The distant group of NO reductases is excluded from this overview.

	Cytochrome <i>bd</i> quinol oxidases	Heme-copper oxidases (excl. NO reductases)
Subunits	SU I, II (catalytic)	SU I, II (catalytic), SU III, IV, etc. (non-catalytic)
Redox centers	3 hemes, no copper centers	2 hemes, 2 copper centers
PMF	Yes	Yes
Proton pump	No	Yes
Electron donors	Ubiquinol	Cytochrome <i>c</i>
q^+/e^-	1 ($4H^+/O_2$)	1.5 – 2 ($6 – 8 H^+/O_2$)
O_2 affinity	very high ($K_{M,O_2} \sim 3\text{-}20\text{ nM}$ ^{14,15})	high (e.g. <i>bo</i> ₃ $K_{M,O_2} = 100\text{ nM}$ ¹⁵)

The oxidases of the heme-copper subclass have been more extensively studied than those of the cytochrome *bd* quinol oxidases. The structural properties and catalytic mechanism of heme-copper oxidases are therefore more known and better understood in comparison to those of the quinol oxidases. The heme-copper oxidases have been studied for over 50 years, yet the mechanism behind their ability to pump protons across cellular membranes continues to intrigue biochemists.

Although the members of the enzyme classes may differ to some degree in structure or heme content, the general belief is that many of the mechanistic principles behind proton pumping apply to all. The catalytic subunits of the well-studied microbial A-type cytochrome *c* oxidases, such as cytochrome *aa*₃ oxidase, are very similar to the human mitochondrial cytochrome *c* oxidase. Research has focused on the mechanism of O-O bond splitting, which happens instantly and requires 4 electrons, whereas the redox centers in the active site of the enzyme hold only 3. The origin of the fourth electron has been ascribed to a nearby amino acid residue, which transiently forms a (neutral) radical until the next electron is transferred to the active site via intramolecular electron transport^{16,17}. Other research on cytochrome *aa*₃ oxidase has focused on describing the mechanism behind proton pumping. The stoichiometry of proton pumping is fairly constant with turnover for most heme-copper oxidases, although the ratio of protons pumped over electrons accepted can differ between enzymes. In order to maintain this constant level of proton pumping, a mechanism through which the proton flow is kept unidirectional, minimizing proton backflow, is believed to be in place in all proton-pumping oxidases.

The cytochrome *bd* oxidases, that do not have sequence homology with the heme-copper oxidases, do not pump protons and therefore have a lower bioenergetic efficiency than the heme-copper oxidases. At the same time they do have a higher affinity for oxygen, which makes them efficient oxygen scavengers. The cytochrome *bd* oxidases are therefore believed to be expressed especially in the presence of H_2O_2 and NO stress, to act as a guard against oxidative damage¹⁸.

Microorganisms living in different conditions seem to have evolved their own ways to help them adapt to their surroundings through fine-tuning the expression of their respiration machinery. A microbe living in a low-stress environment may strive for the highest energy conservation possible, while under conditions of oxidative stress, it could be beneficial to sacrifice some bioenergetic efficiency for a better protection against oxidative damage.

Aim of this research

With all the variety that exists among the terminal oxidases, it is surprising that there appear to be many mechanistic similarities. In order to better define in which aspects the different terminal oxidases differ, or are the same, we have subjected a few exemplary bacterial terminal oxidases to a hyperfast mixing and freeze quenching treatment using the MHQ apparatus developed in our lab¹⁹. With this approach we were able to study the wild type enzymes in detail, focusing in particular on the formation of transient radicals during the various steps of the catalytic cycle and the importance of such radicals for O-O bond splitting and proton pumping. Another goal of our work was to further characterize the elusive P_M state of cytochrome *c* oxidase, which is the first intermediate in which the O-O bond is broken. Most efforts to isolate the P_M state rely on artificial reactions and/or mutant versions of enzymes and they are not necessarily representative for the *in vivo* wild type activity. Using the MHQ technique we have strived to accumulate the 'natural' P_M intermediate in order to collect relevant information on this step of the catalytic cycle.

We have performed microsecond kinetic analysis on a quinol oxidase (cytochrome *bdI* oxidase from *Escherichia coli*), a Type A cytochrome *c* oxidase (cytochrome *aa*₃ oxidase from *Paracoccus denitrificans*) and a Type B cytochrome *c* oxidase (cytochrome *ba*₃ oxidase from *Thermus thermophilus*). Stopped-flow UV-vis spectroscopy in the millisecond-to-second time range was combined with microsecond freeze hyperquenching and low temperature UV-vis and EPR spectroscopy in the micro- to millisecond time range to obtain a full overview of catalytic turnover of the enzymes.

References

1. Hooke, R **1665**, *Micrographia: Or Some Physiological Descriptions of Minute Bodies Made by Magnifying Glasses, with Observations and Inquiries Thereupon*, Courier Dover Publications, New York.
2. El Albani, A *et al.* **2010**, 'Large colonial organisms with coordinated growth in oxygenated environments 2.1 Gyr ago', *Nature*, vol. 466, pp. 100-104. doi: 10.1038/nature09166
3. Bengtson, S, Belivanova, V, Rasmussen, B & Whitehouse, M **2009**, 'The controversial "Cambrian" fossils of the Vindhyan are real but more than a billion years older', *Proceedings of the National Academy of Sciences of the United States of America*, vol. 106, pp. 7729-7734. doi: 10.1073/pnas.0812460106
4. Schopf, JW, Kudryavtsev, AB, Czaja, AD & Tripathi, AB **2007**, 'Evidence of Archean life: Stromatolites and microfossils', *Precambrian Research*, vol. 158, pp. 141-155. doi: 10.1016/j.precamres.2007.04.009
5. Schopf, JW **2006**, 'Fossil evidence of Archaean life', *Philosophical Transactions of the Royal Society B: Biological Sciences*, vol. 361, pp. 869-885. doi: 10.1098/rstb.2006.1834
6. Raven, PH & Johnson, GB **2002**, *Biology*, McGraw-Hill Inc., New York.
7. Darwin, CR **1859**, *On the Origin of Species by Means of Natural Selection, or the Preservation of Favoured Races in the Struggle for Life*, John Murray, London.
8. Margulis, L **1999**, *Symbiotic planet: a new look at evolution*, Basic books, New York.
9. Nass, MMK & Nass, S **1963**, 'Intramitochondrial fibers with DNA characteristics: I. Fixation and Electron Staining Reactions', *The Journal of Cell Biology*, vol. 19, no. 3, pp. 593-611.
10. Ris, H & Plaut, WS **1962**, 'Ultrastructure of DNA-containing areas in the chloroplast of *Chlamydomonas*', *The Rockefeller University Press*, vol. 13, no. 3, pp. 383-391.
11. Hu, GB **2014**, 'Whole Cell Cryo-electron tomography suggest mitochondria divide by budding', *Microscopy and microanalysis*, vol. 20, no. 4, pp. 1180-1187. doi: 10.1017/S1431927614001317
12. Possingham, JV & Rose, RJ **1976**, 'Chloroplast Replication and Chloroplast DNA Synthesis in Spinach Leaves', *Proceedings of the Royal Society B: Biological Sciences*, vol. 193, no. 1112, pp. 295-305. doi: 10.1098/rspb.1976.0047
13. Mitchell, P **1961**, 'Coupling of Phosphorylation to Electron and Hydrogen Transfer by a Chemi-Osmotic type of Mechanism', *Nature*, vol 191, pp. 144 - 148. doi: 10.1038/191144a0
14. D'mello, R, Hill, S & Poole, RK **1996**, 'The cytochrome bd quinol oxidase in *Escherichia coli* has an extremely high oxygen affinity and two oxygen-binding haems: implications for regulation of activity in vivo by oxygen inhibition', *Microbiology*, vol. 142, pp. 755-763. doi: 10.1099/00221287-142-4-755
15. Rice, CW & Hempfling, WP **1978**, 'Oxygen-limited continuous culture and respiratory energy conservation in *Escherichia coli*', *Journal of Bacteriology*, vol. 134, pp. 115-124.
16. Wiertz, FG, Richter, OM, Ludwig, B & De Vries, S **2007**, 'Kinetic resolution of a tryptophan-radical intermediate in the reaction cycle of *Paracoccus denitrificans* cytochrome c oxidase', *Journal of Biological Chemistry*, vol. 282, pp. 31580-31591. doi: 10.1074/jbc.M705520200
17. De Vries, S **2008**, 'The role of the conserved tryptophan²⁷² of the *Paracoccus denitrificans* cytochrome c oxidase in proton pumping', *Biochimica et Biophysica Acta*, vol. 1777, pp. 925-928. doi: 10.1016/j.bbabo.2008.05.008
18. Mason, MG, Shepherd, M, Nicholls, P, Dobbin, PS, Dodsworth, KS, Poole, RK & Cooper, CE **2009**, 'Cytochrome bd confers nitric oxide resistance to *Escherichia coli*', *Nature Chemical Biology*, vol. 5, pp. 94-96. doi: 10.1038/nchembio.135
19. Cherepanov, AV & De Vries, S **2004**, 'Microsecond freeze-hyperquenching: development of a new ultrafast micro-mixing and sampling technology and application to enzyme catalysis', *Biochimica et Biophysica Acta*, vol. 1656, pp. 1-31. doi: 10.1016/j.bbabo.2004.02.006

Chapter II

Energy conversion and conservation by cytochrome oxidases

Angela Paulus, Simon de Vries

Adapted from:
Copper-Oxygen Chemistry, John Wiley & Sons, Inc., Hoboken, NJ, USA, 2011, 107-129

Table of contents

I.	Introduction
II.	Structural features of heme-copper oxidases
III.	Electron transfer
IV.	Proton conducting pathways
V.	Proton transfer reactions
A.	Proton pumping
B.	Uncoupled & decoupled mutants
VI.	Electron transfer reactions in the catalytic cycle
A.	Overview
B.	The individual steps of the catalytic cycle
C.	Radical formation
1.	Radical formation in the reaction with hydrogen peroxide
2.	Radical formation in the reaction with molecular oxygen
VII.	Conclusion and future prospects
References	
Figures and captions	

Abbreviations

ATP	adenosine triphosphate
CcO	cytochrome <i>c</i> oxidase
ENDOR	electron nuclear double resonance
EPR	electron paramagnetic resonance
EXAFS	extended X-ray absorption fine structure
FTIR	fourier transform infrared spectroscopy
H ₂ O ₂	hydrogen peroxide
N ₂ O	nitrous oxide
NO	nitric oxide

I. Introduction

Aerobic organisms are found in all three Domains of Life: archaea, bacteria and eukarya. In the aerobic organisms, oxygen serves as the terminal electron acceptor gathering the excess reducing equivalents produced in cellular metabolism, thereby making the overall chemistry of the cell electroneutral. The reduction of oxygen by membrane-bound terminal oxidases is usually coupled to the generation of a proton motive force, which enables the cell for example to produce ATP and to import nutrients. Three evolutionary independent classes of terminal oxidases occur in nature: The heme-copper oxidases, the cytochrome *bd* oxidases and the di-iron oxidases. The heme-copper oxidases are highly efficient proton pumps with a stoichiometry of eight protons translocated per oxygen reduced. The cytochrome *bd* oxidases are not proton pumps, but the reaction is electrogenic due to the uptake of four protons per water molecule formed from one side of the membrane. The cytochrome *bd* oxidases thus have half the bioenergetic efficiency of the heme-copper oxidases. The membrane-bound di-iron oxidases occur mainly in plant mitochondria and they do not translocate protons. All free energy of the reduction of oxygen to water is released in the form of heat, which is used as a signal for flowering.

The superfamily of heme-copper oxidases comprises not only the cytochrome oxidases, which catalyze the reduction of molecular oxygen to water, but also the NO reductases, which reduce NO to N₂O.¹⁻⁶ The close relation between oxidases and NO reductases is illustrated in studies showing that the latter enzymes quite efficiently catalyze the reduction of oxygen to water⁷ while the cytochrome oxidases can reduce NO to N₂O, albeit at a low rate.⁸ These observations pertaining to function suggest a high similarity between the structures of oxidases and NO reductases, as is also borne out by the sequence similarities between the two types of enzymes in the superfamily and their comparable biophysical properties.^{7,9,10} The reduction of oxygen (Eq. 1) by cytochrome oxidases (but not by NO reductases) generates a proton electrochemical gradient across the cytoplasmic or mitochondrial membrane. Four protons are used for the formation of water and four are pumped across the membrane according to:



where H⁺_C are protons taken up from the cytoplasm (or mitochondrial matrix) and H⁺_P protons ejected to the periplasm (or mitochondrial intermembrane space).¹¹⁻¹⁵ Instead of cytochrome *c*, azurin, 4Fe-4S ferredoxins, ubiquinol or menaquinol may serve as electron donor. The quinones for example are the reductants to the cytochrome *bo*₃ of *Escherichia coli*.¹⁶

Bioinformatic analysis combined with 3D-structural information has led to the classification of the superfamily of heme-copper oxidases into three oxidase families (Type A, B and C)¹⁷; a more recent bioinformatic search has identified eight oxidase families (Type A-H) and five NO reductase families.¹⁸ The Type D-H oxidases occur predominantly in the archaea and structural and kinetic characterization of these enzymes is presently very limited.

Crystal structures have been determined for Type A oxidases {e.g. cytochrome *aa*₃ from *Paracoccus denitrificans* (1QLE)¹⁹, *Rhodobacter sphaeroides* (2GSM)²⁰, *E. coli bo*₃ oxidase (1FFT)²¹, mitochondrial cytochrome *aa*₃ (2DYR)²²} and for Type B oxidases {*Thermus thermophilus* cytochrome *ba*₃ (1XME)²³}, but not for Type C, the *cbb*₃ oxidases.

This review discusses the details of the catalytic mechanism of the Type A and Type B oxidases highlighting electron transfer-coupled proton pumping. For these oxidases a wealth of kinetic data are available that can be related to their known structures. Recent

reviews covering cytochrome *bd* oxidases and archaeal oxidases are found in ²⁴ and ^{18,25}, respectively.

II. Structural features of heme-copper oxidases

Cytochrome *c* oxidases are multi-subunit enzymes. Subunit I harbors the entire binuclear active site (heme Fe-Cu_B) and the heme center that acts as the direct electron donor to the binuclear center. The electron transfer pathway extends to the Cu_A center in subunit II, near the cytochrome *c* binding site. The precise location of the quinol binding site in e.g. the *bo*₃ oxidases is not known, but it may reside at the interface of subunits I and II. The proton transfer pathways are mainly located in subunit I, a few residues being contributed by subunit II. Purified bacterial enzyme preparations consisting of subunits I and II only, are capable of reducing oxygen at high rates and they display full proton pumping capacity.²⁶ All oxidases contain a third subunit, an integral membrane subunit, which binds phospholipids; however, the function of subunit III is not known. In some oxidases subunit I and III are fused to a single subunit.²⁷ Bacterial oxidases usually contain a small fourth subunit of unknown function that consists of a single transmembrane alpha-helix. Mitochondrial cytochrome oxidases may contain up to thirteen subunits. The mitochondrial subunits I, II and III are encoded by the mitochondrial DNA, pointing to their bacterial origin. The additional subunits are encoded by the nuclear DNA and appear not essential for catalytic activity per se. Some subunits are expressed in a tissue-specific or oxygen-dependent way.²⁸

The active site where molecular oxygen binds, consists of a mono-histidine bound five-coordinate high spin heme (heme *a*₃, *o*₃ or *b*₃) and a mono-copper site (Cu_B) ligated by three histidine residues (Fig. 1). The direct electron donor to the binuclear center is a low spin bis-histidine heme center (heme *a* or *b*), which receives its electrons from Cu_A or directly from the substrate quinol. The six histidine residues that serve as ligands to the metal centers are strictly conserved. Cu_A is a Cu²⁺-Cu¹⁺/Cu¹⁺-Cu¹⁺ mixed-valence center in which the two copper atoms are 2.5 Å apart.²⁹

III. Electron transfer

Rates of electron tunneling between the cofactors can be predicted within a factor 5-10 error with the square-barrier approximation, which neglects any influence of the tunneling medium.³⁰ For every ~1.7 Å increase in tunneling distance the rate of electron transfer decreases by an order of magnitude. The best estimations for tunneling rates are obtained when the tunneling distance is determined as the shortest 'edge-to-edge' distance between the cofactors rather than the metal-to-metal distance. Cu_A is located at a distance of 16.1 Å from the low spin heme *a* and at 18.9 Å from heme *a*₃.³¹ The edge-to-edge distance between heme *a* and heme *a*₃ is 4.7 Å (metal-to-metal 13 Å).³² The two metals of the binuclear center are separated by 5.3 Å in bacterial and 4.5 Å in mammalian cytochrome *c* oxidase and they are antiferromagnetically coupled in the resting enzyme through a bridging peroxide residue.^{33,34}

The rates of electron transfer from Cu_A to heme *a* and from heme *a* to the binuclear center are calculated as 8.7·10⁴ s⁻¹ and 6.5·10⁸ s⁻¹.³¹ Direct measurements of electron transfer rates yield values close to the calculations (2·10⁴ s⁻¹^{35,36} and 7·10⁸ s⁻¹³⁷ respectively). The rate of direct electron transfer from Cu_A to heme *a*₃ is calculated at ~250 s⁻¹, which is not insignificant in respect to the turnover rate of ~1000 e⁻ s⁻¹.³¹ The short-circuit between Cu_A and heme *a*₃ is generally assumed not to be functional and might be suppressed to physiologically insignificant rates in case this reaction path would have a high reorganization energy.

In addition to the metal containing cofactors, aromatic residues might participate directly in electron transfer. The binuclear center is surrounded by a number of conserved aromatic residues (Fig. 1), which can form neutral radicals during the reaction with oxygen and/or hydrogen peroxide.³⁸⁻⁴⁰ Furthermore, cytochrome *c* oxidases from each of the three subtypes harbor a covalent crosslink of a histidine Cu_B ligand (H276) to its neighboring tyrosine (Y280).⁴¹ The crosslink is formed post-translationally, presumably during the first turnover. Its strict conservation among Type A, B and C oxidases suggests a vital role in the mechanism of cytochrome *c* oxidase. Due to its unique electronic properties the His-Tyr crosslink can be regarded as a cofactor that might mediate electron and proton transfer.

IV. Proton conducting pathways

The protons that are taken up by cytochrome oxidase are conducted along proton pathways that consist of chains of hydrogen-bonded functional groups and water-filled cavities, forming effective proton relay networks. The proton-conducting chains also appear to contain 'gaps', so that conformational changes are necessary for delivery of protons to the binuclear center or to the proton loading site. Proton transfer rates may be modulated through these conformational changes.

At least two proton conducting pathways were revealed by the X-ray crystal structure of the bovine enzyme.^{42,43} The shorter pathway, which starts from the N-side of the membrane near a lysine residue (K354), is made up of residues from both helix VI and VIII of subunit I and is called the K-pathway (Fig. 2b). The K-pathway extends to the strictly conserved Y280 near the active site via T351 and S291 and conducts only two of the total of eight protons taken up during turnover. The K-pathway is used specifically in the reductive phase of the cycle. Six out of the eight protons (including all four pumped protons) are conducted by the much longer D-pathway (Fig. 2a). The D-pathway is located between D124 on the N-side of the membrane and the E278 near the binuclear centre and comprises the side chains of residues in helix III and IV of subunit I. Residues contributing to the D-pathway in *Paracoccus denitrificans* are: D124, N199, N131, Y35, S134, S193 and E278. The E278 at the end of the pathway in Type A1 oxidases is lacking in Type A2 oxidases. Type A2 oxidases may have a tyrosine residue at a similar position, sometimes with a neighboring serine residue to form a YS-motif. The K- and the D-pathway are otherwise very well conserved among Type A1 and A2 oxidases.

Sequence comparison indicates that the residues of the D- or K-pathway are not at all conserved in Type B oxidases. The crystal structure of the cytochrome *ba₃* (Type B) oxidase, indicates the presence of K-like and D-like proton conducting pathways.⁴⁴ Recent mutational analyses of the Type B *ba₃* oxidase have, however, shown that the four protons required for the formation of water and the pumped protons are delivered via the K-like pathway.⁴⁵ The K-pathway in Type B oxidases is formed by E15 (subunit II), T312, S309, Y248, S261 and Y237 (all located in subunit I). Mutations in the K-pathway severely diminish proton pumping and electron transfer rates in both the reductive and the oxidative phases of the reaction. Mutations to the putative D-like proton pathway were shown to have much smaller effects or none at all. This behavior is completely different from that of Type A oxidases, where mutations blocking the D-pathway result in selective inhibition of the oxidative phase and abolished proton pumping. Type C oxidases are suggested to use only one proton transfer pathway, similar to Type B oxidases.⁴⁶

Based on the crystal structures additional putative proton conducting pathways have been suggested for Type A and B oxidases. In Type A oxidases of mammalian^{43,47} and bacterial origin⁴² there is a chain of protonatable residues starting at an aspartate (D407, *B. taurus*) or a glutamate residue (E442, *P. denitrificans*), leading towards heme *a*. The pathway

is named after the first residue from the N-side that is conserved between the bacterial and the mammalian enzymes (H448). The H-pathway in *P. denitrificans* may also be referred to as E-pathway.⁴⁸ The residues of the H-pathway are only weakly conserved between mammalian and *P. denitrificans* oxidase and are not conserved in cytochrome *bo*₃ from *E. coli*. In addition to that, H-pathway mutants display high residual activity. The H-pathway may influence electron transfer from heme *a* to the binuclear center through the many H-bond interactions between heme *a* and its surroundings, but it is probably not a proton transfer pathway.

The third putative proton pathway in Type B oxidases is the Q-pathway,^{49,50} which leads from a glutamine residue to the histidine ligand of heme *a*₃. Residues of the Q-pathway are not conserved among Type B oxidases and mutations blocking the pathway do not affect activity or proton pumping.⁴⁵ Therefore, the Q-pathway does not appear to function as a proton entry pathway. It was suggested that the Q-pathway is involved in the release of protons to the proton exit pathway.⁵⁰

V. Functional aspects of cytochrome *c* oxidase

A. Proton pumping

Studies on cytochrome *c* oxidase in whole cells, coupled mitochondria or incorporated in lipid membrane vesicles have been carried out to determine the stoichiometry of proton pumping (Table I). For Type A and C oxidases it is firmly established that eight protons are taken up during turnover, yielding an overall stoichiometry of 2 H⁺/e⁻. The stoichiometry of proton pumping alone is 1 H⁺/e⁻, as four protons that are taken up are consumed in the chemical reduction of oxygen to water. It is tacitly assumed that all cytochrome *c* oxidases have the same total stoichiometry, although there are indications that the overall H⁺/e⁻ ratio for Type B oxidases is smaller (~1.5 H⁺/e⁻), yielding a stoichiometry of 0.5 H⁺/e⁻ for proton pumping (Table I). A significant difference in the stoichiometry of proton pumping may be a reflection of the different structures of the proton pathways in Type A and Type B oxidases. In particular, the glutamate residue E278 in Type A oxidases that is involved in (gating) proton transfer appears to lack a protonatable equivalent in Type B oxidases. In *T. thermophilus* *ba*₃ oxidase there is an isoleucine residue in this position, which may compromise the efficiency of the proton translocation process. On the other hand, the relatively low proton pumping stoichiometry of the Type B *ba*₃ oxidase may simply be due to suboptimal experimental conditions. *T. thermophilus* thrives at 95°C, whereas proton pumping experiments are performed at temperatures below 65°C. The observation that the Type B oxidase from *Acidianus ambivalens*⁵¹ pumps protons at H⁺/e⁻ = 1 strengthens the belief that under the right circumstances all cytochrome oxidases translocate protons at the same maximum stoichiometry of 2 H⁺/e⁻. The effect of the specific experimental conditions on proton pumping efficiency has been observed also in Type A oxidases^{52,53} and in Type C oxidases.⁵⁴

Gating of proton pumping is necessary in order to prevent backflow of protons across the membrane. This backflow results in a lowered net H⁺/e⁻ ratio and in dissipation of the membrane potential and/or proton motive force. The gating residue in Type A CcO's, acting as a valve or switch, is proposed to be E278.⁵⁵ This residue is not conserved in Type A2 and B oxidases, but might be functionally replaced by the YS motif. The pK_a value for E278 is high (pK_a = 9.4)⁵⁶, but in fact close to that expected for the tyrosine of the YS motif. Another possible candidate to gate proton pumping is the strictly conserved W272, which was suggested to direct proton transfer through redox linked activity.^{39,57}

B. Uncoupled & decoupled mutants

Point mutations in cytochrome *c* oxidases can affect the kinetics of proton uptake and thereby the stoichiometry of translocation. These mutant enzymes may reveal clues to the principles underlying proton pumping. Particularly interesting are the uncoupled mutant oxidases, which show significant or even increased oxygen reductase activity, with a severely decreased coupling of proton pumping. The energy conservation efficiency for these enzymes is low compared to the wild type enzyme. In fully uncoupled mutants, proton pumping is lacking and the only contribution to the membrane potential comes from the uptake of protons and electrons from different sides of the membrane for the reduction of oxygen to water. In so-called decoupled mutants proton translocation, proton pumping and respiration are all inhibited.

Several studies on site-directed mutants of the *aa*₃ terminal oxidase from *Rhodobacter sphaeroides* have been reported.⁵⁸⁻⁶² Some of these mutants show a decreased coupling between electron transfer and proton translocation.⁵⁹ Substitution of the *R. sphaeroides* asparagine residues N139 or N207 (N131/N199 in *P. denitrificans*) by aspartate, for example, abolishes proton pumping while electron transfer activity is retained. The asparagines are located in the neck of the D-pathway and proposed to be involved in the organisation of the water chain along the pathway. The mutants display a modified pH dependency for the **P_R** to **F** transition, which was interpreted as an increase in the pK_a of E278 compared to the wild type value (10.9 instead of 9.4).⁵⁹ The decrease in coupling efficiency might therefore be explained by an increased proton affinity of E278. This would prevent facile proton release towards the P-side, while proton transfer to the binuclear site is maintained due to the even higher proton affinity of the specific heme-Fe and Cu_B ligand states in the binuclear site. On the other hand, electrostatic calculations on the equivalent *P. denitrificans* mutant do not support this view. The influence of a mutation in the N131/N199 region (20 Å away) on the pK_a of E278 was predicted to be only minor.⁶³

In crystallized samples of the N131D mutant the water chain that connects the residues of the D-pathway appears structurally perturbed.⁶⁴ Four water molecules that are readily distinguished in the wild type crystal structure appear missing in the mutant, suggesting higher mobility of the molecules in the water chain, which may disrupt a Grotthuss-type proton transfer along the chain. The direct environment of E278 was also altered in the mutant. The E278 side chain was found to adopt two distinct orientations (pointing towards and away from the D-pathway) in the same sample, indicating that the function of E278 as a proton 'switch' or 'valve' may be impeded by the mutation. In view of the above, the observation that the S189A mutation was without effect on oxygen reduction activity or proton pumping efficiency, is unexpected.⁶⁵ In the S189A mutant, the serine residue, which is normally hydrogen-bonded to water and located only 7 Å from E278 in the D-pathway, is replaced by the non-polar alanine. Such a mutation might easily distort or disrupt the direct environment of E278 and the precise structure of the chain of water molecules. Apparently, the structure of the water chain in the D-pathway is rather robust and is not significantly affected by the hydrogen-bonding state of S189.

Mutation of the uncharged S189 residue to a negatively charged aspartate (S189D) results in uncoupling of the proton pump, which led to the suggestion that it is the alteration of the electrostatic potential within the pathway that uncouples electron transfer from proton translocation.⁶⁵ However, that is not plausible, because the N131T mutation, which does not affect the electrostatic potential, also results in uncoupling.⁶⁶ The activity and stoichiometry of proton pumping in D-pathway double mutants (D124N/N131D) are surprisingly unaffected,⁶⁷ i.e. the two mutations appear compensatory. At present there is no single explanation for the effect of mutations on D-pathway residues.

Some mutants of CcO are only partially decoupled, i.e. they do pump protons, but with lower stoichiometry. An example of such a mutant is the W164F mutant, which maintains 40% of wild type activity and pumps protons at half the stoichiometry.⁶⁸ The mutated tryptophan residue is located in the region above the hemes and is hydrogen-bonded to the δ -propionates of both hemes *a* and *a*₃. Mutation of the tryptophan to a phenylalanine creates more space for the D-pathway E278 residue to adopt the conformation pointing away from the proton pathway. This might prevent fast reprotonation of E278 by the D-pathway and/or increase the rate of proton back flow by reprotonation from the P-side. In both cases the apparent proton pumping efficiency decreases. The pH dependence of the proton pumping reaction in the wild type and mutant enzymes suggests that there is a pH-sensitive proton back flow that becomes more significant at high pH.⁶⁸

VI. Catalytic cycle

A. Overview

The reduction of oxygen to water is a complex reaction, involving no less than 13 components (8 H^+ , 4 e^- , O_2) and perhaps as many steps, some of which have yet to be uncovered. The catalytic cycle of cytochrome *c* oxidase can be divided into two parts (Fig. 3): The reductive phase ($\text{O}_\text{H} \rightarrow \text{MV}$) and the oxidative phase ($\text{MV} \rightarrow \text{O}_\text{H}$). The reductive phase starts with the fully oxidized enzyme (O_H) and proceeds via the one-electron reduced state (E) to the two-electron reduced form (MV) or further to the artefactual four-electron reduced state (R). In the natural cycle of CcO molecular oxygen binds as soon as the enzyme is two-electron reduced (MV), a four-electron reduced state (R) does not accumulate in the cell under aerobic conditions. However, the R state is easy to produce experimentally and a suitable state to study properties of initial catalytic intermediates. The oxidative phase constitutes the reaction between oxygen and the two- or four-electron reduced enzyme (MV or R , respectively) and proceeds to the fully oxidized enzyme O_H , (but not O) via a number of partially oxidized intermediates. The oxidative phase includes heterolytic scission of the O-O bond in a reaction that requires four electrons and a proton.

B. The individual steps of the catalytic cycle

The reaction scheme that contains all known kinetically competent intermediates and the suggested proton pumping steps (omitting the uptake of the four chemical protons) is depicted in Fig. 3. The redox states of the metal centers in the fully oxidized enzyme O_H are Cu_A^{2+} , a_3^{3+} , a_3^{3+} and Cu_B^{2+} . Electrons from substrates like cytochrome *c* or ubiquinol enter the enzyme via Cu_A and are further transferred, via heme *a*, to the binuclear center. The first electron transfer yields E . The formation of E occurs in two steps. The electron is initially shared between the Cu_A and heme *a* metallo-centers which are in electronic equilibrium³⁶ and in a subsequent proton-dependent step transferred to Cu_B .⁶⁹ The second electron arriving via Cu_A produces the Mixed Valence (MV) state of the enzyme. In MV , the reduced active site heme *a*₃ binds oxygen forming (A), the ferrous-oxy complex. Oxygen binds transiently to Cu_B^{1+} before binding to heme *a*₃. The intermediate A appears to decay to P_M with a half-life of only $\sim 32\text{ }\mu\text{s}$,³⁹ a rate that is dependent on $[\text{O}_2]$. It was established by resonance Raman spectroscopy that the O-O bond is broken in the P state.⁷⁰ In the mixed valence state only three of the required four electrons are available for O-O bond splitting ($\text{Fe}_{a_3}^{2+} \rightarrow \text{Fe}_{a_3}^{4+}$; $\text{Cu}_\text{B}^{1+} \rightarrow \text{Cu}_\text{B}^{2+}$). The fourth electron and the proton are donated by a nearby amino acid residue, suggested as Y280.⁷¹ As a result of the heterolytic O-O bond splitting the heme *a*₃ has reacted to the oxoferryl form ($\text{Fe}_{a_3}^{4+}=\text{O}^{2-}$) while the other oxygen atom ends up at Cu_B^{2+}

as a hydroxo-ligand. The subsequent third substrate electron reduces the YO[•] radical (Y280*) to its anion YO⁻. The **P_R** state thus formed no longer harbors a radical. **P_R** is indistinguishable from **P_M** by its optical spectrum, but not by EPR.^{72,73} From **P_R** to **F** (t_{1/2}~27 μs), two protons are taken up from the N-side of the membrane through the proton conducting pathways. One proton protonates the YO⁻ to Y280, and the other proton is released to the P-side of the membrane. The transition from the **F** (oxoferryl) to the recently described³⁹ **F_W*** state forms the rate-limiting step of the cycle with t_{1/2}~1.2 ms. It involves the uptake of one proton from the N-side and the release of one proton to the P-side, as well as the transient formation of a neutral radical (W272*).³⁹ This radical is proposed to facilitate and gate proton pumping in a redox dependent manner.⁵⁷ In the **F** → **F_W*** transition, the oxoferryl heme *a*₃ is reduced to Fe(III)-OH⁻ by an electron from the nearby W272, yielding W272*, and protonated by a proton from E278. Since the W272* was determined to be a tryptophan *neutral* radical it was proposed that the W272 proton is ejected to the periplasm upon oxidation of W272 to W272*.³⁹ E278 is replenished with a proton from the D-pathway and in the **F_W*** → **O_H** transition the W272* is reduced to W272⁻ by an electron from the Cu_A/heme *a* redox pair with a t_{1/2} of 30 – 60 μs.³⁹ In its anionic form, the W272⁻ is a very strong base (pK_a>15) and is able to attract the newly arrived proton at E278. The deprotonated glutamate is once again protonated by a proton from the D-pathway. In total, two protons are taken up via E278, one from W272 is ejected to the P-side, while the W272 electron reduces the oxo-ferryl intermediate, which brings the overall stoichiometry of the **F** → **O_H** transition to 2 H⁺/e⁻, as found experimentally. According to this model⁵⁷ proton pumping is directly coupled to the redox activity of the strictly conserved residue W272, which provides both the thermodynamic driving force and the unidirectionality required for proton pumping.

We consider it very likely that the O-O bond breaking proceeds in the same way in either the fully reduced or mixed valence enzyme.^{5,39} The contrasting view^{12,74} is that in the two-electron reduced enzyme O-O splitting occurs as described above, involving Y280, but in the four-electron reduced enzyme, the fourth electron to split the O-O bond is donated by heme *a*.

The **O_H** state, depicted as part of the cycle in Fig. 3, is the activated (also pulsed or fast, see e.g.⁷⁵) oxidized form of CcO that has just finished a turnover cycle. This state is known to pump protons during the reductive phase,⁷⁶ whereas the oxidized ‘resting’ enzyme does not (although some reports disagree)¹³. The states **O_H** and **O** can also be distinguished by their cyanide binding kinetics.⁷⁵ **O_H** binds CN⁻ by at least a factor of 100 more rapidly than **O**. The ligands to the active site metals in the **O** state have been proposed as H₂O for heme *a*₃ and OH⁻ for Cu_B²⁺.⁴² However, more recent crystallographic and EXAFS studies and careful redox titrations by Mochizuki *et al.* provide evidence for the presence of peroxide as a bridging ligand between heme *a*₃ and Cu_B in the resting enzyme.^{34,77-79} The catalytically relevant ‘high-energy’ **O_H** might have OH⁻ ligands at both metal centers (e.g.⁷⁴). In the absence of substrates the active form of CcO relaxes back to the resting state on a time scale of minutes.

A branched, rather than a linear sequential, mechanism for CcO was suggested by Szundi *et al.* (see⁸⁰, or the review with Einarsdóttir⁸¹). This mechanism is linear between **F** and **A**, but branches into two parallel pathways for **A** → **F**. Equilibrium exists between the **P**- and **F**-states in this model and the interconversion between **P** and **F**, involving the uptake of a proton by the binuclear center, is pH dependent (**P** being the more stable species at high pH). It is possible that the kinetics of oxidation of reduced CcO appear as a series of unidirectional sequential transitions under regular experimental conditions, even if the mechanism is in reality branched or contains rapid protonic equilibria.

C. Radical formation

Over the past decade several groups have reported the formation of radicals in cytochrome oxidases from various organisms. Radicals have been observed both in the reaction with oxygen or with hydrogen peroxide. The reaction between hydrogen peroxide and oxidized CcO is very slow compared to the oxidation of reduced (or mixed valence) CcO by molecular oxygen. The P_M and F^\bullet states that are formed after addition of H_2O_2 are relatively stable enabling analysis by EPR spectroscopy. However, the actual reaction that occurs upon mixing H_2O_2 with *oxidized* oxidase is different from the reaction of *reduced* oxidase with molecular oxygen. The H_2O_2 acts as a two-electron oxidant to the oxidized oxidase, converting the heme a_3 iron to the $Fe^{4+}=O^{2-}$ oxoferryl and abstracting one electron from the enzyme. This electron is donated by a nearby amino acid residue, which results in formation of an organic radical. The P_M/F^\bullet generated in this way is obtained from $O_{(H)}$ by moving in reversed direction through the catalytic cycle, which is essentially irreversible. In addition, a true peroxy intermediate has never been detected in cytochrome oxidases. The role in the catalytic cycle of radicals formed by H_2O_2 is therefore questionable.

1. Radical formation in the reaction with hydrogen peroxide

Addition of H_2O_2 to oxidized CcO from *Paracoccus denitrificans* leads to formation of a tyrosine radical, Y167*.^{82,83} The Y167* is not formed in the W272F mutant, suggesting that Y167* is a secondary radical produced via radical migration in the enzyme involving a W272 radical. While a neutral W272* is formed in the reaction with oxygen³⁹ the Y167* has so far been detected only in the presence of H_2O_2 . The Y167F mutant retains 62% of the activity of the wild type oxidase, which renders a specific role in catalysis as yet unclear.⁸³

The broad radical signal observed in the F^\bullet state of the enzyme from bovine heart mitochondria treated with H_2O_2 was assigned to a tryptophan radical cation, based on ENDOR studies, and not to a tyrosine radical. A narrow EPR signal that was not linked to the kinetics of turnover, but probably the result of a peroxide side reaction, was attributed to a porphyrin cation radical.³⁸ F^\bullet may be converted to P_M simply by changing the pH suggesting a change in electronic equilibrium between the two states. Since the P_M state did not appear to have an EPR detectable radical signal, the authors proposed that the radical in P_M resides wholly on the His276-Tyr280 pair and is EPR silent due to spin coupling with Cu_B^{2+} .³⁸ W164 was put forward as the most likely candidate for generation of the radical signal,³⁸ although involvement of W272 or W323 was not excluded. All three tryptophan residues are highly conserved (W272 even strictly) and located close to the binuclear centre.

Svistunenko and co-workers addressed the apparent discrepancy between the proposed radical origins in bovine and bacterial CcO treated with H_2O_2 .⁸⁴ These authors show by EPR simulation studies that the signal detected in the bovine oxidase can be nicely simulated as originating from Y129, the equivalent of the Y167 residue in *P. denitrificans*. This study resolves the discrepancy that appeared to exist between the bacterial and bovine oxidases.

2. Radical formation in the reaction with molecular oxygen

Studies on the rapid reaction of reduced CcO with oxygen to detect kinetically competent radicals present an extra challenge. One approach is to use E278 mutants, in which the reaction does not proceed noticeably beyond P_R . Gorbikova *et al.*⁸⁵ analyzed the E278Q mutant during oxidation of its fully reduced form directly after photo dissociation of CO. The FTIR spectrum observed for P_R contained a contribution from the H276 cross-linked Y280 in its deprotonated form. Furthermore, the development of an electric potential during formation

of **P** was consistent with proton transfer across the distance between Y280 and the bound oxygen.⁸⁵ Formation of a Y280 radical could not be resolved in these experiments, but the observation of the deprotonated Y280 may suggest its involvement in O-O bond splitting in the **P_M** state.

Although the direct detection of a radical by EPR of CcO in the **P_M** state has so far failed, radicals have been observed in the His-Tyr model compound in the absence or presence of copper^{81,86} and in a CcO biomimetic compound brought to the **P_M** state containing Cu_B²⁺.⁸⁶ The apparent EPR silence of **P_M** in CcO as prepared in³⁸ should therefore not be taken for granted. **P_M** prepared by the triple-trapping method is not EPR silent but shows the EPR signal of Cu_B²⁺,^{70,71} which was apparently not observed in³⁸. In addition, there are several ways of preparing **P_M**, each yielding a state with slightly different properties.⁸⁷ Because a Y280* has not been detected, it remains undecided whether Y280 is indeed the primary donor of the proton and the electron needed for O-O bond scission. Calculations⁸⁸ may point to another residue as proton and/or electron donor to break the O-O bond, possibly W272.

A neutral W272* was recently observed in the reaction between CcO and molecular oxygen studied by means of microsecond freeze-hyperquenching combined with optical and EPR spectroscopy.^{39,40} The observed W272* was proposed as an intermediate in the second part of the catalytic cycle, but not in the initial O-O bond breaking reaction. The W272* is formed in the **F** → **O_H** transition with a $t_{1/2}$ ~ 1.2 ms, which led to the proposal of the intermediate state **F_{W*}** (Fig. 3) between **F** and **O_H**. The rate of W272* formation is close to the turnover rate of the CcO and represents the rate-limiting step of the reaction.³⁹ There is no disagreement in the literature that the rate-limiting step occurs in the transition from **F** to **O_H** (e.g.^{57,81}), and this reaction appears experimentally as a relatively slow (~ 1 ms) electron transfer from heme *a* to heme *a*₃. However, the rate of ~ 1 ms rate for this step is an apparent rate. It is the application of optical techniques like UV-Vis and resonance Raman spectroscopy in the majority of the work on CcO's that has led to the above assignment for the rate-limiting step. However, the optical techniques did not enable detection of the W272*, for which 'time-resolved' EPR spectroscopy is needed. Electron transfer between heme *a* and heme *a*₃ proceeds on the nanosecond time scale^{31,37,79} and is thus definitely not 'intrinsically slow'. We can now ask and try to answer the question as to why reduction of the oxo-ferryl by W272 (Fig. 3) is so slow, or to put it slightly differently: Why does the **A** → **F** transition take ~ 60 μs and the **F** → **F_{W*}** → **O_H** transitions approximately 1.2 ms?, a twentyfold difference in rates; or if one takes the view that it is really heme *a* to heme *a*₃ electron transfer that is limiting, why a million fold slower? After all, the two reaction sequences above include similar steps like proton translocation, proton pumping and electron transfer in which metallo-centers and aromatic amino-acid residues forming radicals play a role, thus a large difference in rates is not to be expected a priori. To change the rate of electron transfer from heme *a* to heme *a*₃ by a factor of a million (~ 1 ns to ~ 1 ms) would require a change in relative reduction potentials or reorganization energies of 0.35 – 0.4 eV during the reaction, which seems unlikely. To explain the low rate of reduction of heme *a*₃ by W272, the reduction potential of W272 must be higher than that of the metal centers in the binuclear site by a similar amount (0.35 – 0.4 eV), thus in the range of ~ 0.7 – 0.8 V. This value is not far from that of 'free' tryptophan (~ 1 V) at pH ~ 7. The actual reduction potential of Y280 (~ 0.9 V at pH 7 for 'free' tyrosine) may quite well match the value needed for the O-O bond splitting in the **A** → **F** transition. The reduction potentials of W272 and heme *a*₃ may not match perfectly, explaining the twenty-fold difference in rate between the **A** → **F** and **F** → **O_H** transitions. On the other hand, the actual reduction potential of W272 might be the result of a compromise because W272 might provide the electron and the proton to break the O-O bond in the **A** → **F** transition and serve as the reductant for heme *a*₃ in the **F** → **F_{W*}** transition.

VII. Conclusion and future prospects

The Type A, B and C oxidases are all proton pumps. With the possible exception of the Type B thermophilic cytochrome *ba*₃ the stoichiometry of proton pumping is 1 H⁺/e⁻. Crystal structures that are available for Type A and B oxidases indicate a high 3D-structural conservation of the metallo-electron transfer centers. Sequence comparison of subunit I of the Type C *cbb*₃ oxidases suggests a topology for the redox centers that is similar to that in Type A and Type B oxidases leading to the conclusion that electron transfer pathways are highly similar in all cytochrome oxidases. This is perhaps unexpected in view of the quite loose distance constraint for rapid electron transfer, i.e. metallo-centers must be located within ~ 15 Å. Proton transfer pathways appear to be far less conserved than electron transfer pathways. Type A oxidases have two proton transfer pathways (D and K), Type B only one (the K proton pathway). This too is surprising, since the Grotthuss mechanism for proton transfer requires formation of hydrogen bonds between many strategically placed acid-base groups, polar side chains and/or water molecules in a hydrophobic environment for which a distance constraint of less than 2.5 Å applies. Nature has apparently found many solutions to cope with these latter restrictions. Recent experiments have implicated tyrosine and tryptophan radicals as competent reaction intermediates in O-O bond cleaving and proton pumping, respectively. In these reactions the aromatic residues act both as electron and as proton donors, a capacity exceeding that of the metallo centers. To complete their complex catalytic cycle, the cytochrome oxidases need the participation of six rather than four redox centers. Future studies on the precise roles of aromatic residues in O-O bond breaking and proton pumping will aid to advance our knowledge on the link between electron transfer and proton pumping, or energy conversion and energy conservation.

References

1. Wasser, I. M.; de Vries, S.; Moenne-Loccoz, P.; Schroder, I.; Karlin, K. D. *Chem Rev* **2002**, *102*, 1201-34.
2. Richter, O. M.; Ludwig, B. *Rev Physiol Biochem Pharmacol* **2003**, *147*, 47-74.
3. Michel, H.; Behr, J.; Harrenga, A.; Kannt, A. *Annu Rev Biophys Biomol Struct* **1998**, *27*, 329-56.
4. Hendriks, J.; Oubrie, A.; Castresana, J.; Urbani, A.; Gemeinhardt, S.; Saraste, M. *Biochim Biophys Acta* **2000**, *1459*, 266-73.
5. Cherepanov, A. V.; De Vries, S. *Biochim Biophys Acta* **2004**, *1656*, 1-31.
6. Babcock, G. T.; Wikstrom, M. *Nature* **1992**, *356*, 301-9.
7. Girsch, P.; deVries, S. *Biochimica Et Biophysica Acta-Bioenergetics* **1997**, *1318*, 202-216.
8. Giuffre, A.; Stubauer, G.; Sarti, P.; Brunori, M.; Zumft, W. G.; Buse, G.; Soulimane, T. *Proc Natl Acad Sci U S A* **1999**, *96*, 14718-23.
9. Hendriks, J. H.; Jasaitis, A.; Saraste, M.; Verkhovsky, M. I. *Biochemistry* **2002**, *41*, 2331-40.
10. Hayashi, T.; Lin, M. T.; Ganesan, K.; Chen, Y.; Fee, J. A.; Gennis, R. B.; Moenne-Loccoz, P. *Biochemistry* **2009**, *48*, 883-890.
11. Wikstrom, M. *Biochim Biophys Acta* **2004**, *1655*, 241-7.
12. Verkhovsky, M. I.; Belevich, I.; Bloch, D. A.; Wikstrom, M. *Biochim Biophys Acta* **2006**, *1757*, 401-7.
13. Ruitenber, M.; Kannt, A.; Bamberg, E.; Fendler, K.; Michel, H. *Nature* **2002**, *417*, 99-102.
14. Faxen, K.; Gilderson, G.; Adelloth, P.; Brzezinski, P. *Nature* **2005**, *437*, 286-9.
15. Belevich, I.; Verkhovsky, M. I.; Wikstrom, M. *Nature* **2006**, *440*, 829-32.
16. Puustinen, A.; Verkhovsky, M. I.; Morgan, J. E.; Belevich, N. P.; Wikstrom, M. *Proc Natl Acad Sci U S A* **1996**, *93*, 1545-8.
17. van der Oost, J.; de Boer, A. P.; de Gier, J. W.; Zumft, W. G.; Stouthamer, A. H.; van Spanning, R. J. *FEMS Microbiol Lett* **1994**, *121*, 1-9.
18. Hemp, J.; Gennis, R. B. *Results Probl Cell Differ* **2008**, *45*, 1-31.
19. Harrenga, A.; Michel, H. *J Biol Chem* **1999**, *274*, 33296-9.
20. Qin, L.; Hiser, C.; Mulichak, A.; Garavito, R. M.; Ferguson-Miller, S. *Proc Natl Acad Sci U S A* **2006**, *103*, 16117-22.
21. Abramson, J.; Riistama, S.; Larsson, G.; Jasaitis, A.; Svensson-Ek, M.; Laakkonen, L.; Puustinen, A.; Iwata, S.; Wikstrom, M. *Nat Struct Biol* **2000**, *7*, 910-7.
22. Shinzawa-Itoh, K.; Aoyama, H.; Muramoto, K.; Terada, H.; Kurauchi, T.; Tadehara, Y.; Yamasaki, A.; Sugimura, T.; Kurono, S.; Tsujimoto, K.; Mizushima, T.; Yamashita, E.; Tsukihara, T.; Yoshikawa, S. *Embo J* **2007**, *26*, 1713-25.
23. Hunsicker-Wang, L. M.; Pacoma, R. L.; Chen, Y.; Fee, J. A.; Stout, C. D. *Acta Crystallogr D Biol Crystallogr* **2005**, *61*, 340-3.
24. Junemann, S. *Biochim Biophys Acta* **1997**, *1321*, 107-27.
25. Schroder, I. In *Archaea: new models for prokaryotic biology*; Blum, P., Ed.; Caister Academic Press, 2008; pp 1-26.
26. Solioz, M.; Carafoli, E.; Ludwig, B. *J Biol Chem* **1982**, *257*, 1579-82.
27. Mather, M. W.; Springer, P.; Hensel, S.; Buse, G.; Fee, J. A. *J Biol Chem* **1993**, *268*, 5395-408.
28. Castello, P. R.; Woo, D. K.; Ball, K.; Wojcik, J.; Liu, L.; Poyton, R. O. *Proceedings of the National Academy of Sciences of the United States of America* **2008**, *105*, 8203-8208.
29. Blackburn, N. J.; Barr, M. E.; Woodruff, W. H.; Vanderhoost, J.; Devries, S. *Biochemistry* **1994**, *33*, 10401-10407.
30. Moser, C. C.; Chobot, S. E.; Page, C. C.; Dutton, P. L. *Biochim Biophys Acta* **2008**, *1777*, 1032-7.
31. Moser, C. C.; Page, C. C.; Dutton, P. L. *Philos Trans R Soc Lond B Biol Sci* **2006**, *361*, 1295-305.

32. Solomon, E. I.; Sundaram, U. M.; Machonkin, T. E. *Chem Rev* **1996**, *96*, 2563-2606.
33. Van Gelder, B. F.; Beinert, H. *Biochim Biophys Acta* **1969**, *189*, 1-24.
34. Mochizuki, M.; Aoyama, H.; Shinzawa-Itoh, K.; Usui, T.; Tsukihara, T.; Yoshikawa, S. *J Biol Chem* **1999**, *274*, 33403-11.
35. Adelroth, P.; Brzezinski, P.; Malmstrom, B. G. *Biochemistry* **1995**, *34*, 2844-9.
36. Farver, O.; Grell, E.; Ludwig, B.; Michel, H.; Pecht, I. *Biophys J* **2006**, *90*, 2131-7.
37. Pilet, E.; Jasaitis, A.; Liebl, U.; Vos, M. H. *Proceedings of the National Academy of Sciences of the United States of America* **2004**, *101*, 16198-16203.
38. Rich, P. R.; Rigby, S. E.; Heathcote, P. *Biochim Biophys Acta* **2002**, *1554*, 137-46.
39. Wiertz, F. G.; Richter, O. M.; Ludwig, B.; de Vries, S. *J Biol Chem* **2007**, *282*, 31580-91.
40. Wiertz, F. G.; Richter, O. M.; Cherepanov, A. V.; MacMillan, F.; Ludwig, B.; de Vries, S. *FEBS Lett* **2004**, *575*, 127-30.
41. Buse, G.; Soulimane, T.; Dewor, M.; Meyer, H. E.; Bluggel, M. *Protein Sci* **1999**, *8*, 985-90.
42. Ostermeier, C.; Harrenga, A.; Ermiler, U.; Michel, H. *Proceedings of the National Academy of Sciences of the United States of America* **1997**, *94*, 10547-10553.
43. Tsukihara, T.; Aoyama, H.; Yamashita, E.; Tomizaki, T.; Yamaguchi, H.; Shinzawa-Itoh, K.; Nakashima, R.; Yaono, R.; Yoshikawa, S. *Science* **1996**, *272*, 1136-1144.
44. Soulimane, T.; Buse, G.; Bourenkov, G. P.; Bartunik, H. D.; Huber, R.; Than, M. E. *Embo J* **2000**, *19*, 1766-76.
45. Chang, H. Y.; Hemp, J.; Chen, Y.; Fee, J. A.; Gennis, R. B. *Proc Natl Acad Sci U S A* **2009**, *106*, 16169-73.
46. Hemp, J.; Han, H.; Roh, J. H.; Kaplan, S.; Martinez, T. J.; Gennis, R. B. *Biochemistry* **2007**, *46*, 9963-72.
47. Yoshikawa, S.; Shinzawa-Itoh, K.; Nakashima, R.; Yaono, R.; Yamashita, E.; Inoue, N.; Yao, M.; Fei, M. J.; Libeu, C. P.; Mizushima, T.; Yamaguchi, H.; Tomizaki, T.; Tsukihara, T. *Science* **1998**, *280*, 1723-9.
48. Pfizner, U.; Odenwald, A.; Ostermann, T.; Weingard, L.; Ludwig, B.; Richter, O. M. *J Bioenerg Biomembr* **1998**, *30*, 89-97.
49. Pereira, M. M.; Santana, M.; Teixeira, M. *Biochim Biophys Acta* **2001**, *1505*, 185-208.
50. Koutsoukakis, C.; Soulimane, T.; Varotsis, C. *Biophys J* **2004**, *86*, 2438-44.
51. Gomes, C. M.; Backgren, C.; Teixeira, M.; Puustinen, A.; Verkhovskaya, M. L.; Wikstrom, M.; Verkhovsky, M. I. *FEBS Lett* **2001**, *497*, 159-64.
52. Lepp, H.; Brzezinski, P. *Biochim Biophys Acta* **2009**, *1790*, 552-7.
53. Capitanio, N.; Capitanio, G.; De Nitto, E.; Boffoli, D.; Papa, S. *Biochemistry* **2003**, *42*, 4607-12.
54. Raitio, M.; Wikstrom, M. *Biochimica Et Biophysica Acta-Bioenergetics* **1994**, *1186*, 100-106.
55. Kaila, V. R.; Verkhovsky, M. I.; Hummer, G.; Wikstrom, M. *Proc Natl Acad Sci U S A* **2008**, *105*, 6255-9.
56. Namslauer, A.; Aagaard, A.; Katsonouri, A.; Brzezinski, P. *Biochemistry* **2003**, *42*, 1488-98.
57. de Vries, S. *Biochim Biophys Acta* **2008**, *1777*, 925-8.
58. Busenlehner, L. S.; Branden, G.; Namslauer, I.; Brzezinski, P.; Armstrong, R. N. *Biochemistry* **2008**, *47*, 73-83.
59. Han, D.; Namslauer, A.; Pawate, A.; Morgan, J. E.; Nagy, S.; Vakkasoglu, A. S.; Brzezinski, P.; Gennis, R. B. *Biochemistry* **2006**, *45*, 14064-74.
60. Lee, H. J.; Ojemmy, L.; Vakkasoglu, A.; Brzezinski, P.; Gennis, R. B. *Biochemistry* **2009**, *48*, 7123-31.
61. Mitchell, D. M.; Adelroth, P.; Hosler, J. P.; Fetter, J. R.; Brzezinski, P.; Pressler, M. A.; Aasa, R.; Malmstrom, B. G.; Alben, J. O.; Babcock, G. T.; Gennis, R. B.; Ferguson-Miller, S. *Biochemistry* **1996**, *35*, 824-8.
62. Namslauer, I.; Brzezinski, P. *Proc Natl Acad Sci U S A* **2009**, *106*, 3402-7.
63. Olkhova, E.; Helms, V.; Michel, H. *Biophys J* **2005**, *89*, 2324-31.

64. Durr, K. L.; Koepke, J.; Hellwig, P.; Muller, H.; Angerer, H.; Peng, G.; Olkhova, E.; Richter, O. M.; Ludwig, B.; Michel, H. *J Mol Biol* **2008**, *384*, 865-77.
65. Namslauer, A.; Lepp, H.; Branden, M.; Jasaitis, A.; Verkhovsky, M. I.; Brzezinski, P. *J Biol Chem* **2007**, *282*, 15148-58.
66. Lepp, H.; Salomonsson, L.; Zhu, J. P.; Gennis, R. B.; Brzezinski, P. *Biochim Biophys Acta* **2008**, *1777*, 897-903.
67. Branden, G.; Pawate, A. S.; Gennis, R. B.; Brzezinski, P. *Proc Natl Acad Sci U S A* **2006**, *103*, 317-22.
68. Ribacka, C.; Verkhovsky, M. I.; Belevich, I.; Bloch, D. A.; Puustinen, A.; Wikstrom, M. *Biochemistry* **2005**, *44*, 16502-12.
69. Belevich, I.; Bloch, D. A.; Belevich, N.; Wikstrom, M.; Verkhovsky, M. I. *Proc Natl Acad Sci U S A* **2007**, *104*, 2685-90.
70. Proshlyakov, D. A.; Ogura, T.; Shinzawa-Itoh, K.; Yoshikawa, S.; Appelman, E. H.; Kitagawa, T. *J Biol Chem* **1994**, *269*, 29385-8.
71. Proshlyakov, D. A.; Pressler, M. A.; DeMaso, C.; Leykam, J. F.; DeWitt, D. L.; Babcock, G. T. *Science* **2000**, *290*, 1588-1591.
72. Hansson, O.; Karlsson, B.; Aasa, R.; Vanngard, T.; Malmstrom, B. G. *Embo J* **1982**, *1*, 1295-7.
73. Morgan, J. E.; Verkhovsky, M. I.; Palmer, G.; Wikstrom, M. *Biochemistry* **2001**, *40*, 6882-92.
74. Wikstrom, M. *Biochim Biophys Acta* **2000**, *1458*, 188-98.
75. Moody, A. J. *Biochim Biophys Acta* **1996**, *1276*, 6-20.
76. Verkhovsky, M. I.; Jasaitis, A.; Verkhovskaya, M. L.; Morgan, J. E.; Wikstrom, M. *Nature* **1999**, *400*, 480-483.
77. Powers, L.; Chance, B.; Ching, Y.; Angiolillo, P. *Biophys J* **1981**, *34*, 465-98.
78. Scott, R. A.; Schwartz, J. R.; Cramer, S. P. *Biochemistry* **1986**, *25*, 5546-55.
79. Koepke, J.; Olkhova, E.; Angerer, H.; Muller, H.; Peng, G.; Michel, H. *Biochim Biophys Acta* **2009**, *1787*, 635-45.
80. Szundi, I.; Van Eps, N.; Einarsdottir, O. *Biochemistry* **2003**, *42*, 5074-90.
81. Einarsdottir, O.; Szundi, I. *Biochim Biophys Acta* **2004**, *1655*, 263-73.
82. MacMillan, F.; Kannt, A.; Behr, J.; Prisner, T.; Michel, H. *Biochemistry* **1999**, *38*, 9179-84.
83. Budiman, K.; Kannt, A.; Lyubenova, S.; Richter, O. M.; Ludwig, B.; Michel, H.; MacMillan, F. *Biochemistry* **2004**, *43*, 11709-16.
84. Svistunenko, D. A.; Wilson, M. T.; Cooper, C. E. *Biochim Biophys Acta* **2004**, *1655*, 372-80.
85. Gorbikova, E. A.; Belevich, I.; Wikstrom, M.; Verkhovsky, M. I. *Proc Natl Acad Sci U S A* **2008**, *105*, 10733-7.
86. Collman, J. P.; Devaraj, N. K.; Decreau, R. A.; Yang, Y.; Yan, Y. L.; Ebina, W.; Eberspacher, T. A.; Chidsey, C. E. *Science* **2007**, *315*, 1565-8.
87. Ji, H.; Yeh, S. R.; Rousseau, D. L. *FEBS Lett* **2005**, *579*, 6361-4.
88. Blomberg, M. R.; Siegbahn, P. E.; Wikstrom, M. *Inorg Chem* **2003**, *42*, 5231-43.
89. Pereira, M. M.; Verkhovskaya, M. L.; Teixeira, M.; Verkhovsky, M. I. *Biochemistry* **2000**, *39*, 6336-40.
90. Alge, D.; Wastyn, M.; Mayer, C.; Jungwirth, C.; Zimmermann, U.; Zoder, R.; Fromwald, S.; Peschek, G. A. *IUBMB Life* **1999**, *48*, 187-97.
91. Kannt, A.; Soulimane, T.; Buse, G.; Becker, A.; Bamberg, E.; Michel, H. *FEBS Lett* **1998**, *434*, 17-22.
92. Toledo-Cuevas, M.; Barquera, B.; Gennis, R. B.; Wikstrom, M.; Garcia-Horsman, J. A. *Biochim Biophys Acta* **1998**, *1365*, 421-34.
93. Gleissner, M.; Kaiser, U.; Antonopoulos, E.; Schafer, G. *J Biol Chem* **1997**, *272*, 8417-26.

Figures and captions

Fig. 1: The active site of cytochrome *c* oxidase highlighting the conserved aromatic residues in Type A and Type B oxidases (with the exception of W164, which occurs only in Type A oxidases) and all four redox-active metal centers.

Fig. 2: Proton conducting pathways in the type A1 cytochrome *c* oxidase (cytochrome *aa*₃ from *P. denitrificans*). Residues contributing to the proton conducting pathways are shown in green. Cu_B and the di-copper center Cu_A are indicated in red, hemes *a* and *a*₃ in grey and the heme iron atoms in cyan.

a) D-pathway: protons taken up through this pathway are transferred to W272 (magenta) and released to the P-side via the Mn²⁺ ion, as in the **F_{W*}** to **O_H** transition (see below and ³⁹). Alternatively, the protons taken up through the D-pathway may be transferred to the binuclear center to bind to metallo-oxo/hydroxo reaction intermediates.

b) K-pathway: all protons that are taken up through this pathway are transferred to the binuclear center and play a role only in the reduction of oxygen to water, not in proton pumping.

Fig. 3: Schematic overview of the binuclear centre (heme *a*₃ – Cu_B) and nearby protonatable residues during the catalytic cycle of cytochrome *c* oxidase. Intermediate states are indicated by capital letters (**O_H**, **E**, etc.). H_i⁺: protons taken up from the proton conducting pathways, H_o⁺: protons released to the periplasmic space, e⁻: electrons destined for the binuclear site, YOH: tyrosine280, WH: tryptophan272. Cu_A and heme *a*, the electron donors to the binuclear site, and **R**, the artifactual four-electron fully reduced enzyme, are omitted from the drawing. **O** represents the enzyme as isolated; this form of the enzyme contains a peroxide residue bridging *a*₃ and Cu_B, and is not part of the catalytic cycle.³⁴

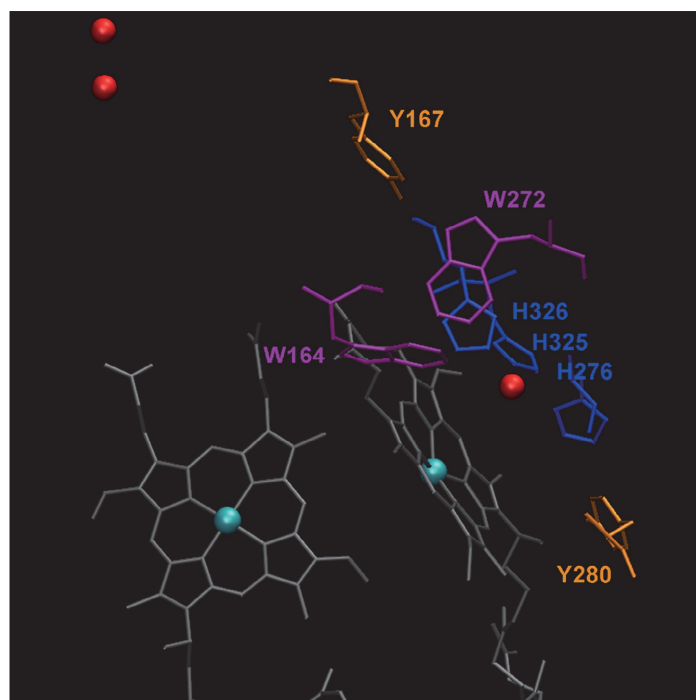


Fig. 1

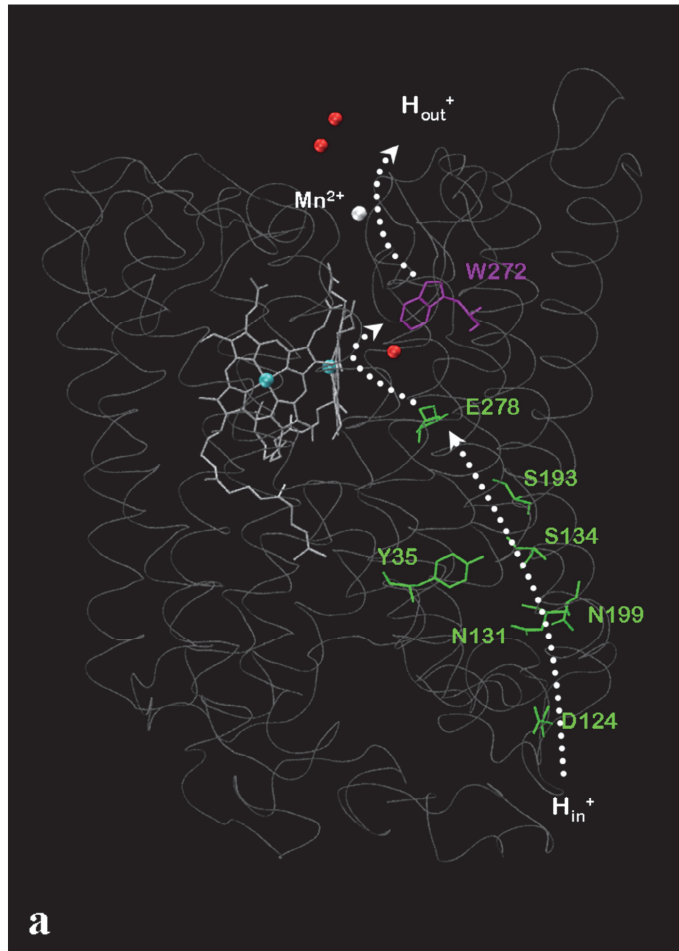


Fig. 2a

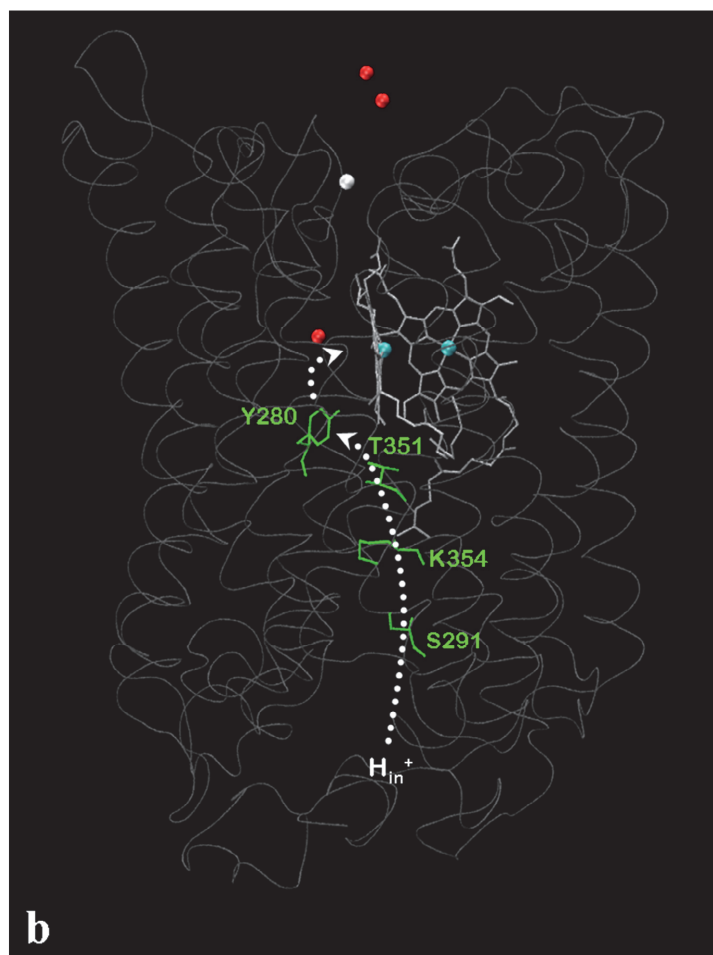


Fig. 2b

Table I:
Overview of the proton pumping stoichiometries determined for CcO's from various sources.

Species	CcO type	hemes	Pumping H ⁺ /e ⁻ ratio	Literature reference	Complex
<i>B. taurus</i> ^a	A	<i>aa</i> ₃	1.1	Solioz <i>et al.</i> 1982 ²⁶	<i>aa</i> ₃
<i>P. denitrificans</i> ^b	A	<i>aa</i> ₃	1.04	Dürr <i>et al.</i> 2008 ⁶⁴	<i>aa</i> ₃
<i>R. marinus</i> ^b	A	<i>caa</i> ₃	1	Pereira <i>et al.</i> 2000 ⁸⁹	<i>caa</i> ₃
<i>Synechocystis</i> <i>sp</i>					
<i>PCC6803</i> ^b	A	<i>aa</i> ₃	0.9	Alge <i>et al.</i> 1999 ⁹⁰	<i>aa</i> ₃
<i>T. thermophilus</i> ^b	B	<i>ba</i> ₃	0.4-0.5	Kannt <i>et al.</i> 1998 ⁹¹	<i>ba</i> ₃
<i>R. sphaeroides</i> ^b	C	<i>cbb</i> ₃	0.6-1.1	Toledo-Cuevas <i>et al.</i> 1998 ⁹²	<i>cbb</i> ₃
<i>S. acidocaldarius</i> ^c	A	<i>bb</i> ₃	3 ^d		SoxM
	B	<i>aa</i> ₃	1.2	Gleissner <i>et al.</i> 1997 ⁹³	SoxABC
<i>A. ambivalens</i> ^c	B	<i>aa</i> ₃	1	Gomes <i>et al.</i> 2001 ⁵¹	D
<i>P. oguniense</i> ^c	A	<i>aa</i> ₃	unknown		DoxBC
	B	<i>aa</i> ₃	unknown		PoxC
<i>A. permix</i> ^c	A	<i>aa</i> ₃	unknown		PoxI
	B	<i>ba</i> ₃	unknown		CO-2
					CO-1

a) Eukaryote

b) Bacterium

c) Archaeon

d) Sum of the H⁺/e⁻ ratios for the *bb*₃-type oxidase proton pump and for the electrogenic reaction of the *bc*₁-like complex

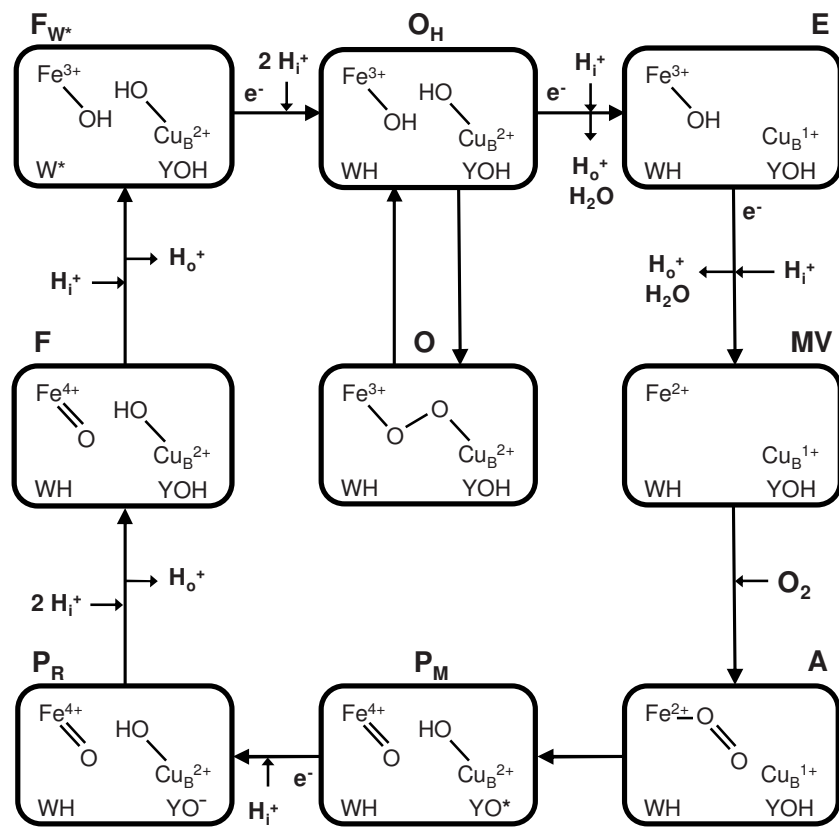


Fig. 3

Chapter III

Oxoferryl “P” intermediates of cytochrome aa_3 oxidase

Angela Paulus, Simon de Vries, Wilfred Hagen

Summary

The true P_M state of cytochrome *c* oxidase (CcO) is not easily captured, as it only transiently accumulates during the oxidation of the reduced molecule. There are different ways to trap cytochrome *c* oxidase in a P_M -like state, e.g. by exposing the enzyme to oxygen after it was incubated with CO or by using a mutant of CcO, in which the catalytic cycle cannot progress beyond this state. The intermediates observed in such experiments may differ from the true P_M intermediate that is part of the natural turnover of CcO. This chapter describes the accumulation of the true P_M intermediate and the comparison with the CO-induced P state. Even with the use of microsecond freeze-hyperquenching (MHQ) the accumulation of the P_M state proved very challenging. The comparison with the CO-induced P-state (P_{CO/O_2}) however clearly showed that the two compounds have very different kinetics and slightly different spectral features. It is concluded that the CO-incubated oxygen-reacted P_{CO/O_2} is not a valid model compound for the true P_M intermediate.

Introduction

During the reduction of oxygen, redox sites in cytochrome *c* oxidase (CcO) donate a total of four electrons to the O-O bond splitting reaction, one of which originates from an amino acid residue close enough to participate in the active site chemistry^{1,2}. The Y280 residue is conserved among several types of oxidases and it is located within H-bonding distance of the ligating O_2 , which makes it an excellent candidate for electron donation to O_2 reduction. The expected characteristic signal for a Y280 neutral radical was never observed however, perhaps due to a very short lifetime of the radical-containing intermediate, or due to spin-spin coupling rendering the radical EPR silent. The oxygen reduction by CcOs is believed to involve a number of transient intermediates, as depicted in figure 1, each described by the presence of a ligand in the active site, the reduction level of the redox-active groups and the presence or absence of an amino acid radical. In addition, the proton-loading site (PLS) may transiently hold (a) proton(s) in the course of the catalytic cycle. The PLS most likely consists of a cluster of residues that are under the strong influence of the heme a_3 propionic acids, with the ability to accept and release protons³. For the Type A CcOs, the F to O_H transition may be presented as a two-step process, kinetically defined by the formation and decay of a neutral amino acid radical tentatively assigned to W272⁴ (if not noted otherwise, the amino acid numbering refers to the cytochrome aa_3 oxidase from *P. denitrificans*).

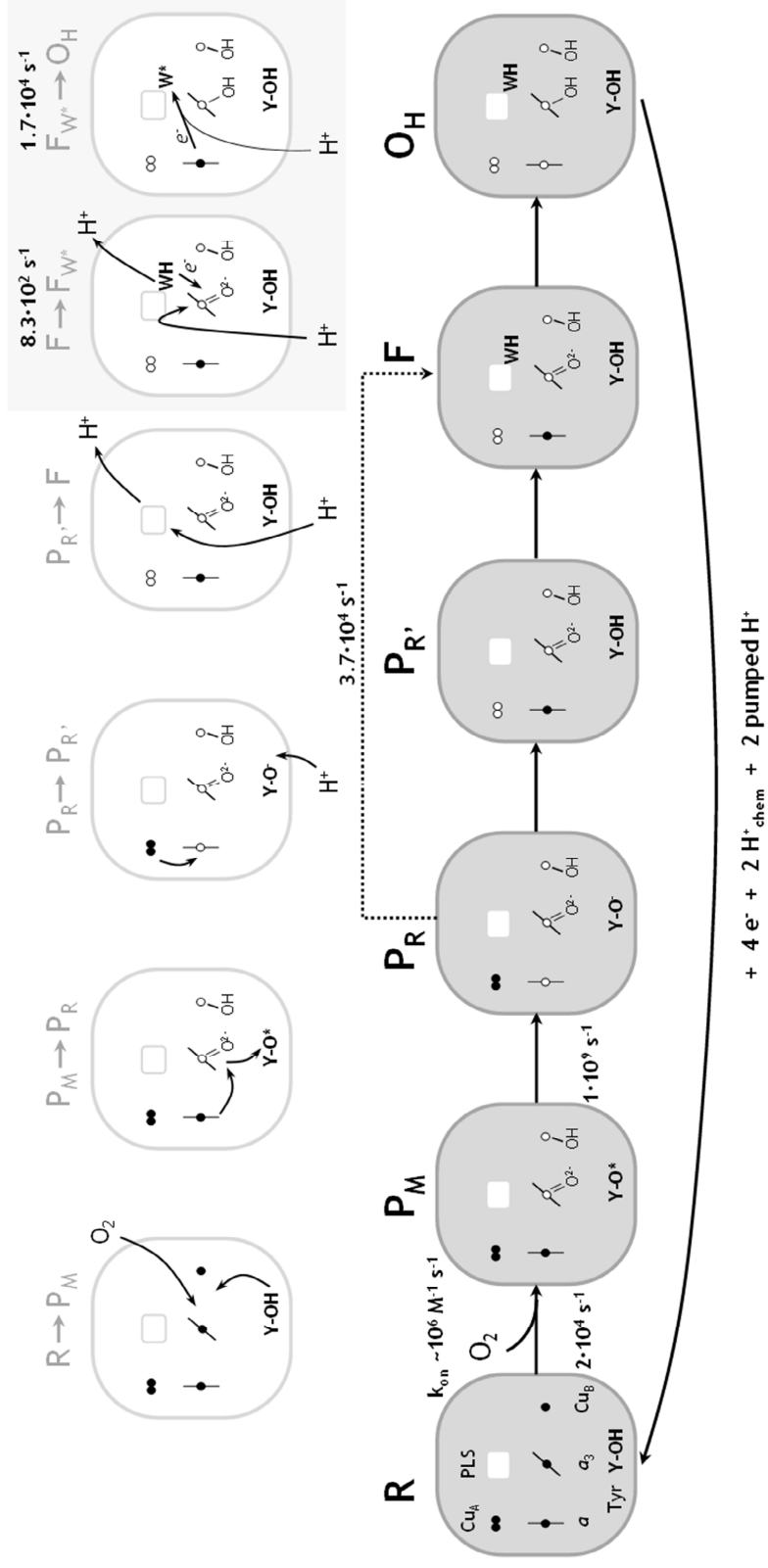


Figure 1 (adapted from A. Paulus 2015⁵): The catalytic cycle of cytochrome *aa*₃ oxidase. The grey boxes represent the different intermediates of the cycle. The white boxes display electron transfer, proton binding and release processes that occur between the different intermediates. The reaction constants (1/τ) indicated at the corresponding reaction steps came from kinetic modelling of experimental data. The Tyr* is reduced in P_M → P_R and presumably reprotonated in P_R'. Proton uptake and proton release events were not measured, but they are proposed to take place between P_R and O_H⁶. **Description:** When the four-electron reduced enzyme (R) is exposed to O₂, the high-spin heme *a*₃ binds oxygen and the O-O bond is split⁷ using the electrons from the active site heme *a*₃/Cu_B and an electron and a proton from Tyr280⁸ (R → P_M). The Tyr* radical is rapidly reduced (~ 1 ns) by the electron from heme *a* to form the P_R state. The first proton uptake event (for reprotonation of YO[•]) correlates with electron transfer from Cu_A to heme *a* (P_R → P_R'). A second proton is then taken up from the negative side of the membrane to form the F state of the enzyme. The oxidative phase of the cycle of cytochrome *aa*₃ oxidase involves a transient Trp radical (W272*). The F to O_H transition of cytochrome *aa*₃ oxidase is therefore depicted as two sequential transitions, F to F_{W*} and F_{W*} to O_H^{4,9,10}. In F to F_{W*} a proton is released from the Trp and an electron is donated to the heme *a*₃, creating the Trp radical. The curved arrow designates the proton involved in the reduction of the oxo-ferryl heme *a*₃ to the ferric hydroxyl state and may involve residue E278⁹ and/or the so-called proton loading site (PLS). The electron residing at the heme *a*₃ together with a second proton taken up in this step convert the W272* back to the protonated Trp as the oxidized enzyme (O_H) is formed again.

The cytochrome *aa*₃ oxidase from *P. denitrificans* is known to form several oxoferryl intermediates during the reaction with oxygen (P_M, P_R, F, F_{W*}), each with different spectral characteristics that arise in part from the presence or absence of a neutral or reduced radical in the vicinity of the active site^{4,11}. Although P_M and P_R are named after the redox state of the enzyme at the moment of O₂ binding (Mixed valence vs. fully Reduced), we believe both are formed (transiently) during every turnover, regardless of the amount of electrons present when O₂ binds. Artificial oxoferryl states of the enzyme, with or without radicals, can be generated through reaction with CO and O₂ (P_{CO/O2}) or with H₂O₂ (P_H; Y167 in *P. denitrificans*^{2,12,13} or Y129/Y244 in *B. taurus*^{13,14}), but these may not play a role in the natural catalytic cycle of CcO.

This chapter describes our efforts to obtain a radical fingerprint for the naturally occurring P_M state of CcO, which is the first state after the O-O bond has been broken (see Figure 2).

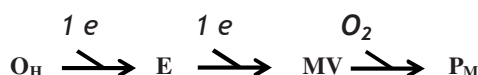


Figure 2: Part of the catalytic cycle of cytochrome *aa*₃ oxidase, from the oxidized enzyme (O_H) to the P_M intermediate. E: the one-electron reduced intermediate of CcO; MV: the two-electron reduced intermediate of CcO.

Our approach has involved the combination of hyperfast freeze-quenching and (stopped-flow) UV-vis and EPR spectroscopic analysis. A comparison between P_M and the CO-generated P state of CcO is made to assess the validity of using P_{CO/O2} as a model compound for P_M.

Materials and methods

Single mixing stopped-flow (SF) spectroscopy (CcO vs. cyt *c*)

Purified Mn²⁺-depleted cytochrome *aa*₃ oxidase from *P. denitrificans*¹⁵ was diluted in 20 mM HEPES buffer (0.05% dodecyl-β-D-maltoside (LM), pH 7.2 or 8.0) and mixed in an (anaerobic) stopped-flow setup with horse heart cytochrome *c* (hcc) or yeast cytochrome *c* (ycc). Before injection into the stopped-flow setup the cytochrome *c* solutions were reduced

with ascorbate (asc). The CcO was activated by reduction with asc/PES (phenazine ethosulfate) and oxidation by exposure to the air to yield the pulsed state¹⁶. The ascorbate was used in a small excess, or the enzyme solutions were run over a PD10 desalting column shortly before the experiment. The enzyme concentrations were calculated from the optical absorbance with $\epsilon_{550} = 29.5 \text{ mM}^{-1}\text{cm}^{-1}$ for reduced cytochrome *c* and $\epsilon_{\text{Soret}} = 158 \text{ mM}^{-1}\text{cm}^{-1}$ for oxidized cytochrome *aa*₃ oxidase. The experiments were performed at 10 °C.

Sequential mixing stopped-flow (SF) spectroscopy (CcO vs. cyt *c*)

Purified Mn²⁺-depleted cytochrome *aa*₃ oxidase from *P. denitrificans*¹⁵ was diluted in 20 mM HEPES buffer (0.05% dodecyl- β -D-maltoside (LM), pH 8.0). The pulsed cytochrome *aa*₃¹⁶ oxidase was mixed with ascorbate-reduced hcc or ycc in a sequential mixing stopped-flow setup. All enzyme solutions were eluted over a PD10 column to remove excess reductant prior to injection into the SF system. The experiments were performed at 10 °C. In the first mixing step the cytochrome *aa*₃ and cytochrome *c* were mixed in a ~1:1 ratio at low ionic strength (5-20 mM). After a predetermined delay of max 100 ms the second mixing took place at the optimal ionic strength for CcO turnover. The two-electron reduced MV CcO rapidly reacted with O₂ present in the reaction medium to form P_M.

Microsecond freeze-hyperquenching (MHQ)

The single and sequential mixing cytochrome *c* stopped-flow experiments were repeated in the MHQ setup (using a cold plate to quench the reactions¹⁰) at higher protein concentrations. The experiments were performed at 9±2 °C. In the sequential mixing experiments the ionic strengths of the buffers were further optimized for our purpose (to be 56 mM after the second mix). The delay between mixes, that was readily adjustable in the SF apparatus, is related to the nozzle type and flow rate in MHQ experiments. The delay was varied between 40 and 280 ms.

Electron Paramagnetic Resonance (EPR) spectroscopy

The MHQ frozen powder was packed into an EPR tube with a filter at the bottom as described¹⁰. The tubes were kept in liquid nitrogen during and after packing. EPR spectroscopy was performed on a Bruker EC106 and samples were cooled by a home-built He-flow system¹⁷.

Generation of P_{CO/O2} (single mixing stopped-flow spectroscopy)

Purified resting Mn²⁺-depleted cytochrome *aa*₃ oxidase from *P. denitrificans*¹⁵ was diluted in 100 mM HEPES buffer (0.05% LM) at neutral pH (7.2) in an infusion bottle. The solution was degassed and subsequently exposed to a flow of carbon monoxide (CO) for 10 minutes. The enzyme solution was incubated overnight at room temperature and 1 atm CO. After the incubation the CcO/CO vial was decapped inside an anaerobic chamber to allow the excess CO to escape from the solution. The CO-bound CcO was rapidly mixed in the stopped-flow setup vs. oxygen-saturated buffer at 10 °C, yielding P_{CO/O2}. The surroundings of the inlets of the SF system were flushed continuously with high quality argon gas (Ar 6.5) and the syringes were flushed with anaerobic buffer directly before the injection of the cytochrome *aa*₃ oxidase.

Results

The reaction was studied under *in vivo*-like conditions (using cyt *c* as the electron donor and activated/pulsed cytochrome *c* oxidase as the primary electron acceptor) to minimize the observation of artefacts not relevant to the natural mechanism of CcO. In order to effectively accumulate P_M , the two-electron reduced ‘mixed valence’ state (MV) must be reacted with an excess of O_2 . Simply mixing the CcO with cyt *c* in a 1:2 ratio was expected to result in a mixture of states, in which P_M may not even be prominent. It was therefore decided to accumulate MV with cyt *c* through sequential mixing, optimizing the enzyme concentrations in both mixes and the delay time in between the mixes for the highest yield of 2-electron reduced CcO directly after the second mix. The one- and two-electron reduction of CcO were first characterized in a stopped-flow apparatus, using a single mixing and a sequential mixing setup, before reproducing the reaction in our MHQ setup.

One-electron reduced state “E” (single mixing SF)

We have used both horse heart cyt *c* and yeast cyt *c* (figure 3) for the accumulation of E. In oxygen consumption measurements the yeast cyt *c* was shown to have a lower off-rate than the horse heart cyt *c*, which suits the goal of producing 1-electron reduced CcO. The experiments were performed at pH 7.2 (the *in vivo* pH of the environment of *P. denitrificans* CcO) and pH 8.0 (at which the intermediate P states of CcO are more stable and accumulate to higher concentrations^{12,18}).

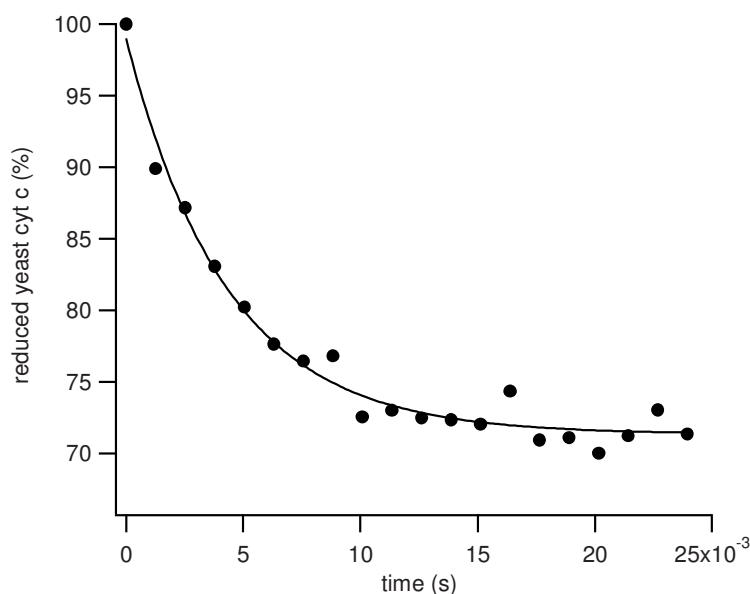


Figure 3: Oxidation of yeast cytochrome *c* by *P. denitrificans* cytochrome *aa*₃ oxidase in a stopped-flow apparatus at 10 °C and pH 8, $I = 40$ mM. k_{obs} of fit = 230 s^{-1} .

The oxidation of yeast cyt *c* fits a single exponential (figure 3). The reaction apparently reaches equilibrium after 20 ms, while there is still reduced cyt *c* left. This is explained by the slow off-rate of yeast cyt *c* on the binding site. It is assumed that all molecules of CcO have

bound a molecule of cyt *c* after 20 ms which remains transiently attached, and this is the best moment for the introduction of the second equivalent of cyt *c* (i.e. the second mix).

When the formation of E is monitored as an increase of absorbance at 608 nm, a curve such as the one in figure 4 displays the window of opportunity for the second mix (after formation and before significant decay of E). These data were fit with the oxidation rate of cyt *c* and reveal a relatively stable E state. No decay of the absorbance at 608 nm was detected during the 0.126 s time course of the experiment. It was therefore decided that the second mix should take place between 20 and 200 ms after the first mix. Given the observed stability of E and the ~1:1 ratio of cyt *c* oxidized : CcO reduced we can assume that the accumulation of E approximates 100%. The extinction coefficient for the E state minus the pulsed oxidized enzyme at 608 nm in the stopped-flow difference spectra is $8.0 \text{ mM}^{-1}\text{cm}^{-1}$.

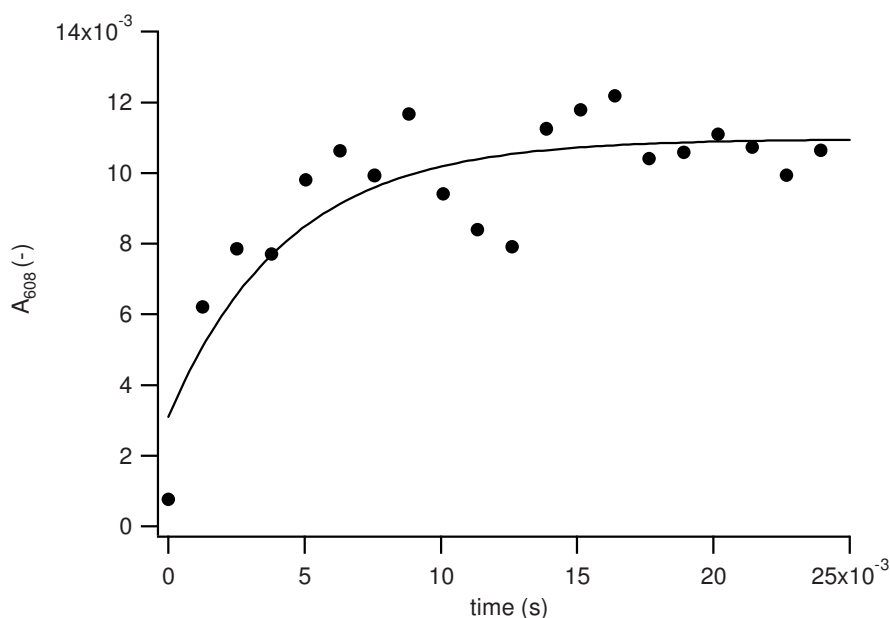


Figure 4: increase in absorbance at 608 nm by *P.denitrificans* cytochrome *aa*₃ oxidase due to reduction by yeast cyt *c* in a stopped-flow apparatus at 10 °C and pH 8, I = 40 mM. k_{obs} of fit = 230 s^{-1} .

Two-electron reduced O₂-reacted state “P_M” (sequential mixing SF)

As the stopped-flow apparatus was never absolutely anaerobic, the formation of MV could only be observed indirectly, through the formation of P_M and P_R. Oxygenated solutions were used at all times in the second mix to ensure that the oxygen concentration was not rate-limiting for the formation of P_M from E. The first mix was the (one-electron) reduction of CcO by reduced yeast cyt *c* (YCC) or horse heart cyt *c* (HCC), while the second mix was always with horse heart cyt *c*. Ionic strengths of the solutions were varied to optimize the binding and release rates of the two types of cyt *c*. The ionic strength of the reaction mixture after the second mix was optimal for exchange of cyt *c* (I~100 mM).

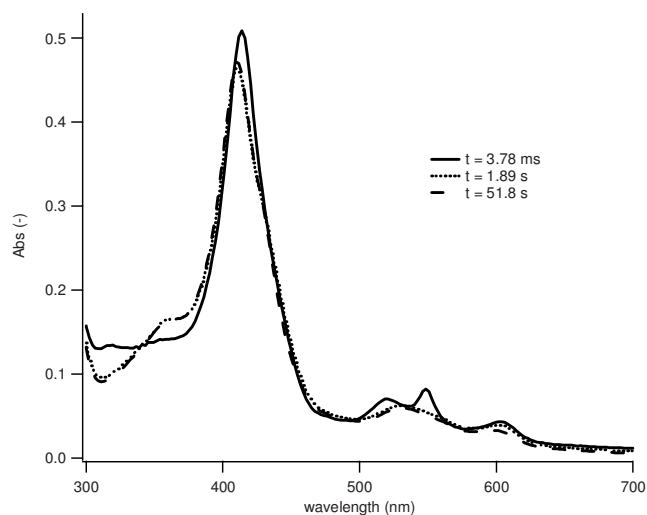


Figure 5: Oxidation of reduced horse heart cyt *c* by (yeast *c* – bound) CcO (550 nm) and formation of the P intermediate of CcO (610 nm) in a sequential mixing stopped-flow apparatus at 10 °C and pH 8, I = 100 mM. The first mix with yeast cyt *c* at low ionic strength, followed by a delay of 125 ms, precedes the data acquisition. Data was collected with a split time base: 500 measurements in 1.89 s, followed by 50 measurements in 50 s. Samples were mixed in a molar (2:2):1 ratio and a volumetric (1:1):2 ratio, resulting in a final 1:2 ratio of CcO : cyt *c*.

The yield of P was monitored through the absorbance at 610 nm (figures 5, 6). The spectral data show that indeed only the oxidation of the second equivalent of cyt *c* is detected in the stopped-flow spectrophotometer. The yeast cyt *c* from the first mix was oxidized within the delay time of 125 ms.

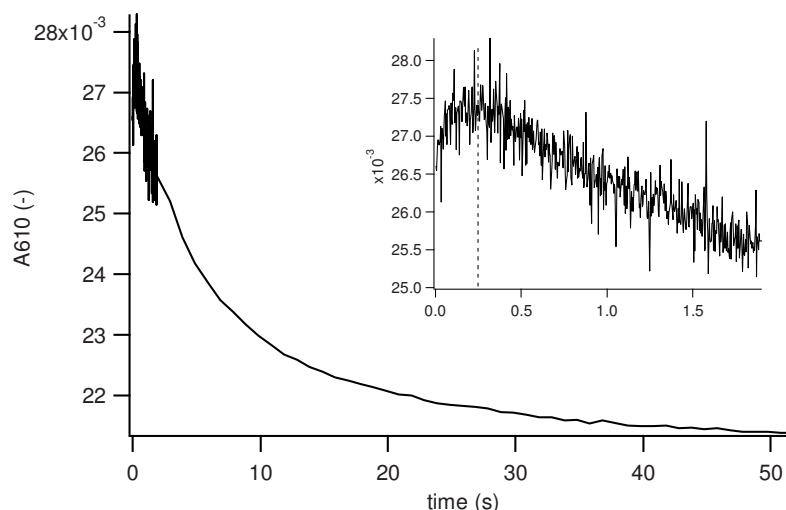


Figure 6: Formation of the P intermediate of CcO (610 nm) in a sequential mixing stopped-flow apparatus at 10 °C and pH 8, I = 100 mM. The first mix with yeast cyt *c* at low ionic strength, followed by a delay of

125 ms, precedes the data acquisition. Samples were mixed in a molar (2:2):1 ratio and a volumetric (1:1):2 ratio, resulting in a final 1:2 ratio of CcO : cyt *c*.

Both the formation and decay of P were faster when the concentration of reduced cyt *c* in the second mix was higher. The highest P yield was at ~250 ms after the second mix when the cyt *c* was added to the CcO in a 1:1 ratio (figure 6), or at 32 ms after the second mix when the cyt *c* was added at 20x that concentration. The apparent rate of formation of the 610 nm species exceeds the rate of its decay by >50 times (22 s^{-1} vs. $\sim 0.4\text{ s}^{-1}$). The oxidation of the second equivalent of cyt *c* progresses exponentially at 3.4 s^{-1} across the formation and decay of P_M . It appears that the second cyt *c* equivalent is oxidized almost 70 times slower than the first equivalent ($\tau \sim 290\text{ ms}$ and 4.3 ms , respectively). There was no difference between the maximum population of P_M after mixing YCC/CcO vs. HCC compared to mixing HCC/CcO vs. HCC.

The optical spectrum of P_M was constructed by subtracting the spectral contributions of reduced and oxidized cyt *c* from the total spectral data (figure 7). The spectrum of P_M thus obtained may also contain (smaller) populations of other states of CcO, such as the pulsed oxidized state which is spectrally similar to P_M . If the accumulation of P_M is assumed to be 100%, the extinction coefficient of the $1.4\text{ }\mu\text{M}$ of P_M in this reaction can be calculated ($\epsilon_{604} \sim 21\text{ mM}^{-1}\text{cm}^{-1}$).

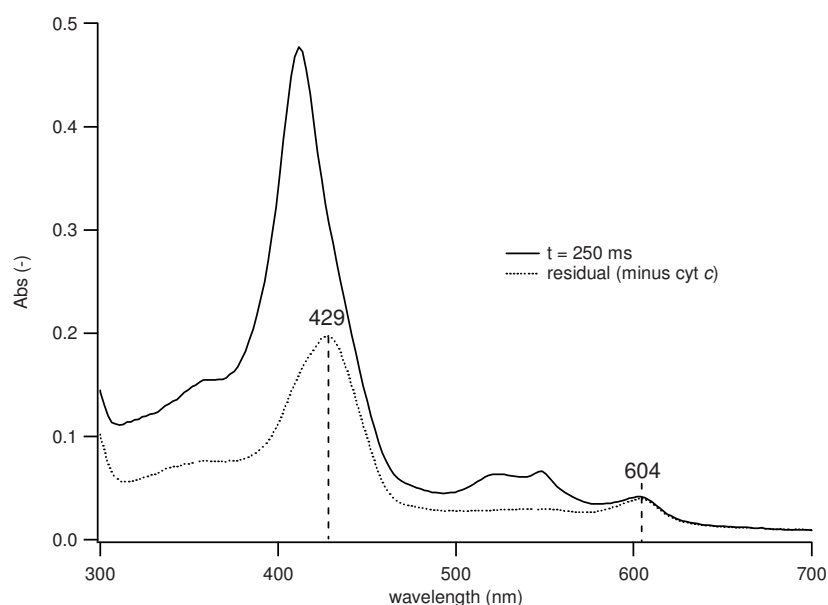


Figure 7: Raw (-) and residual (···) spectra after subtraction of the spectral contributions of cyt *c*. Time point 250 ms is at the moment of highest yield of P_M in the reaction.

Two-electron reduced O_2 -reacted state " P_M " (single mixing SF)

The formation of P_M in a single mixing reaction was performed for the purpose of comparison to the sequential mixing results. In the case of a single mix between CcO and reduced horse

heart cyt *c* the maximum P_M yield was observed in ~ 30 ms and the formation and decay of the absorbance at 608 nm for P_M (figure 8) fitted the rates determined in the sequential mixing experiments (150 s^{-1} and 1.5 s^{-1} , respectively). By simulation it was calculated that with fast O_2 -binding ($\sim 15\text{ }\mu\text{s}$) and the experimentally observed rates for formation and decay of P_M , the accumulation of P_M could be up to 95%.

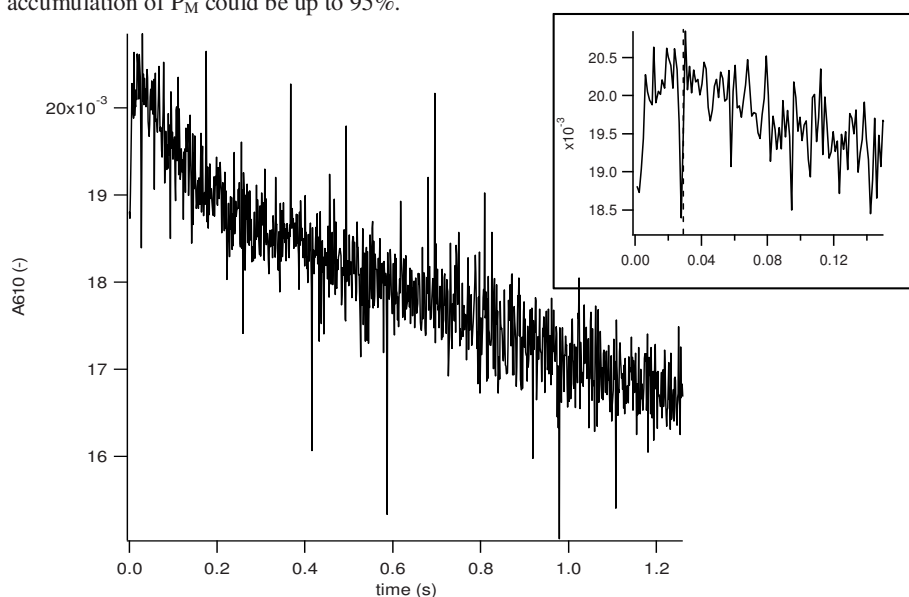


Figure 8: Formation of the P intermediate of CcO (608 nm) in a single mixing stopped-flow apparatus at $10\text{ }^{\circ}\text{C}$ and $\text{pH } 8$, $I = 56\text{ mM}$. Pulsed CcO was mixed *vs.* reduced horse heart cyt *c* in a molar 1:2 ratio.

The sequential mixing did not result in a higher yield of P_M than was achieved in the single mixing experiment, which is perhaps not very surprising in retrospect. It was observed in the sequential mixing experiment that the second equivalent of cyt *c* was oxidized $\sim 70\times$ slower than the first equivalent, indicating that the second electron transfer to CcO is rate-limiting for the formation of the mixed valence state. Therefore, splitting up the reaction in two one-electron steps does not help to obtain a higher yield of MV , and subsequently P_M .

MHQ with CcO /cyt *c* (single mixing, “E”)

Pulsed cytochrome *c* oxidase was mixed *vs.* reduced horse heart cyt *c* 1:1 to form the E state of the enzyme. The frozen powder samples were analysed with low temperature UVvis spectroscopy (figure 9). Note that the spectral characteristics of enzyme samples are often shifted by a few nanometers in low-temperature measurements.

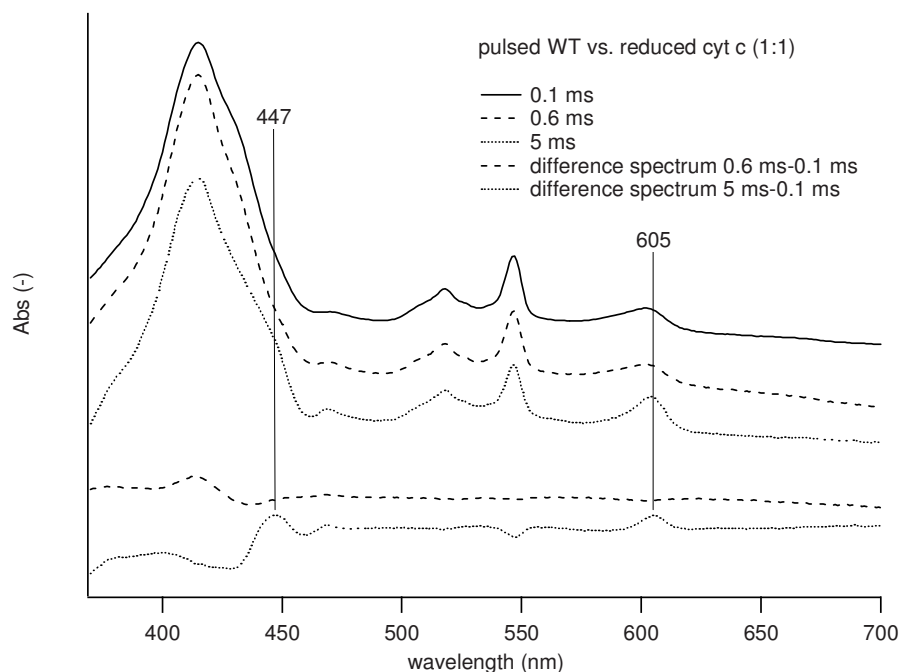


Figure 9: Spectra of the frozen powder samples collected after 0.1, 0.5 and 6 ms reaction time, as well as the difference spectra depicting the spectral changes due to the reaction between the three time points.

The raw spectra were normalized for differences in absolute enzyme concentration based on the intensity of the spectral features of *cyt c* in the spectra combined with the rate of *cyt c* oxidation that was determined in the SF experiments ($\sim 230 \text{ s}^{-1}$). The spectra after 100 and 600 μs are very similar, but the 5 ms spectrum shows a much more intense alpha band that has red-shifted slightly. The increase of the 605 nm absorbance coincides with an increasing Soret absorbance around 447 nm, as is clear from the difference spectrum. These spectral developments suggest that the first electron that is taken up is transferred no further than heme a ¹⁹.

MHQ with CcO/*cyt c* (sequential mixing, “P_M”)

Since it did not matter for the maximum population of P_M which *cyt c* was used, it was preferred to use only horse heart *cyt c*, in excess in the second mix, for sequential mixing MHQ experiments. The use of just one type of *cyt c* shortened the sample preparation time and facilitated multicomponent analysis of the spectral data.

Pulsed CcO was mixed vs. reduced horse heart *cyt c* in a molar (2:2):1 ratio. Apart from the incomplete oxidation of the *cyt c*, the sequential samples did not show significant changes in the spectra between 0.4 and 6 ms (figure 10). The only change in the alpha region absorbance of CcO was an increase in the absorbance around 606 nm, but the amplitude was barely above the noise level.

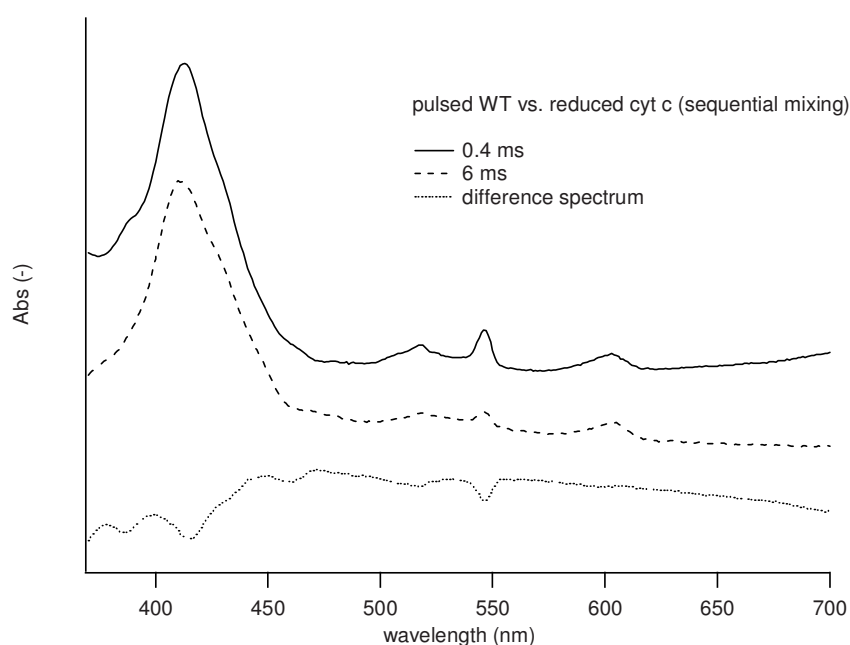


Figure 10: Spectra of the frozen powder samples collected after 0.4 and 6 ms reaction time, as well as the difference spectrum depicting the spectral changes due to the reaction between the two time points.

The formation of oxoferryl CcO (P, F) from pulsed CcO and reduced cyt *c* was clearly slow compared to the reaction of FR CcO with oxygen⁴. Although studying reaction times in the ms range is possible with the MHQ technique, the practical consequence is a much lower time resolution of consecutive data points (samples) in a series. In addition, the sequential volumetric 1:1 mixing diluted the enzyme samples four times in total, and the EPR spectra of the reacted samples were too weak to detect the radical in P_M. Further concentration of the starting material was not possible due to severe increase in viscosity and, as a consequence, incomplete mixing in the MHQ setup. Adjustment of the volumetric ratio of enzyme vs. substrate also resulted in insufficient mixing and retarded kinetics of cyt *c* oxidation (data not shown). The sequential mixing MHQ was found unsuitable for the study of a transient radical signal in CcO and work continued with the regular single-mixing MHQ setup.

MHQ with CcO/cyt *c* (single mixing, “P_M”)

For the single mixing MHQ experiments a 1:‘many’ molar ratio of CcO to cyt *c*, mixed in equal volumes, was used. A maximum P_M population of >90% of all CcO molecules was expected based on the stopped-flow experiments, assuming that the slightly different reaction conditions (e.g. the absolute enzyme concentration) did not have a significant effect on the reaction kinetics.

The samples showed changes in the spectrum of CcO across the first 5 ms, although the Soret peak was obscured by the contribution of cyt *c*. In addition, the Soret band was too intense to

assume linearity with the protein concentration. The difference spectrum, representing the spectral changes between 0.1 and 5 ms, shows a distinct increase in the absorbance at 605 nm (figure 11, inset), similar to the experiment with a 1:1 ratio of CcO to cyt *c*. This helps understand the finding that hardly anything changed in the CcO spectrum between 0.4 and 6 ms in the sequential samples. In those experiments, the uptake of the first electron had already taken place (for the larger part) in the dead time between mixes, before the addition of the second equivalent of reduced cyt *c*. The spectra therefore only show spectral changes as a result of uptake of a second electron. Apparently, these changes are very small.

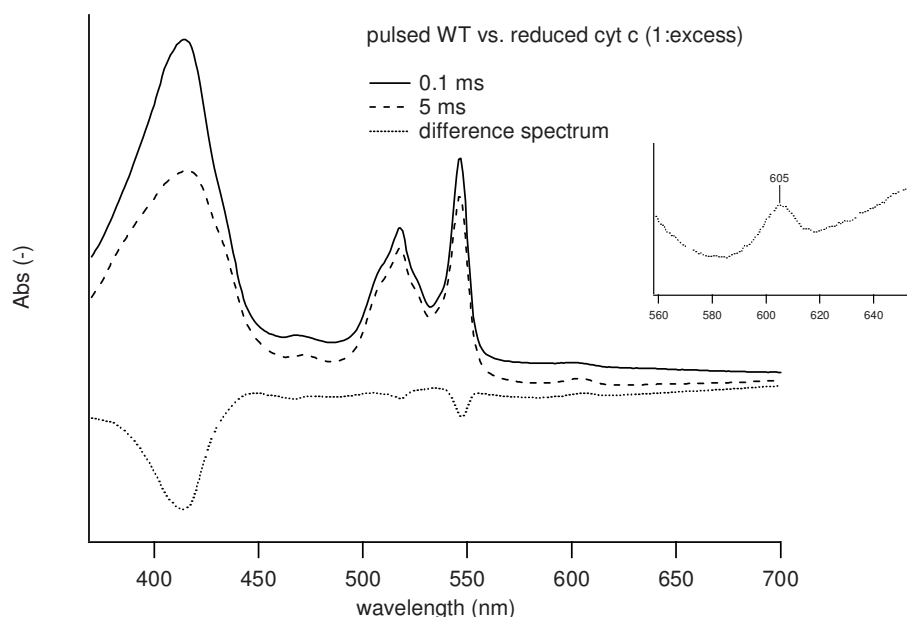


Figure 11: Spectra of the frozen powder samples collected after 0.1 and 5 ms reaction time, as well as the difference spectrum depicting the spectral changes due to the reaction between the two time points. **Inset:** alpha region of the difference spectrum

MHQ with ascorbate-reduced CcO (single mixing, “P_M”)

In addition to the experiments with cyt *c*, the kinetics of the CcO were studied by mixing the fully reduced (FR) state of the enzyme vs. O₂-saturated buffer, focusing on the formation and decay of P_M during the full turnover of the enzyme. The oxidation reaction of the fully reduced CcO with oxygen was sampled at 130 and 400 μ s (figure 12). The oxidation of the hemes is clear from the Soret changes (decrease at 446 nm and increase at 427 nm). A shoulder in the alpha band appears to lose intensity at 602 nm. This is quite unexpected, since absorbances below 604 nm are generally ascribed to more oxidized species of CcO.

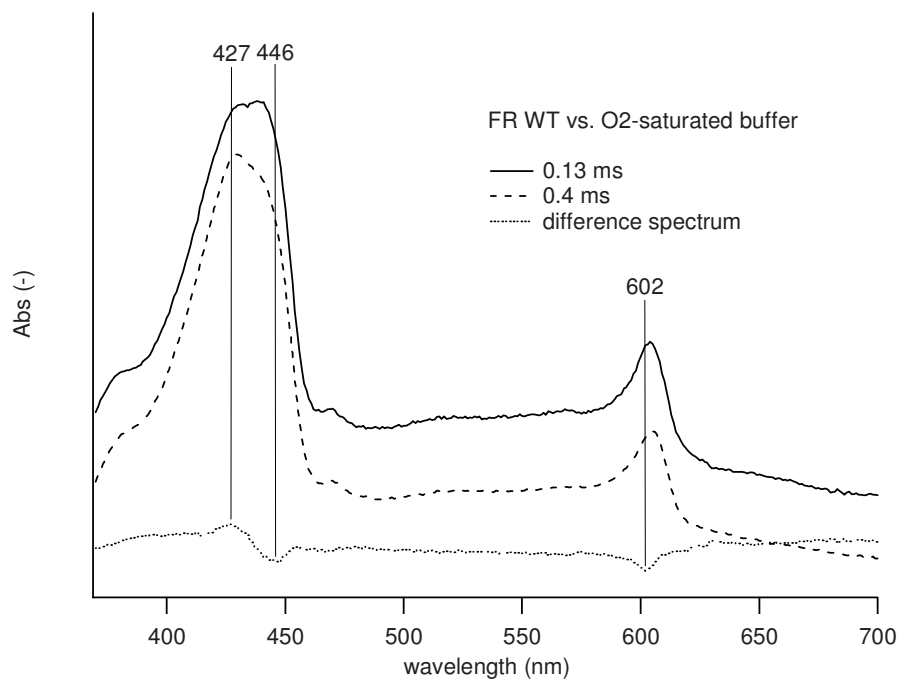


Figure 12: Spectra of the fully reduced CcO after reaction with O₂ for 130 μ s or 400 μ s, as well as the difference spectrum depicting the spectral changes due to the reaction between the two time points.

EPR spectroscopy

The reaction samples from MHQ were analyzed with EPR spectroscopy. The UV vis spectra of the samples with two equivalents of reduced cyt *c* (sample ageing times 0.4 and 6 ms) resembled that of a fully reduced oxygen-reacted sample that included a radical signal (tentatively assigned to W272⁴) (see 6 ms spectrum in figure 13, upper trace). The similarity suggests that it is the same radical species in both the P_M and the F_{W*} state that was detected, even though the line at $g=2.018$ seems much broader in the P_M sample. It is possible that the spectrum contains a contribution from a (broad) tyrosine radical on top of the signal observed in F_{W*}.

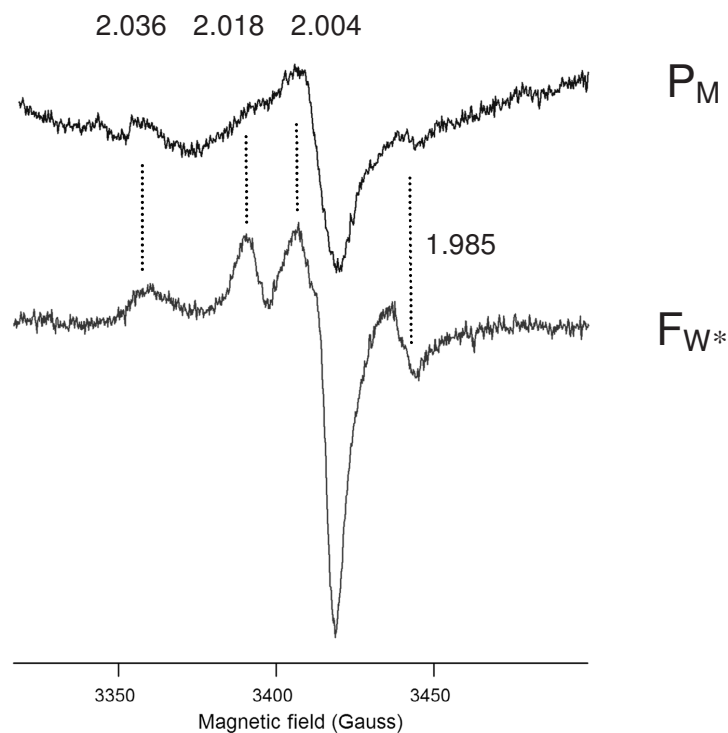


Figure 13: The vertical lines align the peaks of the W272* of F_W^* with that of the radical obtained in the P_M state. The curved baseline of the upper spectrum is due to a contribution of oxidized Cu_A .

P_{CO/O_2}

The validity of the assumption that P_M and P_{CO/O_2} (formed after oxidation of the CO-incubated reduced CcO) are the same species was investigated by assessing the stability of both forms in the stopped-flow setup. The decay rate of P_M was $\sim 1.5 \text{ s}^{-1}$, with a 100x higher rate of formation, as discussed above. The P_{CO/O_2} , however, displayed a much lower rate of decay and therefore a much higher stability than P_M in the stopped-flow cuvette (figure 14). In addition, the alpha band absorbance of the CO/O_2 -induced P state was red-shifted by a few nm, to 612 nm (figure 15).

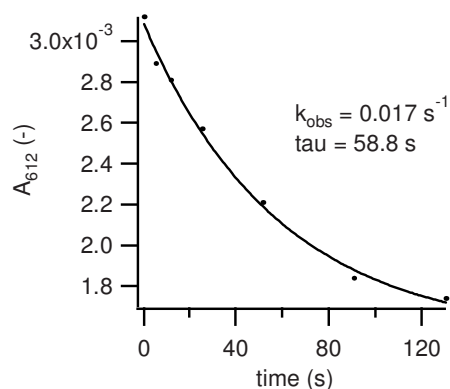


Figure 14: Decay of the P_{CO/O_2} form of CcO (612 nm) in a single mixing stopped-flow apparatus. CO-incubated CcO was mixed vs. oxygen-saturated buffer.

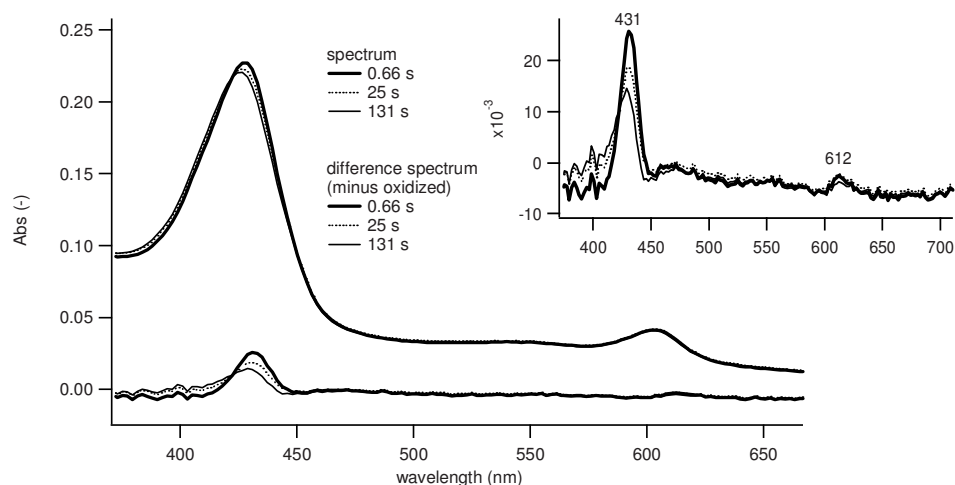


Figure 15: Spectral developments after mixing CO-incubated CcO vs. oxygen-saturated buffer. Main graph: optical and difference-to-oxidized spectra; insert: enlarged difference-to-oxidized spectra.

Discussion

Altogether, the optical spectra of the oxygen-reacted cyt *c*-reduced CcO samples have little to reveal. The minor developments in the optical spectrum, particularly in the alpha region, were not well resolved in these UV-vis data. It was observed, however, that the uptake of the first electron by CcO brings about a much larger change in the spectrum than uptake of consecutive electrons.

Of all the data with cyt *c*, the spectra that most resemble the data collected with FR CcO are the experiments with an excess of cyt *c*, where the rate of electron donation by cyt *c* is least

limiting. The alpha band resides at 604 nm in both cases, whereas the alpha bands of the 1:1 and sequential mixing samples are at 602 and 603 nm, respectively. The more reducing equivalents are readily available (either in or around the oxidase), the more reduced the CcO will be 5 ms into the reaction. With the limited amount of spectral data available for this reaction, and given the inaccuracy caused by small differences in reaction temperature and deviations of the concentrations of the protein samples used, it is not possible to calculate reliable rates for cyt *c* oxidation and stepwise oxygen reduction from the data presented here. However, the oxidation rate of cyt *c* in the MHQ does seem consistent with that in SF, since the spectra in figure 9 were successfully normalized using the rate value from the corresponding SF experiment.

Judging from the UVvis data described above, the P_M and P_{CO/O_2} may not be very similar at all. Both the spectrum of P_{CO/O_2} itself and its kinetic properties do not match the characteristics of the P state that was obtained in the kinetic experiments with cyt *c*- or ascorbate-reduced CcO, neither was an intermediate with these spectral characteristics (alpha band at 612 nm) observed at any point in the reaction in the kinetic range that was studied, both in the SF and in the MHQ experiments. Insights and conclusions from experiments using the P_{CO/O_2} state of CcO should be viewed in that light and are not necessarily applicable to the kinetically relevant P_M intermediate.

Conclusions

In the stopped-flow experiments with the P intermediate of the reaction of MV-CO with oxygen it was observed that P_{CO/O_2} differs from P_M both in optical spectrum and in stability. P_{CO/O_2} must therefore be structurally different from the naturally occurring P intermediates and it is not a valid model compound for P_M . We found that P_M hardly accumulated, in spite of our efforts to manage the reduction of CcO by cyt *c*, indicating that the transition to P_R is very rapid (probably ~1 ns). P_R is spectrally very similar to P_M , but it does not harbour the supposed amino acid radical. P_R dominated the kinetic optical analysis due to its much longer lifetime (slower decay) compared to P_M . As a consequence of the poor accumulation of P_M in these experiments, no support was found in the EPR data that a radical was transiently formed during turnover. *In vivo*-like studies of enzyme kinetics can be as elegant as they are relevant, yet they are limited by the intrinsic kinetic properties of the enzyme. A different approach is required (*e.g.* using altered variants of the enzyme, or through molecular dynamic simulations) for effective trapping of CcO in the P_M state and further characterization of the amino acid radical.

References

1. Proshlyakov, DA, Pressler, MA & Babcock, GT 1998, 'Dioxygen activation and bond cleavage by mixed-valence cytochrome c oxidase', *Proceedings of the National Academy of Sciences of the United States of America*, vol. 95, pp. 8020-8025.
2. MacMillan, F, Kannt, A, Behr, J, Prisner, T & Michel, H 1999, 'Direct evidence for a tyrosine radical in the reaction of cytochrome c oxidase with hydrogen peroxide', *Biochemistry*, vol. 38, pp. 9179-9184.
3. Lu, J & Gunner, MR 2014, 'Characterizing the proton loading site in cytochrome c oxidase', *Proceedings of the National Academy of Sciences of the United States of America*, vol. 111, pp. 12414-12419. doi: 10.1073/pnas.1407187111
4. Wiertz, FG, Richter, OM, Ludwig, B & de Vries, S 2007, 'Kinetic resolution of a tryptophan-radical intermediate in the reaction cycle of *Paracoccus denitrificans* cytochrome c oxidase', *Journal of Biological Chemistry*, vol. 282, pp. 31580-31591. doi: 10.1074/jbc.M705520200
5. Paulus, A, Werner, C, Ludwig, B & de Vries, S 2015, 'The cytochrome ba₃ oxidase from *Thermus thermophilus* does not generate a tryptophan radical during turnover: Implications for the mechanism of proton pumping', *Biochimica et Biophysica Acta*, vol. 1847, pp. 1093-1100. doi: 10.1016/j.bbabo.2015.05.013
6. Von Ballmoos, C, Ädelroth, P, Gennis, RB & Brzezinski, P 2012, 'Proton transfer in ba₃ cytochrome c oxidase from *Thermus thermophilus*', *Biochimica et Biophysica Acta*, vol. 1817, pp. 650-657. doi: 10.1016/j.bbabo.2011.11.015
7. Einarsdottir, O, Funatogawa, C, Soulimane, T & Szundi, I 2012, 'Kinetic studies of the reactions of O₂ and NO with reduced *Thermus thermophilus* ba₃ and bovine aa₃ using photolabile carriers', *Biochimica et Biophysica Acta*, vol. 1817, pp. 672-679. doi: 10.1016/j.bbabo.2011.12.005
8. Kaila, VR, Verkhovsky, MI & Wikström, M 2010, 'Proton-coupled electron transfer in cytochrome oxidase', *Chemical Reviews*, vol. 110, pp. 7062-7081. doi: 10.1021/cr1002003
9. De Vries, S 2008, 'The role of the conserved tryptophan₂₇₂ of the *Paracoccus denitrificans* cytochrome c oxidase in proton pumping', *Biochimica et Biophysica Acta*, vol. 1777, pp. 925-928. doi: 10.1016/j.bbabo.2008.05.008
10. Wiertz, FG, Richter, OM, Cherepanov, AV, MacMillan, F, Ludwig, B & de Vries, S 2004, 'An oxo-ferryl tryptophan radical catalytic intermediate in cytochrome c and quinol oxidases trapped by microsecond freeze-hyperquenching (MHQ)', *FEBS Letters*, vol. 575, pp. 127-130.
11. Yu, MA, Egawa, T, Shinzawa-Itoh, K, Yoshikawa, S, Yeh, SR, Rousseau, DL & Gerfen, GJ 2011, 'Radical formation in cytochrome c oxidase', vol. 1807, pp. 1295-1304. doi: 10.1016/j.bbabo.2011.06.012
12. Budiman, K, Kannt, A, Lyubenova, S, Richter, OM, Ludwig, B, Michel, H & MacMillan, F 2004, 'Tyrosine 167: the origin of the radical species observed in the reaction of cytochrome c oxidase with hydrogen peroxide in *Paracoccus denitrificans*', *Biochemistry*, vol. 43, pp. 11709-11716.
13. Svistunenko, DA, Wilson, MT & Cooper, CE 2004, 'Tryptophan or tyrosine? On the nature of the amino acid radical formed following hydrogen peroxide treatment of cytochrome c oxidase', *Biochimica et Biophysica Acta*, vol. 1655, pp. 372-380.
14. Yu, MA, Egawa, T, Shinzawa-Itoh, K, Yoshikawa, S, Guallar, V, Yeh, SR, Rousseau, DL & Gerfen, GJ 2012, 'Two tyrosyl radicals stabilize high oxidation states in cytochrome c oxidase for efficient energy conservation and proton translocation', *Journal of the American Chemical Society*, vol. 134, pp. 4753-4761.
15. Hendler, RW, Pardhasaradhi, K, Reynafarje, B & Ludwig B 1991, 'Comparison of energy-transducing capabilities of the two- and three-subunit cytochromes aa₃ from *Paracoccus denitrificans* and the 13-subunit beef heart enzyme', *Biophysical Journal*, vol. 60, pp. 415-423.
16. Moody, AJ 1996, 'As prepared' forms of fully oxidised haem/Cu terminal oxidases', *Biochimica et Biophysica Acta*, vol. 1276, pp. 6-20.

17. Von Wachenfeldt, C, de Vries, S & van der Oost, J 1994, 'The CuAsite of the caa3-type oxidase of *Bacillus subtilis* is a mixed-valence binuclear copper centre', *FEBS Letters*, vol. 340, pp. 109–113. doi: 10.1016/0014-5793(94), 80182-7
18. Wilson, MT, Jensen, P, Aasa, R, Malmström, BG & Vänngård, T 1982, 'An investigation by e.p.r. and optical spectroscopy of cytochrome oxidase during turnover', *Biochemical journal*, vol. 203, pp. 483-492.
19. Kobayashi, K, Une, H & Hayashi, K 1989, 'Electron transfer process in cytochrome oxidase after pulse radiolysis', *Journal of Biological Chemistry*, vol. 264, pp. 7976-7980.

Chapter IV

The cytochrome *ba*₃ oxidase from *Thermus thermophilus* does not generate a tryptophan radical during turnover; implications for the mechanism of proton pumping

Angela Paulus, Carolin Werner, Bernd Ludwig, Simon de Vries

Adapted from:
Biochimica et Biophysica Acta, 2015, 1847:1093-1100

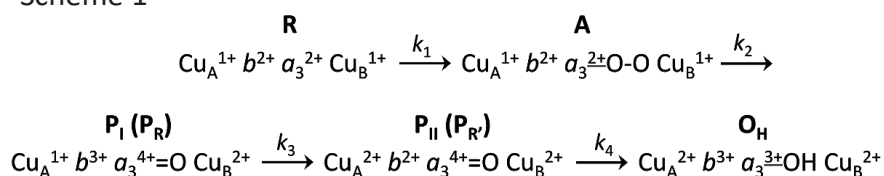
Abstract

Oxygen reduction by cytochrome *ba*₃ oxidase from *Thermus thermophilus* was studied by stopped-flow and microsecond freeze-hyperquenching analyzed with UV-Vis and EPR spectroscopy. In the initial phase the low-spin heme *b*₅₆₀ is rapidly and almost completely oxidized ($k_{\text{obs}} > 33000 \text{ s}^{-1}$) whereas Cu_A remains nearly fully reduced. The internal equilibrium between Cu_A and heme *b*₅₆₀ with forward and reverse rate constants of 4621 s^{-1} and 3466 s^{-1} , respectively, indicates a $\sim 7.5 \text{ mV}$ lower midpoint potential for Cu_A compared to heme *b*₅₆₀. The formation of the oxidized enzyme is relatively slow (693 s^{-1}). In contrast to the *Paracoccus denitrificans* cytochrome *aa*₃ oxidase, where in the last phase of the oxidative half cycle a radical from the strictly conserved Trp272 is formed, no radical is formed in the cytochrome *ba*₃ oxidase. Mutation of the Trp229, the cytochrome *ba*₃ oxidase homologue to the Trp272, did not abolish the activity, again in contrast to the *Paracoccus* cytochrome *aa*₃ oxidase. Differences in the proton pumping mechanisms of Type A and Type B oxidases are discussed in view of the proposed role of the strictly conserved tryptophan residue in the mechanism of redox-linked proton pumping in Type A oxidases. In spite of the differences between the Type A and Type B oxidases we conclude that protonation of the proton-loading site constitutes the major rate-limiting step in both respective catalytic cycles.

1. Introduction

Cytochrome *ba*₃ oxidase is a membrane-bound heme-copper oxidase that catalyzes the reduction of molecular oxygen to water, accompanied by proton pumping. In *Thermus thermophilus*, electrons are donated to cytochrome *ba*₃ oxidase one-by-one by cytochrome *c*₅₅₂¹ that docks at the positive side of the membrane, while the protons are taken up from the negative side of the membrane, resulting in the formation of a proton electrochemical gradient. The electrons are transferred from Cu_A at the docking site via the low-spin heme *b* to the high-spin heme *a*₃-Cu_B binuclear center. When the fully (four-electron) reduced enzyme is exposed to oxygen at neutral pH, the electron transfer reactions following binding of oxygen depicted in Scheme 1 are observed²⁻⁴:

Scheme 1



Scheme 1: R is the four-electron reduced enzyme that binds O₂ and A the oxygenated complex in which O₂ is bound to heme *a*₃. P_I (P_R), P_{II} (P_R') reflect the various heme *a*₃ oxo-ferryl states (see also text below and Fig. 5 including protonation states of the various states) and finally O_H, the oxidized pulsed activated enzyme.

The rates of the reactions are estimated at $k_1 = 100.000 \text{ s}^{-1}$, $k_2 = 200.000 \text{ s}^{-1}$, $k_3 = 18.000 \text{ s}^{-1}$ and $k_4 = 1000 \text{ s}^{-1}$, with [O₂] = 90 μM for the reaction at ambient temperature (20-25 °C)^{2,3}. These rates were observed in time-resolved spectroscopic studies using photolabile O₂ carriers in the absence of CO. In contrast, the rate of CO dissociation has been shown to limit the rate of oxygen binding dramatically in flow-flash studies on cytochrome *ba*₃ oxidase^{2,3},

as a result of which the kinetics of oxygen binding and O-O bond breaking are usually not resolved⁴⁻⁷ although they apparently were in⁸.

In pulse radiolysis experiments of cytochrome *ba*₃ oxidase where the reductive half-cycle is studied through single-electron injection, electron transfer from Cu_A to heme *b*₅₆₀ indicated an approximately 16 mV lower midpoint potential of heme *b*₅₆₀ compared to that of Cu_A. Because the midpoint potentials of Cu_A, heme *b*₅₆₀ and heme *a*₃ are rather similar, the first electron taken up by the oxidized enzyme distributes over at least three redox active groups (Cu_A, heme *b*₅₆₀ and heme *a*₃)⁹. In studies of the oxidative half-cycle the low-spin heme *b*₅₆₀ is transiently rereduced in P_{II} (P_R)^{2,8}.

In addition to the enzymatic O₂-reduction, cytochrome *ba*₃ oxidase is capable of proton pumping, that is the translocation of protons that do not take part in the reduction of O₂ to H₂O. The stoichiometry of proton pumping by cytochrome *ba*₃ oxidase is lower than that of Type A CcOs (~ 0.5 H⁺/e instead of 1 H⁺/e)^{4,10,11}. The basis for this difference has been proposed to be due to different timing of electron and proton transfer events between the two enzymes¹⁰, or be related to the lowered proton uptake activity of the proton pathway in cytochrome *ba*₃ oxidase¹²⁻¹⁴ or to differences in the intramolecular electron transfer vs. Type A CcOs^{10,15-17}. A proton gating mechanism is required to prevent the leaking back of protons towards the negative side of the membrane. In the Type A oxidases, several proton gating mechanisms are proposed, some of which include an important role for an amino acid residue at the end of the proton conducting D-pathway (E278 for example in bacterial *aa*₃ CcOs)¹⁸⁻²⁰ while other mechanisms are based on unidirectionality of the chemistry of proton transfer: In *P. denitrificans* CcO a tryptophan neutral radical from the conserved W272 is formed during the reaction that was studied by freeze-quench/EPR²⁰ and this redox active W272 was proposed to act as an unidirectional redox-linked proton pump in the F to O_H transition^{(21,22}, see Fig. 5); in *B. taurus* CcO heme *a* and the mitochondrially conserved Asp51 direct proton translocation through the H-channel^{23,24}. A recent study suggests that all CcOs maximally pump 1 H⁺/e but that the Type B and C oxidases, which only possess a single K-proton transfer pathway, are more susceptible to proton back leak depending on the experimental conditions (high proton-motive force), because they lack the D-proton pathway characteristic of Type A oxidases²⁵. However, the stoichiometry of ~ 0.5 H⁺/e has been found at low proton-motive force, and been rationalized in terms of the mechanism of the cytochrome *ba*₃ oxidase^{4,10,15}.

This work describes studies of the early reaction steps of reduced cytochrome *ba*₃ oxidase with oxygen by means of rapid kinetics and EPR spectroscopy. Our results are discussed in the light of current mechanisms of electron transfer and proton transfer/proton pumping for cytochrome *ba*₃ oxidase and cytochrome *aa*₃ oxidase.

2. Materials and Methods

2.1 Growth and preparation of mutants

T. thermophilus *ba*₃ oxidase was prepared^{26,27} and the activities were measured as in²⁴. The two enzyme preparations displayed the same behavior in the reported experiments and were therefore treated as one in the analysis. Mutant sequences of *T. thermophilus* *ba*₃ oxidase were introduced using the QuikChange Site-Directed Mutagenesis kit (Stratagene). The following primer sequences were applied:

W229Q CCCTTGGTCGCGCGCACCCCTCTTCCAGTGGACG

W229H TTGGTCGCGCGCACCCCTCTTCCACTGGACGG

Mutants in the *P. denitrificans* *aa*₃-type oxidase were generated and the oxidase complex purified as in ²⁸.

2.2 Stopped-flow (SF) kinetic experiments

Pre-steady state kinetic experiments were performed with an Applied Photophysics SX20 stopped-flow spectrometer (dead time 2-3 ms) with a 150W Xe arc lamp and thermostatted syringes. The setup was incubated with approximately 5 mM dithionite and thoroughly flushed with anaerobic buffer to ensure anaerobicity of the system. The enzyme samples were reduced with 10 mM ascorbate and either 0.2 or 1 μ M PES in an anaerobic chamber prior to loading in the stopped-flow apparatus using gastight Hamilton syringes. The enzyme samples were mixed vs. oxygen-saturated buffer at 5, 10 or 40 °C and data was collected between 2.5 ms and 1.26 s after mixing. The cytochrome *ba*₃ concentration in the final reaction mixture was 1-4 μ M in 50 mM Tris HCl pH 8 (200 mM NaCl, 0.02% lauryl maltoside).

2.3 Microsecond freeze-hyperquenching (MHQ) experiments

Samples were reduced in an anaerobic chamber with 10 mM ascorbate and either 0.2 or 1 μ M PES and loaded into the MHQ setup ^{21, 29} using a gastight Hamilton syringe. Samples were mixed vs. oxygen-saturated buffer and the reaction was stopped by freeze-quenching after reaction times ranging from ~ 100 μ s to ~ 20 ms at 9 ± 2 °C. The frozen powder was collected in liquid nitrogen and stored at cryo-temperatures until further analysis. The final cytochrome *ba*₃ oxidase concentration in the reaction mixture was ~ 75 μ M in 50 mM Tris HCl pH 8 (200 mM NaCl, 0.02% lauryl maltoside).

2.4 Low-temperature UV-Vis spectral analysis

The UV-Vis optical spectra of the frozen powder samples were measured using an Olis DW2000 double beam spectrophotometer, flushed with cold nitrogen gas (-165 °C) to prevent reaction progress during measurements. Cuvettes were prepared by injection of frozen powder sample mixed with melting isopentane (-160 °C) into the pre-cooled cell, followed by immediate freezing in liquid nitrogen. The spectra were baseline and scatter corrected and normalized to the total area of the γ -band ³⁰. Slight variations in spraying conditions and sample handling cause a scatter of approximately $\pm 10\%$.

2.5 X-band Electron paramagnetic resonance spectroscopy (EPR)

The MHQ frozen powder was packed into an EPR tube with a filter at the bottom as described ³⁰. The tubes were kept in liquid nitrogen during and after packing. EPR spectroscopy was performed on a Bruker EC106 and samples were cooled by a home-built He-flow system ³¹.

2.6 Data analysis

Kinetic simulations were performed with an algorithm developed in-house that numerically calculates up to 12 consecutive reversible first order reactions and that runs under IGOR Pro (6.06). This calculation yields the overall time course of the formation and decay of enzyme intermediate states. Calculated rate constants are accurate to $\pm 20\%$ of the quoted values.

3. Results

3.1 Stopped-flow experiments

As preparation for the MHQ measurements, a stopped-flow study of the cytochrome *ba*₃ oxidase was performed to observe the behavior of the enzyme at temperatures below room temperature (9 ± 2 °C in MHQ experiments). The kinetics of heme *b*₅₆₀ oxidation at 5, 10 and 40 °C are displayed in Figure 1A. Particularly at the lowest temperature, 5°C, the net oxidation of heme *b*₅₆₀ does not go to completion, as the reduction level of heme *b*₅₆₀ was never below ~ 35% in these measurements. The rate of the reduction of heme *b*₅₆₀ by the asc/PES system decreases less with decreasing temperature than the subsequent enzymatic steps, resulting in a significant reduction level of heme *b*₅₆₀ during steady state turnover at the lower temperatures.

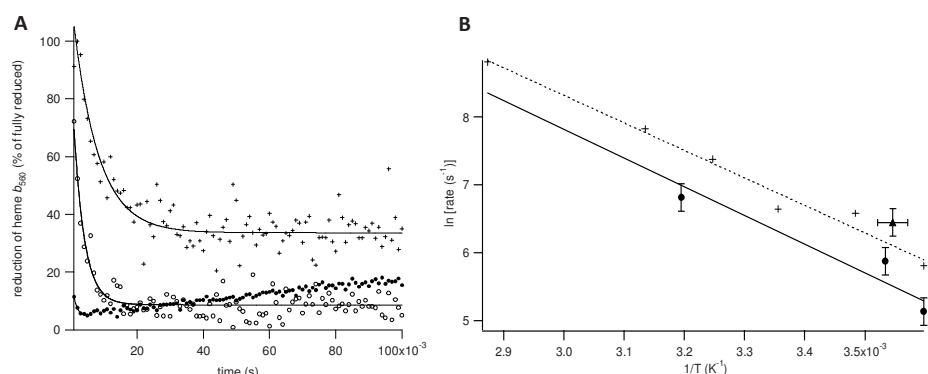


Figure 1: Kinetic analysis of the oxidation of heme *b*₅₆₀. **A**) Kinetic traces of the oxidation of heme *b*₅₆₀ in the reaction of fully reduced cytochrome *ba*₃ oxidase with oxygen, in the presence of a reducing agent (asc/PES). The level of reduction is expressed relative to the reduction level of the heme *b*₅₆₀ prior to mixing with oxygen (100%). Part of the oxidation of heme *b*₅₆₀ was not observed because it occurred in the dead time of the stopped flow setup (~ 2.5 ms). The data are shown for the reaction at 40 °C (●), 10 °C (○) and 5 °C (+). Only the initial oxidation phase, before the gradual onset of equilibrium, was used for the calculation of the rate of oxidation of heme *b*₅₆₀. Calculated values for the rate of oxidation of heme *b*₅₆₀ are 142 s⁻¹ at 5 °C, 313 s⁻¹ at 10 °C and 912 s⁻¹ at 40 °C. **B**) Arrhenius plot displaying the temperature dependence of the rate of heme *b*₅₆₀ oxidation (●: stopped-flow data; ▲: MHQ data point (693 s⁻¹ (see below) 9 ± 2 °C); +: data from pulse radiolysis studies¹⁶). The activation energy of the oxidation of heme *b*₅₆₀ that can be calculated from the fit through the pulse radiolysis data is approximately 34 kJ/mol. The set of data acquired with the stopped-flow apparatus yields an *E*_a of ~ 36 kJ/mol.

An Arrhenius plot was constructed (Figure 1B) from the observed first-order rate constants for oxidation of heme *b*₅₆₀ at different temperatures, as well as from the data published on the oxidation rate of heme *b*₅₆₀ in pulse radiolysis experiments¹⁶. Although the observed heme *b*₅₆₀ oxidation rates in the stopped-flow experiments are approximately two-fold lower than the rates determined at the same temperature in the pulse radiolysis experiments, our data (*E*_a ~ 36 kJ/mol, Fig. 1B) yield a similar activation energy *E*_a for the oxidation of heme *b*₅₆₀ as calculated from the pulse radiolysis experiments (*E*_a ~ 34 kJ/mol).

3.2 Freeze-quench experiments

In order to study the oxidation reaction of reduced ba_3 with molecular oxygen at shorter times than possible with the stopped-flow apparatus, MHQ experiments were performed in the time interval between 74 μ s and 21 ms at a reaction temperature of 9 ± 2 °C. An overview of UV-Vis spectra of these samples is depicted in Figure 2. The O-O bond breaking reaction was not resolved since it is completed within ~ 15 μ s^{2,3}.

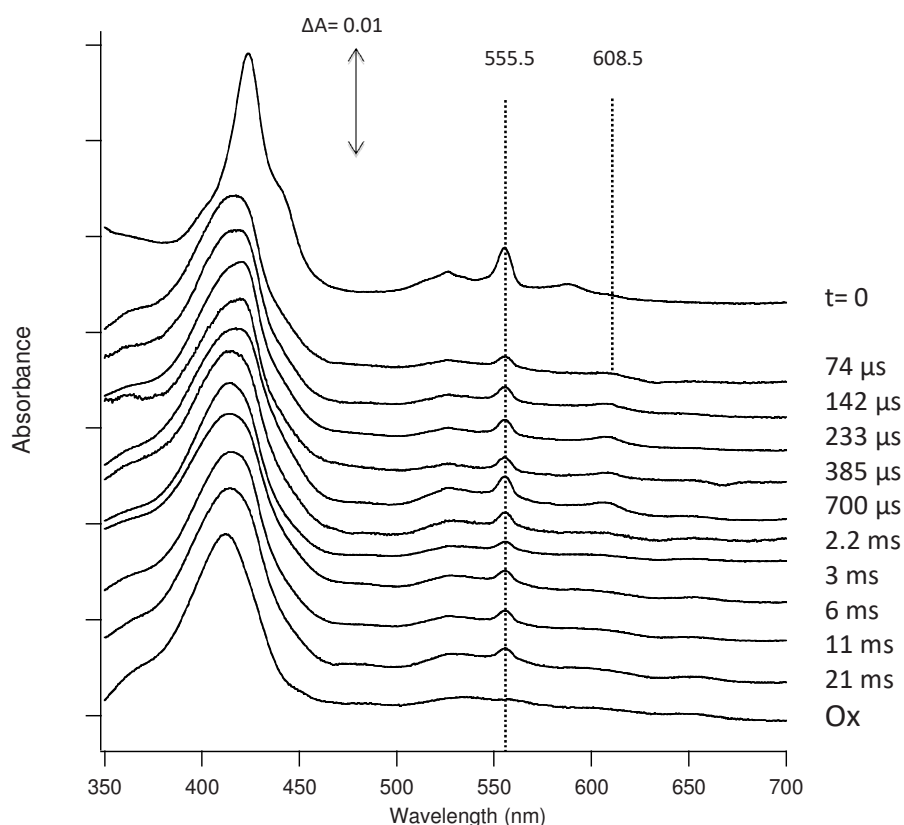


Figure 2: Low temperature UV-Vis spectra of samples obtained with the MHQ technique. Powder samples were mixed with cold isopentane and an aliquot of the mixture was dispensed into a precooled cuvette that was kept at approximately -165 °C throughout the optical measurement. The spectra shown here correspond to a range of reaction times, starting with the unreacted control (top spectrum, 't = 0', fully reduced cytochrome ba_3) and completing the series with the spectrum of fully oxidized cytochrome ba_3 (bottom spectrum, 'Ox'). The two reference spectra for fully reduced and fully oxidized cytochrome ba_3 were collected from manually prepared 'static' samples; all the other spectra originate from samples after MHQ. Wavelengths of interest are indicated by dotted vertical lines (heme b_{560} at 555.5 nm and oxoferryl heme a_3 at 608.5 nm in the low temperature spectra).

As was observed in the stopped-flow experiments, the oxidation of heme b_{560} in the MHQ experiments did not go to completion. This is also reflected in the position of the Soret maximum at 415 nm in the samples reacted for several milliseconds, whereas in the oxidized spectrum the Soret peak resides at 413.5 nm. The α -band shifts from 608.5 nm at the shortest

reaction times to 606.5 nm after 700 μ s, accompanied by a shift of the Soret band from 424 nm to 418 nm. The increase in absorbance at 555.5 nm between 233 μ s and 700 μ s, which coincides with a red shift of the Soret peak, indicates partial rereduction of heme b_{560} in the early stages of the reaction. The reduced heme b_{560} transiently accumulates before it oxidizes to the equilibrium reduction level ($\sim 25\%$).

Both the stopped-flow and freeze-quench experiments (Figs. 1 and 2) show a considerable extent of reduction of heme b_{560} as the reaction approaches equilibrium (20-25 % at $9\pm 2^\circ\text{C}$). This high level of reduction after a single turnover was not observed for cytochrome aa_3 oxidase from *P. denitrificans*²¹. The cytochrome aa_3 oxidase converts back to the pulsed oxidized state after 3 to 6 ms in the presence of ascorbate and 0.5 μ M PES. The partial rereduction of heme b_{560} during oxidation between 233 μ s and 700 μ s has been observed before in flow-flash experiments with or without CO-bound cytochrome ba_3 oxidase^{2,3,8}. The transient formation of the F state (between P_R and O_H) at 580 nm was not observed in our data. The population of the F state is pH dependent and is very low for cytochrome ba_3 oxidase at pH 8¹⁵ compared to pH 10. At a pH closer to neutral, the F to O_H transition of cytochrome ba_3 oxidase occurs at a much higher rate than the P_R to F transition¹⁵ in contrast to cytochrome aa_3 oxidase, where the F to O_H transition is much slower than the preceding step both at neutral and alkaline pH, resulting in significant population of F^{5,21}.

The MHQ frozen powder samples were analyzed by X-band EPR spectroscopy. The EPR spectra of all samples are depicted in Figure 3. The spectra show the oxidation of Cu_A . A small radical that is inherent to the freeze-quench procedure (Fig. 3, top trace, 'MHQ-radical') and possibly due to the ascorbyl radical³² is seen as well. There is no evidence for the formation of a Trp-radical intermediate from the strictly conserved tryptophan in the ba_3 oxidase (W229) as it has been previously observed for the cytochrome aa_3 oxidase^{21,30}. In *P. denitrificans* aa_3 oxidase W272 is essential since the W272M and W272F mutants display no catalytic activity or proton pumping and there is no formation of P or F intermediates upon reaction with hydrogen peroxide³³ or with O_2 (see Supplementary data, Figs. S1 and S2, for UV-vis and EPR spectra of kinetic experiments, $k_{\text{obs}}(\text{O}_2) < 0.4 \text{ s}^{-1}$). In contrast to the *P. denitrificans* aa_3 oxidase mutations in the homologous W229 in the ba_3 cytochrome *c* oxidase (W229Q and W229H) retained approximately 25% of the steady state wild type activity³⁴. Experiments to investigate whether or not proton pumping in this mutant was affected could not be performed in view of the low yield of the mutant proteins.

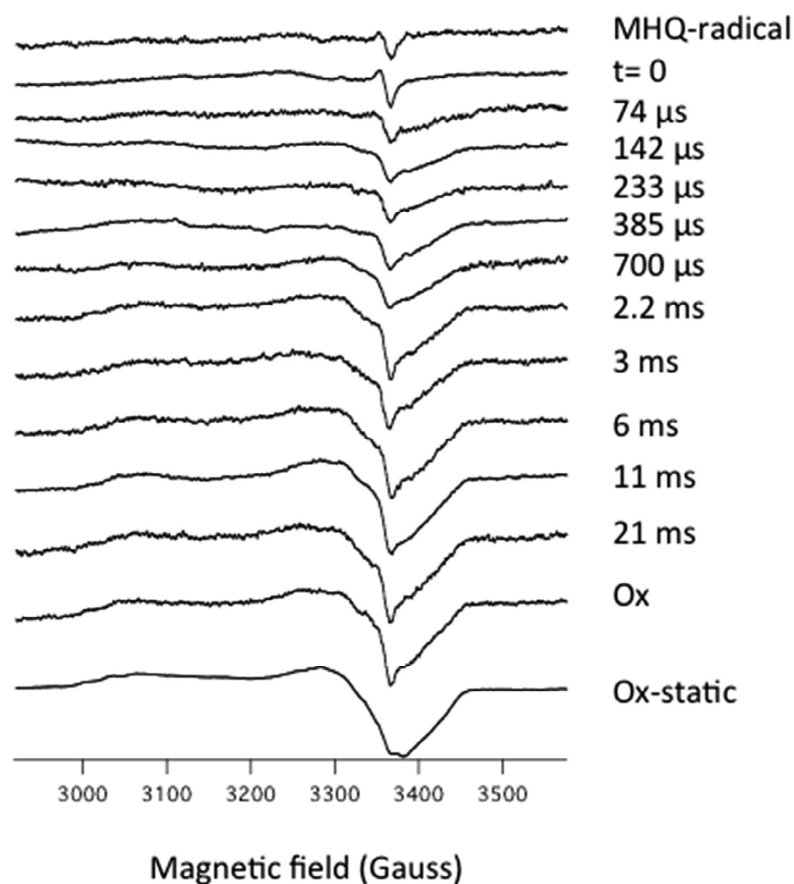
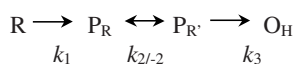


Figure 3: Overview of the EPR spectra of the frozen powder samples of reduced cytochrome *ba*₃ oxidase reacting with O₂ for various times. Top trace 'MHQ-radical' calculated from the difference spectrum of 'Ox' and 'Ox-static'.

The kinetic results from the optical and EPR spectroscopic analyses were combined and fitted to single reaction model for the overall reaction consisting of three consecutive transitions (Fig. 4), in which the first step constitutes both O₂ binding and O-O bond breaking:



with $k_1 \geq 33324 \text{ s}^{-1}$, $k_2 = 4621 \text{ s}^{-1}$, $k_{-2} = 3466 \text{ s}^{-1}$ and $k_3 = 693 \text{ s}^{-1}$.

The simulation based on these rate constants fits the data satisfactorily for the first 2-3 ms. After that period, the net oxidation of heme *b*₅₆₀ and the formation of O_H cease since the system equilibrates to a temperature dependent steady state with $20 \pm 10\%$ reduced heme *b*₅₆₀ due to the presence of excess reductant (see also Fig. 1).

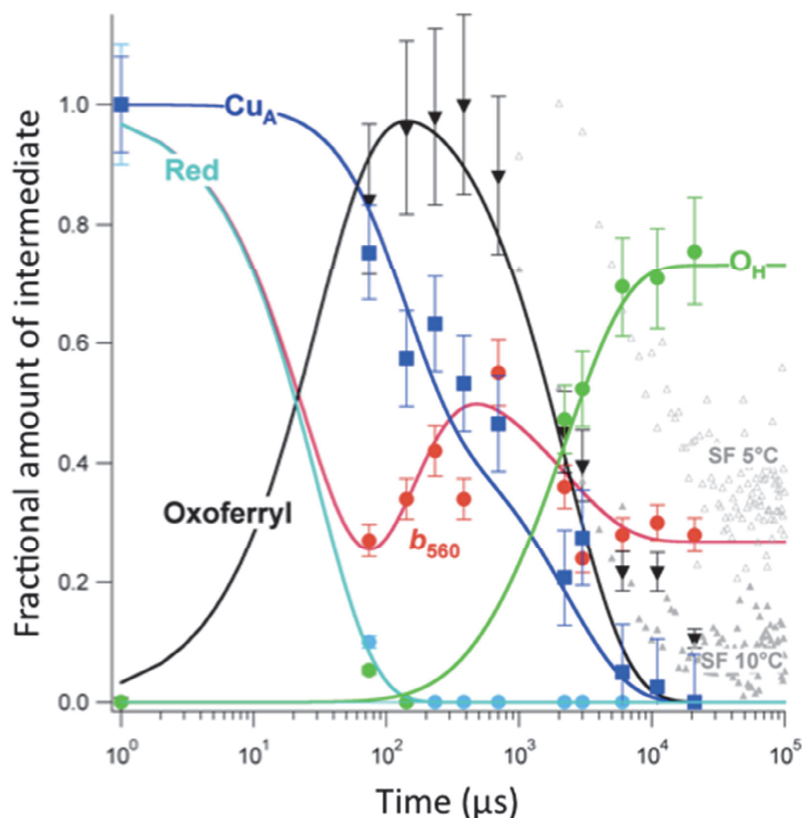


Figure 4: Fits of the kinetics of the various redox centers of cytochrome *ba*₃ oxidase upon reduction of oxygen, based on the kinetic data from the MHQ (EPR) and stopped-flow (UVvis) experiments and on the reaction model above. See text for values of the rate constants used. Depicted are the fractions of total (ranging from 0 to 1) of several reaction intermediates and of the reduction level of redox active centers in the time range between 0 and 100 ms. The simulation approaches a state with approximately 25% reduced heme *b*₅₆₀ and 75% fully oxidized enzyme, in correspondence with the observed spectra and EPR data. Dark blue: reduction level of Cu_A, light blue: fraction of completely reduced enzyme (R), black: fraction of total enzyme with oxoferryl heme *a*₃ (oxoferryl; P_R/P_R′/F), red: reduction level of heme *b*₅₆₀ (*b*₅₆₀), green: fraction of completely oxidized enzyme (O_H), grey: stopped flow data for heme *b*₅₆₀ reduction at 560 nm at 5°C (SF 5°C; open triangles) and 10°C (SF 10°C; filled triangles). Note that the early time points of the data at 5°C indicate a transient reduction profile for heme *b*₅₆₀ as observed in the MHQ experiments, but at a later time owing to the lower reaction temperature.

The oxidation of Cu_A appears biphasic, with a fast and a slow phase that correspond to a heme *b*₅₆₀ reduction phase and a Cu_A-heme *b*₅₆₀ equilibration phase, respectively. The internal equilibrium between heme *b*₅₆₀ and Cu_A is given by forward (*k*₂) and reverse (*k*₋₂) rate constants of 4621 s⁻¹ and 3466 s⁻¹ indicating a 7.5 (± 5.8) mV higher midpoint potential for heme *b*₅₆₀ compared to Cu_A, contrast to earlier pulse radiolysis studies¹⁶, where a 16 mV lower midpoint potential for heme *b*₅₆₀ was reported. However, the sum of *k*₋₂ and *k*₂ (8087 s⁻¹), which is *k*^{obs}₂ is nearly equal to the values of 8380 s⁻¹ and 8500 s⁻¹ for 5 °C and 10 °C, respectively, determined in¹⁶.

The data and analysis shown in Fig. 4 are qualitatively similar to the cytochrome *ba*₃ oxidation kinetics reported in Figs. 2, Scheme 5 and Fig. 5 in ². However, a more direct quantitative comparison cannot be made in view of different experimental temperatures, our lower time resolution and a difference between ours and the kinetic analysis in ² in which in particular the electron transfer between heme *b*₅₆₀ and Cu_A was calculated as an irreversible reaction.

4. Discussion

In this paper the reaction between oxygen and reduced cytochrome *ba*₃ oxidase has been monitored by UV-vis and EPR spectroscopy using stopped-flow and ultrafast freeze-quench methods. The experiments show a clear transient oxidation of heme *b*₅₆₀, in contrast to Type A *aa*₃ oxidases, where the biphasic oxidation of heme *a* is much less pronounced ³⁵. In further contrast to Type A oxidases, mutations in W229 (W272) rendered a 25% active enzyme instead of a completely inactivated enzyme (Figs. S1 and S2), indicating that the conserved tryptophan is not essential for activity in cytochrome *ba*₃ oxidase. Finally, no transient formation of a tryptophan radical from the conserved W272 (W229), which in Type A oxidases is proposed to play a role in proton pumping ^{21,22}, was observed during the reaction of the wild type cytochrome *ba*₃ oxidase. In the following we will first discuss our results in regard to the intramolecular electron transfer kinetics and then focus on the question as to which electron/proton transfer step(s) are limiting the overall rate in Type A and Type B oxidases to ~ 1 ms.

4.1 Intramolecular electron transfer

The oxidation/reduction rates that we observe for heme *b*₅₆₀ in stopped-flow experiments are approximately a factor of 2 lower than observed in pulse radiolysis experiments while yielding a similar activation energy ^{9, 16}. For the freeze experiments MHQ we calculate a similar k^{obs}_2 (~ 8000/s) as in ¹⁶ but the individual values of k_{-2} and k_2 yield a 7.5 mV higher midpoint potential of heme *b*₅₆₀ compared to Cu_A whereas a value of 16 mV lower was previously observed ¹⁶. Although these differences might be due to different experimental techniques, the crucial difference is that the stopped-flow and freeze-quench experiments reported here were performed starting with the reduced enzyme in reaction with O₂, thus monitoring the oxidative half-cycle of the reaction, whereas the pulse radiolysis studies were performed in the absence of oxygen, monitoring injection of a single electron, the initial step of the reductive half-cycle ¹⁶. It thus appears that the energy barrier to overcome for ET between heme *b*₅₆₀ and heme *a*₃ is approximately the same in both half-cycles and is not affected by the reduction and/or ligand state of the binuclear center or that of other redox centers. The different values for the differences in midpoint potential between of heme *b*₅₆₀ and Cu_A can be due to dissimilar electrostatic effects on the redox centers in oxidized enzyme and fully reduced or partly reduced enzyme present during the reaction.

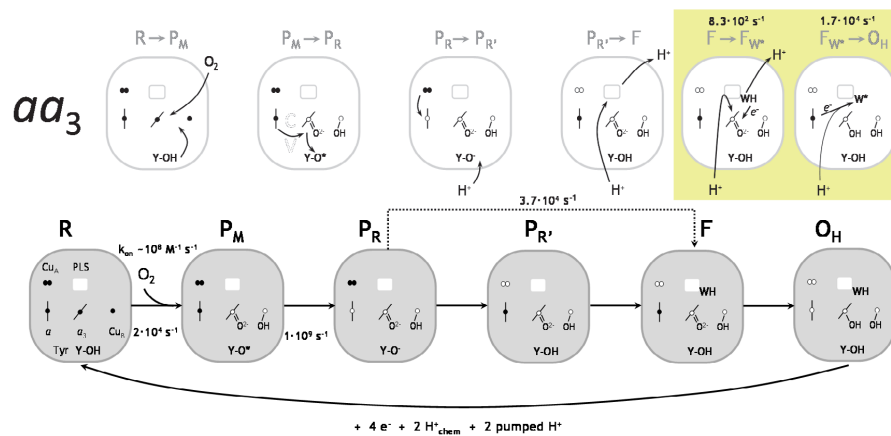
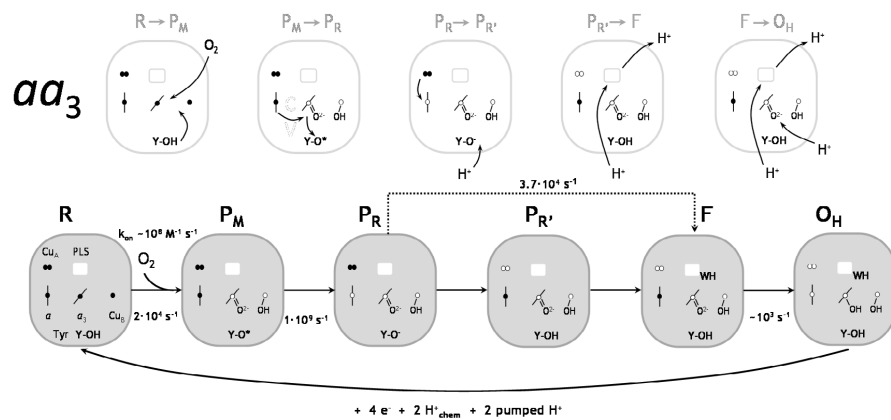
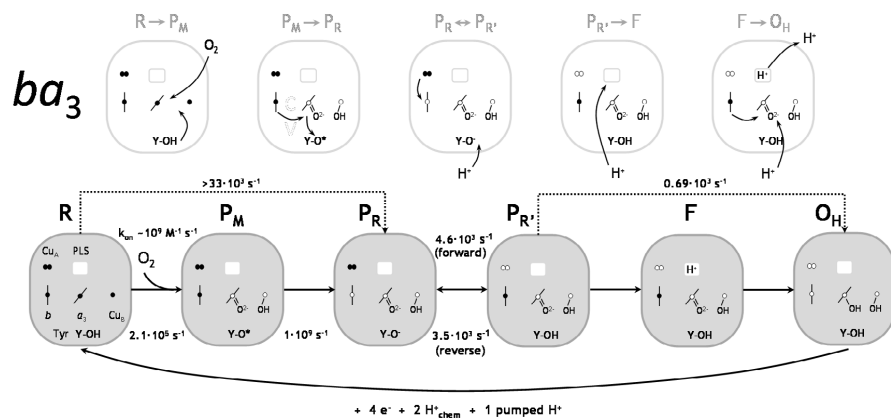


Figure 5: Proposal for the catalytic cycle of cytochrome *ba*₃ oxidase (top scheme) and the comparison to cytochrome *aa*₃ oxidase (bottom two schemes). The grey boxes represent the different intermediates of the cycle. The white boxes display electron transfer, proton binding and release processes that occur between the different intermediates. WH: W229 in cytochrome *ba*₃ oxidase, W272 in cytochrome *aa*₃ oxidase. **Cytochrome *ba*₃ oxidase:** Note that P_M and F were not resolved in our data. The reaction constants (1/τ) from the three-transition kinetic model (Fig. 4) are indicated at the corresponding reaction steps. The Tyr* is reduced in P_M → P_R and presumably reprotonated in P_R'. Proton uptake and proton release events were not measured, but they are proposed to take place between P_R and O_H⁴. Description: When the reduced enzyme (R) is exposed to O₂, the high-spin heme *a*₃ binds oxygen and the O-O bond is split^{2,3} using the electrons from the active site heme *a*₃/Cu_B and an electron and a proton from Tyr237⁵ (R → P_M). The Tyr* radical is rapidly reduced (~ 1 ns) by the electron from heme *b*₅₆₀ to form the P_R state. The first proton uptake event (for reprotonation of YO) correlates with electron transfer from Cu_A to heme *b*₅₆₀ (P_R → P_R'). A second proton is then taken up from the negative side of the membrane to form the F state of the enzyme. After transfer of the electron at heme *b*₅₆₀ to the BNC, followed by uptake of another proton to the catalytic site and the release of the proton at the PLS, the oxidized enzyme (O_H) is formed again. **Cytochrome *aa*₃ oxidase:** The oxidative phase of the cycle of cytochrome *aa*₃ oxidase involves an extra proton-pumping event (P_R → F) and (lower scheme) a transient Trp neutral radical from W272 (shown as W*). The F to O_H transition of cytochrome *aa*₃ oxidase is therefore depicted (see yellow box) as two sequential transitions, F to F_W* and F_W* to O_H^{21,22,30}. The curved arrow designates the proton involved in the reduction of the oxo-ferryl heme *a*₃ to the ferric hydroxyl state and may involve E278²² and/or the PLS.

The transfer of the first electron from heme *b*₅₆₀ to heme *a*₃ (> 33.000 s⁻¹) in the oxidative phase is much faster than that of the second electron (693 s⁻¹), while the rate of ET between Cu_A and heme *b*₅₆₀ is intermediate (~ 4000 s⁻¹, Fig. 5). These specific rate constants produce the observed transient oxidation/rereduction of the heme *b*₅₆₀ (Figs. 1, 4), which has been described before in the literature^{2,8}. The observation of the very rapid initial electron transfer from heme *b*₅₆₀ upon O₂-binding has led to the idea⁸ that the rapid initial ET from heme *b*₅₆₀ may constitute donation of the fourth electron to the active site for O-O bond splitting without the need for formation of a Tyr radical (P_M, Fig. 5). However, the oxidation of heme *a* in cytochrome *aa*₃ oxidase is also transient³⁵, but less extensive due to different relative rate constants for heme *a* oxidation/reduction compared to heme *b*₅₆₀, and the transient oxidation of heme *a* is more difficult to observe due to spectral overlap with heme *a*₃. More specifically, the rates of O₂ binding and O-O bond splitting are approximately ten times faster in cytochrome *ba*₃ oxidase (10⁹ M⁻¹s⁻¹ and 4.8 μs, respectively) than in cytochrome *aa*₃ oxidase^{2,3}. Owing to the short edge-to-edge distance of ~ 5 Å, electron transfer between heme *b*(*a*) and heme *a*₃ is intrinsically very fast (within ~ 1 ns, or with 10⁹ s⁻¹³⁶). As a consequence, the oxidation of heme *b*₅₆₀ occurs immediately after O-O bond splitting and is almost complete after 10 – 20 μs, in which step the Tyr* is reduced. In cytochrome *aa*₃ oxidase the oxidation of heme *a* is slower because the O-O bond splitting takes ~ 40 μs^{3,35}, and the transient heme *a* kinetics are less resolved because the rate of equilibration between Cu_A and heme *a* (~ 60 μs) occur at the same time scale as O-O bond splitting.

For these reasons the transient oxidation/rereduction of the heme *b*₅₆₀, but not of heme *a*, is simply a direct consequence of the different kinetic constants in cytochrome *ba*₃ oxidase and cytochrome *aa*₃ oxidase; there is no indication that the mechanism of O-O bond splitting would be different in Type A oxidases. In addition, we propose that the intermediate P_M that contains the tyrosine radical is a genuine intermediate irrespective of whether the oxidative half-cycle is initiated from the two-electron or four-electron reduced enzyme. The ~ 1 ns rate of electron transfer from heme *b*(*a*) to the binuclear center simply prevents accumulation and detection of P_M and a Tyr* when more than two electrons are present³⁶. In summary, the experimentally observed oxidation rates of heme *b*(*a*) during the oxidative half-cycle are gated by the rates of O₂ binding, of O-O bond splitting and by the Cu_A/heme *b*(*a*) equilibration rate. The next question is, which process gates the slowest heme *b*(*a*) oxidation

phase that occurs between $P_{R\cdot}$ and O_H with $\sim 1 \cdot 10^3 \text{ s}^{-1}$ ($\tau \sim 1 \text{ ms}$) and which constitutes the major rate limiting step of the overall reaction in both Type A and Type B oxidases, because their maximal turnover rates are all close to $\sim 250 \text{ O}_2$ per second^{7, 21, 34, 37, 38}.

4.2 Rate limiting step

A model for catalysis and proton pumping in cytochrome ba_3 oxidase was published recently^{4, 15} where proton uptake and release are part of different reaction steps. The uptake and release of protons are therefore observed separately, in contrast to the Type A oxidases where the proton uptake and release occur simultaneously^{4-7, 10, 39} (Fig. 5). Another difference to the Type A oxidases is that in the cytochrome ba_3 oxidase the F state (580 nm) only accumulates at alkaline pH (~ 10 ^{4, 8}) due to the relatively fast $F \rightarrow O_H$ transition. Our data acquired at pH 8 (Fig. 2) are consistent with the apparent absence of F^{2, 4, 8}.

Based upon our kinetic analysis of the oxidation of cytochrome ba_3 oxidase we ascribe the RLS ($\tau \sim 1 \text{ ms}$) to a process occurring between $P_{R\cdot}$ and O_H . Since the F state was not observed, we conclude that it was poorly populated and that the formation of F from $P_{R\cdot}$ at pH 8 is slow relative to the $F \rightarrow O_H$ transition¹⁵. We therefore propose that the RLS in cytochrome ba_3 oxidase is in fact the $P_{R\cdot}$ to F transition, in contrast to the cytochrome aa_3 oxidase from *P. denitrificans*, where the RLS was assigned to the $F \rightarrow O_H$ transition^{21, 22}, specifically to the formation of F_{W*} from F. The rate of the electron and proton transfer from W272 to heme a_3 , producing the Trp neutral radical (W272*), was calculated at 580 s^{-1} (at 10°C) and proposed as the major RLS in cytochrome aa_3 oxidase^{21, 22}. In the cytochrome ba_3 oxidase, however, we observed no kinetically relevant protein radicals between $P_{R\cdot}$ and F or between F and O_H . The absence of a Trp radical in cytochrome ba_3 oxidase may directly be related to its lower proton pumping stoichiometry. By donating the proton to form the heme $a_3 \text{ Fe}^{3+}\text{-OH}^-$ state in cytochrome aa_3 oxidase, the W272 makes the proton that is taken up from the proton conducting channel available for pumping^{21, 22}. Although we could not assess the proton-pumping capacity of the W229 mutant, the finding that mutation of this residue yields an enzyme that retains 25% of the wild type activity, whereas the equivalent mutation in cytochrome aa_3 oxidase completely inactivates the enzyme (Supplementary data) suggests different roles for this conserved tryptophan residue in the two classes of oxidases. We have previously proposed that in Type A oxidases the tryptophan residue is involved in redox-linked proton pumping^{21, 22}. The apparent absence of oxidation/reduction activity of W229 in the cytochrome ba_3 oxidase provides a basis for the lower proton-pumping capacity of the Type B oxidases compared to the type A oxidases.

We propose that the proton uptake from the negative side of the membrane that occurs during the $P_{R\cdot}$ to F transition comprises the rate-limiting step in cytochrome ba_3 oxidase. In our experiments, we cannot monitor protonation. Thus, the proton taken up in $P_{R\cdot} \rightarrow F$ may either be transferred to the PLS, or it may be used to reprotonate the tyrosinate, depending on the fate of the proton taken up between P_R and $P_{R\cdot}$ in cytochrome ba_3 oxidase (Fig. 5). If we make the comparison to the cytochrome aa_3 oxidase, the formation of W272* is found to coincide with proton uptake to the PLS, without reprotonation of the tyrosinate (the reprotonation of YO^- is usually placed before F^{8, 40} or after O_H ¹⁰, but not between F and O_H). We therefore postulate that it is proton uptake to the PLS that limits the reaction rate of both cytochrome ba_3 oxidase and cytochrome aa_3 oxidase, albeit at different points in their catalytic cycles.

5. Concluding remarks

We conclude that the observed differences in electron transfer kinetics between Type A and Type B oxidases such as transient heme b_{560} oxidation/reduction are merely a reflection of their different rate constants for intramolecular electron transfer and oxygen binding and do not imply formation of different intermediate electronic states. Although the rate-limiting step for the reduction of oxygen occurs at different points of the catalytic cycles of cytochrome ba_3 oxidase and cytochrome aa_3 oxidase, we propose that the actual rate-determining step is proton uptake to the PLS in the F to O_H transition in both enzymes and that this step constitutes the major rate-determining step in steady-state oxidation.

Cytochrome ba_3 oxidase is repeatedly reported to pump less protons/cycle than cytochrome aa_3 oxidase, and this has been suggested to be due to the presence of just a single proton transfer pathway in the former²⁵. Based on the results presented here, we ascribe the lower pumping efficiency to the lack of redox activity of W229 in the cytochrome ba_3 oxidase. We suggest that specific properties of the D-proton pathway in Type A oxidases enable the conserved tryptophan residue (W272) to become redox active and assist in proton pumping.

References

1. Soulimane, T.; Von Walter, M.; Hof, P.; Than, M.E.; Huber, R.; Buse, G. Cytochrome-c552 from *Thermus thermophilus*: a functional and crystallographic investigation *Biochem Biophys Res Commun* **1997**, *237*, 572-576. doi: 10.1110/ps.9.11.2068
2. Szundi, I.; Funatogawa, C.; Fee, J.A.; Soulimane, T. and Ólöf Einarsson, Ó. CO impedes superfast O₂ binding in ba3 cytochrome oxidase from *Thermus thermophilus* *Proc. Natl. Ac. Sci* **2010**, *107*, 21010 – 21015.
3. Einarsson, Ó.; Funatogawa, C.; Soulimane, T.; Szundi, I. Kinetic studies of the reactions of O₂ and NO with reduced *Thermus thermophilus* ba3 and bovine aa3 using photolabile carriers *Biochim Biophys Acta* **2012**, *1817*, 672-679.
4. Von Ballmoos, C.; Ädelroth, P.; Gennis, R. B.; Brzezinski, P. Proton transfer in ba3 cytochrome c oxidase from *Thermus thermophilus* *Biochim Biophys Acta* **2012**, *1817*, 650-657. doi: 10.1016/j.bbabo.2011.11.015
5. Kaila, V. R. I.; Verkhovsky, M. I.; Wikstrom, M. Proton-coupled electron transfer in cytochrome oxidase *Chem Rev.* **2013**, *110*, 7062-7081. doi: 10.1021/cr1002003
6. Brzezinski, P.; Larsson, G. Redox-driven proton pumping by heme-copper oxidases *Biochim Biophys Acta* **2003**, *1605*, 1-13. doi: 10.1016/S0005-2728(03)00079-3
7. Ferguson-Miller, S.; Babcock, G.T. Heme/copper terminal oxidases *Chem Rev* **1996**, *96*, 2889-2907. doi: 10.1021/cr950051s
8. Silvestry, S. A.; Belevich, I.; Jasaitis, A.; Konstantinov, A. A.; Wikstrom, M.; Soulimane, T.; Verkhovsky, M. I. Time-resolved single-turnover of ba3 oxidase from *Thermus thermophilus* *Biochim Biophys Acta* **2007**, *1767*, 1383-1392. doi: 10.1016/j.bbabo.2007.09.010
9. Farver, O.; Chen, Y.; Fee, J.A.; Pecht, I. Electron transfer among the CuA-, heme b- and a3-centers of *Thermus thermophilus* cytochrome ba3 *FEBS lett* **2006**, *580*, 3417-3421. doi: <http://dx.doi.org/10.1016/j.febslet.2006.05.013>
10. Von Ballmoos, C.; Lachmann, P.; Gennis, R.B.; Ädelroth, P.; Brzezinski, P. Timing of electron and proton transfer in the ba3 cytochrome c oxidase from *Thermus thermophilus* *Biochemistry* **2012**, *51*, 4507-4517. doi: 10.1021/bi300132t
11. Kannt, A.; Soulimane, T.; Buse, G.; Becker, A.; Bamberg, E.; Michel, H. Electrical current generation and proton pumping catalyzed by the ba3-type cytochrome c oxidase from *Thermus thermophilus* *FEBS Lett* **1998**, *434*, 17-22. doi: [http://dx.doi.org/10.1016/S0014-5793\(98\)00942-9](http://dx.doi.org/10.1016/S0014-5793(98)00942-9)
12. Soulimane, T.; Buse, G.; Bourenkov, G.P.; Bartunik, H.D.; Huber, R.; Than, M.E. Structure and mechanism of the aberrant ba3-cytochrome c oxidase from *Thermus thermophilus* *The EMBO Journal* **2000**, *19*, 1766-1776. doi: 10.1093/emboj/19.8.1766
13. Mitchell, R.; Rich, P.R. Proton uptake by cytochrome c oxidase on reduction and on ligand binding *Biochim Biophys Acta* **1994**, *1186*, 19-26. doi:10.1016/0005-2728(94)90130-9
14. Kannt, A.; Lancaster, C.R.D.; Michel, H. The coupling of electron transfer and proton translocation: electrostatic calculations on *Paracoccus denitrificans* cytochrome c oxidase *Biophys J* **1998**, *74*, 708-721. doi: 10.1016/S0006-3495(98)73996-7
15. Von Ballmoos, C.; Gennis, R.B.; Ädelroth, P.; Brzezinski, P. Kinetic design of the respiratory oxidases *Proc Natl Acad Sci U S A* **2011**, *108*, 11057-11062. doi: 10.1073/pnas.1104103108
16. Farver, O.; Wherland, S.; Antholine, W.E.; Gemmen, G.J.; Chen, Y.; Pecht, I.; Fee, J.A. Pulse radiolysis studies of temperature dependent electron transfers among redox centers in ba(3)-cytochrome c oxidase from *Thermus thermophilus*: comparison of A- and B-type enzymes *Biochemistry* **2010**, doi: 10.1021/bi100548n
17. Hellwig, P.; Soulimane, T.; Buse, G.; Mäntele, W. Electrochemical, FTIR, and UV/VIS spectroscopic properties of the ba(3) oxidase from *Thermus thermophilus* *Biochemistry* **1999**, *38*, 9648-9658. doi: 10.1021/bi9903401
18. Zheng, X.; Medvedev, D.M.; Swanson, J.; Stuchebrukhov, A.A. Computer simulation of water in cytochrome c oxidase *Biochim Biophys Acta* **2003**, *1557*, 99-107. doi: 10.1016/S0005-2728(03)00002-1

19. Hofacker, I.; Schulten, K. Oxygen and proton pathways in cytochrome c oxidase *Proteins* **1998**, *30*, 100-107. doi: 10.1002/(SICI)1097-0134(199801)30:1<100::AID-PROT9>3.0.CO;2-S
20. Kim, Y. C.; Wikström, M.; Hummer, G. Kinetic gating of the proton pump in cytochrome c oxidase *Proc Natl Acad Sci* **2009**, *106*, 13707–13712. doi: 10.1073/pnas.0903938106
21. Wiertz, F. G.; Richter, O. M.; Ludwig, B.; de Vries, S. Kinetic resolution of a tryptophan-radical intermediate in the reaction cycle of *Paracoccus denitrificans* cytochrome c oxidase *J Biol Chem* **2007**, *282*, 31580-31591. doi: 10.1074/jbc.M705520200
22. De Vries, S. The role of the conserved tryptophan272 of the *Paracoccus denitrificans* cytochrome c oxidase in proton pumping *Biochim Biophys Acta* **2008**, *1777*, 925-928. doi: 10.1016/j.bbabo.2008.05.008
23. Tsukihara, T.; Shimokata, K.; Katayama, Y.; Shimada, H.; Muramoto, K.; Aoyama, H.; Mochizuki, M.; Shinzawa-Itoh, K.; Yamashita, E.; Yao, M.; Ishimura, Y.; Yoshikawa, S. The low-spin heme of cytochrome c oxidase as the driving element of the proton-pumping process *Proc Natl Acad Sci U S A* **2003**, *100*, 15304-15309. doi: 10.1073/pnas.2635097100
24. Yoshikawa, S. and Shimada, A. The mechanism of Cytochrome c Oxidase *Chem. Rev.* **2015**, doi: 10.1021/cr500266a
25. Rauhamäki, V.; Wikström, M. The causes of reduced proton-pumping efficiency in Type B and C respiratory heme-copper oxidases, and in some mutated variants of type A *Biochim Biophys Acta* **2014**, *1837*, 999-1003. doi: 10.1016/j.bbabo.2014.02.020
26. Werner, C.; Richter, O.-M. H.; Ludwig, B. A novel heme a insertion factor gene cotranscribes with the *Thermus thermophilus* cytochrome ba3 oxidase locus *Journal of Bacteriology* **2010**, *192*, 4712-4719. doi: 10.1128/JB.00548-10
27. Chen, Y.; Hunsicker-Wang, L.; Pacoma, R.L.; Luna, E.; Fee, J.A. A homologous expression system for obtaining engineered cytochrome ba3 from *Thermus thermophilus* HB8 *Protein Expr Purif* **2005**, *40*, 299-318. doi: 10.1016/j.pep.2004.11.014
28. Pfützner, U.; Odenwald, A.; Ostermann, T.; Weingard, L.; Ludwig, B.; Richter, O. –M. H. Cytochrome c oxidase (heme aa3) from *Paracoccus denitrificans*: analysis of mutations in putative proton channels of subunit I *J Bioenerg Biomembr* **1998**, *30*, 89-97. doi: 10.1023/A:1020515713103
29. Cherepanov, A. V.; De Vries, S. Microsecond freeze-hyperquenching: development of a new ultrafast micro-mixing and sampling technology and application to enzyme catalysis *Biochim Biophys Acta* **2004**, *1656*, 1-31. doi: 10.1016/j.bbabo.2004.02.006
30. Wiertz, F. G.; Richter, O. M.; Cherepanov, A. V.; MacMillan, F.; Ludwig, B.; de Vries, S. An oxo-ferryl tryptophan radical catalytic intermediate in cytochrome c and quinol oxidases trapped by microsecond freeze-hyperquenching (MHQ) *FEBS Lett* **2004**, *575*, 127-130. doi: 10.1016/j.febslet.2004.08.048
31. Von Wachenfeldt, C.; De Vries, S.; Van der Oost, J. The CuAsite of the caa3-type oxidase of *Bacillus subtilis* is a mixed-valence binuclear copper centre *FEBS lett* **1994**, *340*, 109-113. doi: 10.1016/0014-5793(94)80182-7
32. Yu, M. A.; Egawa, T.; Yeh, S.-R.; Rousseau, D. L.; Gerfen, G. J. EPR characterization of ascorbyl and sulfur dioxide anion radicals trapped during the reaction of bovine Cytochrome c Oxidase with molecular oxygen *J Magn Reson* **2010**, *203*, 213-219. doi: 10.1016/j.jmr.2009.12.017
33. MacMillan, F.; Budiman, K.; Angerer, H.; Michel, H. The role of tryptophan 272 in the *Paracoccus denitrificans* cytochrome c oxidase *FEBS letters* **2006**, *580*, 1345-1349. doi: 10.1016/j.febslet.2006.01.054
34. Werner, C. Identifizierung von CbaX – ein Biogenesefaktor für die Cytochrom ba3 Oxidase aus *Thermus thermophilus* *Dissertation zur Erlangung des Doktorgrades der Naturwissenschaften* **2010**
35. Szundi, I.; Cappuccio, J.; Einarsdottir, O. Amplitude analysis of single-wavelength time-dependent absorption data does not support the conventional sequential mechanism for the reduction of dioxygen to water catalyzed by bovine heart cytochrome c oxidase *Biochemistry* **2004**, *43*, 15746-15758. doi: 10.1021/bi049408p

36. Pilet, E.; Jasaitis, A.; Liebl, U.; Vos, M. H. Electron transfer between hemes in mammalian cytochrome c oxidase *Proc Natl Acad Sci U S A* **2004**, *101*, 16198-16203. doi: 10.1073/pnas.0405032101
37. Ludwig, B. (1986) Cytochrome c oxidase from *Paracoccus denitrificans* *Methods Enzymol.* **126**, 153–159
38. A. Giuffrè, E. Forte, G. Antonini, E. D'Itri, M. Brunori, T. Soulimane, G. Buse, Kinetic properties of ba3 oxidase from *Thermus thermophilus*: effect of temperature. *Biochemistry* **1999**, *38*, 1057-1065
39. Siletsky, S.A.; Konstantinov, A.A. Cytochrome c oxidase: charge translocation coupled to single-electron partial steps of the catalytic cycle *Biochim Biophys Acta* **2012**, *1817*, 476-488. doi: 10.1016/j.bbabi.2011.08.003
40. Popovic, D. M.; Stuchebrukov, A. A. Electrostatic study of the proton pumping mechanism in bovine heart cytochrome c oxidase *Journal of the American Chemical Society* **2004**, *126*, 1858-1871. doi: 10.1021/ja038267w

Supplementary data

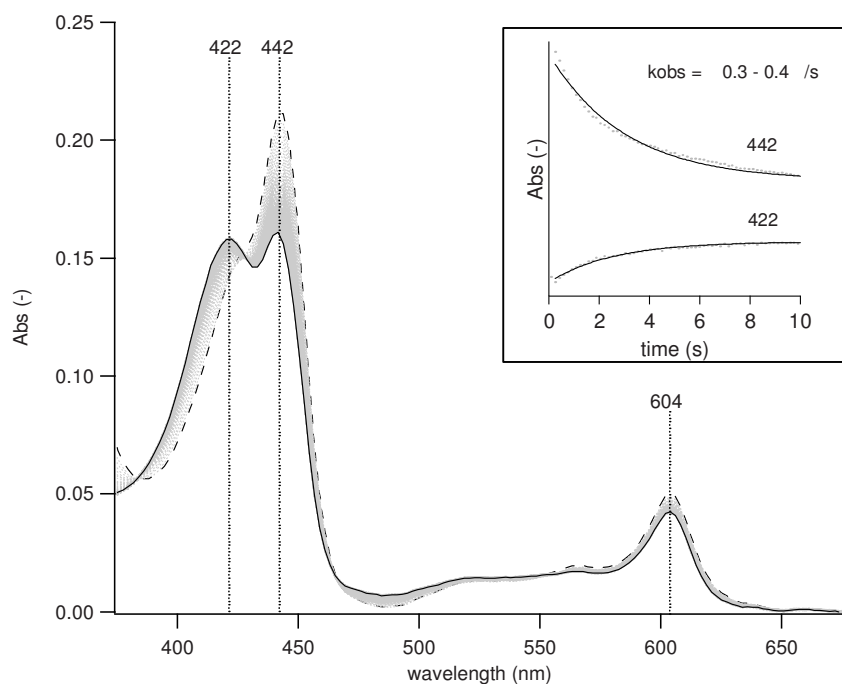


Figure S1:

Kinetic analysis of the oxidation of the fully reduced W272F variant of *P. denitrificans* cytochrome *aa*₃ oxidase at 10 °C. Depicted are the full spectra recorded between 82 ms and 65.5 s of the oxidation by molecular oxygen of the reduced W272F variant, most clearly observed through the absorbance changes at 422 nm, 442 nm and 604 nm. Ascorbate (10 mM) and PES (1 μM) were present to ensure full reduction of the enzyme at the start of mixing with oxygen. The oxygen concentration in the reaction mixture was ~0.6 mM at the start of the reaction. The **inset** shows the kinetic single wavelength data at 422 nm and 442 nm. The single wavelength traces were fitted between 0 s and 10 s reaction time with an exponential ($0.3 \text{ s}^{-1} < k_{\text{obs}} < 0.4 \text{ s}^{-1}$). The extremely low rate and the incompleteness of the oxidation of the W272F enzyme indicates that the enzyme was essentially inactive and is not expected to be capable of reducing O₂ to water.

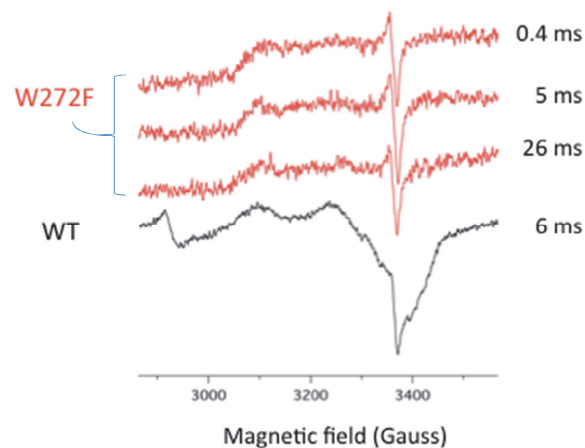


Figure S2:

EPR spectra of the fully reduced W272F variant of *P. denitrificans* cytochrome aa_3 oxidase (top three traces) and wild type enzyme (bottom trace) after reaction with oxygen for the indicated times (for details see legend to Figure S1). All three reaction samples (0.4, 5 and 26 ms) yield a very similar EPR spectrum indicating lack of oxidation. The spectra contain a sharp downward peak at ~ 3370 G, which is due to an artefactual radical produced by the freeze-quench technique. Oxidation of Cu_A and heme a , in the wild type cytochrome aa_3 oxidase from *P. denitrificans* is indicated by the appearance of the signals for heme a and Cu_A (see ^{21,30}). The EPR analysis therefore supports the notion that the W272F mutant is essentially inactive.

Chapter V

Oxoferryl-porphyrin radical catalytic intermediate in cytochrome *bd* oxidases protects cells from formation of reactive oxygen species

Angela Paulus, Sebastiaan Gijsbertus Hendrik Rossius, Madelon Dijk, Simon de Vries

Adapted from:
The Journal of Biological Chemistry, 2012, 287:8830-8838

Abbreviations: QH₂, ubiquinol; ROS, reactive oxygen species; MHQ, microsecond freeze-hyperquenching; DEPMPO, (5-(di-ethoxyphosphoryl)-5-methyl-1-pyrroline N-oxide); dQH₂, decylubiquinol; HRP, horse radish peroxidase.

The superscripts in O¹, Oxy¹, Oxy³, and Red³ refer to the total number of electrons in the heme centers of the enzyme.

The quinol-linked cytochrome *bd* oxidases are terminal oxidases in respiration. These oxidases harbor a low spin heme b_{558} that donates electrons to a binuclear heme b_{595} /heme d center. The reaction with O_2 and subsequent catalytic steps of the *Escherichia coli* cytochrome *bd*-I oxidase were investigated by means of ultra-fast freeze-quench trapping followed by EPR and UV-visible spectroscopy. After the initial binding of O_2 , the O–O bond is heterolytically cleaved to yield a kinetically competent heme d oxoferryl porphyrin-cation radical intermediate (compound I) magnetically interacting with heme b_{595} . Compound I accumulates to 0.75–0.85 per enzyme in agreement with its much higher rate of formation ($20,000\text{ s}^{-1}$) compared with its rate of decay ($1,900\text{ s}^{-1}$). Compound I is next converted to a short lived heme d oxoferryl intermediate (compound II) in a phase kinetically matched to the oxidation of heme b_{558} before completion of the reaction. The results indicate that cytochrome *bd* oxidases like the heme-copper oxidases break the O–O bond in a single four-electron transfer without a peroxide intermediate. However, in cytochrome *bd* oxidases, the fourth electron is donated by the porphyrin moiety rather than by a nearby amino acid. The production of reactive oxygen species by the cytochrome *bd* oxidase was below the detection level of 1 per 1000 turnovers. We propose that the two classes of terminal oxidases have mechanistically converged to enzymes in which the O–O bond is broken in a single four-electron transfer reaction to safeguard the cell from the formation of reactive oxygen species.

Cytochrome *bd* oxidases are membrane-bound heterodimeric terminal oxidases consisting of CydA (57 kDa) and CydB (43 kDa) ¹. These oxidases occur in bacteria and archaea and catalyze the oxidation of ubiquinol or menaquinol ². This reaction is coupled to the generation of a protonmotive force because the four chemical protons consumed per O_2 are taken from the cytoplasmic side of the membrane, whereas the QH_2 -substrate protons are ejected into the periplasm ^{3,4}. Cytochrome *bd* oxidases bear no sequence homology to heme-copper oxidases ¹ and, because they do not pump protons, have a lower bioenergetic efficiency than heme-copper oxidases ^{3,4}. Cytochrome *bd* oxidases generally have a high affinity for oxygen and are suggested to act further as oxygen scavengers and as a protection against H_2O_2 and NO stress ^{5–7}.

Although three-dimensional structures are lacking for cytochrome *bd* oxidases, studies suggest that its three heme groups are all located in CydA. The low spin heme b_{558} is coordinated by His186–Met393, the high spin heme b_{595} by His19, and the chlorin heme d to Glu99 depending on the redox state ^{1,8–15}. The heme normals of b_{558} and b_{595} are parallel to the plane of the membrane ¹⁶, whereas the heme normal of heme d makes an angle of 55° with those of the two other hemes ^{16,17}. A quinone-binding domain has also been identified ^{1,18,19} that stabilizes a semiquinone ²⁰. Spectroscopic studies suggest that hemes d and b_{595} are within 10 \AA ²¹ and form a functional binuclear active site that receives electrons from heme b_{558} , proposed as the direct electron acceptor of QH_2 ^{13,17,22–25}. Raman spectroscopy has identified heme $d^{2+}\text{-}O_2$ (Oxy^1) ³ and heme $d^{4+}\text{=O}$ (F, oxoferryl or compound II) inter-mediate indicating that heme d is the site for binding and conversion of O_2 ^{26–28}.

The current catalytic mechanism, which has been proposed on the basis of flow-flash and stopped-flow kinetic experiments of the reaction between fully reduced enzyme and oxygen, suggests an initial binding of O_2 to heme d to form the Oxy^3 or **A** state ^{29–31}. Oxy^3 is subsequently converted to a peroxy intermediate, **P**, with heme b_{595} and heme d oxidized to their ferric states, while heme b_{558} remains reduced. In the next step (**P** → **F**) electron transfer from heme b_{558} and heme d leads to scission of the O–O bond followed by H_2O release ^{29,30}. The further donation of one electron and a proton to the active site would restore the enzyme to its fully oxidized form O^0 , with a hydroxo-bound heme d iron. However, this form of the

enzyme is probably not part of the normal catalytic cycle³¹. Instead, and under physiological conditions, it is more likely that the two-electron donor QH₂ reduces **F** to Oxy¹ (heme d^{2+} -O₂) followed by reduction by a second QH₂ (yielding Oxy³) to provide the necessary electrons to enter the next catalytic cycle. The as isolated or resting enzyme is usually a mixture of **F** and heme d^{2+} -O₂^{26–28}.

According to the mechanism described above, the O–O bond is broken in two sequential two-electron transfer steps via a peroxy intermediate. This mechanism differs fundamentally from that of the functionally equivalent heme-copper oxidases, which catalyze a single four-electron O–O bond splitting without a peroxy intermediate³². The physiological advantage of the latter mechanism is the possible prevention of ROS. Indeed the production of ROS by the heme-copper oxidases has been found to be undetectably low^{33,34}; in fact (all mitochondrial) ROS production is due to side reactions with O₂ of other respiratory enzymes in their reduced state, notably complex I and complex III^{33–37}. Whether cytochrome *bd* oxidases produce ROS is not known. If they do so, how much ROS is produced and would this be due in consequence to the formation of a peroxy intermediate?

The assignment of a catalytic peroxy intermediate was based solely on the UV-visible spectrum²⁹ and lacks solid biophysical underpinning further preventing conclusions about its possible structure as a side-on, end-on, or heme-bridged peroxy species. To characterize the structure of **P**, the catalytic mechanism of the cytochrome *bd*-I oxidase from *Escherichia coli* was investigated using an ultrafast mixing and freeze-quenching technique (MHQ) that in addition to UV-visible enables EPR spectroscopic analyses^{38,39}.

Our results indicate that cytochrome *bd* oxidases split the O–O bond like the heme-copper oxidases in a single four-electron transfer reaction. However, in cytochrome *bd* oxidases a compound I intermediate is formed, unlike the heme-copper oxidases. The amount of ROS produced by cytochrome *bd* oxidase was below the detection level of 1 per 1000 turnovers. We propose that both classes of terminal oxidases have convergently evolved to enzymes in which the O–O bond is broken in a single four-electron transfer reaction to minimize the cellular production of ROS.

Experimental procedures

Overexpression of Cytochrome bd-I oxidase from E. coli

The cytochrome *bo* and *bd*-II knock-out strain MB30 was a donation by M. Bekker⁴⁰. MB30 was transformed with plasmid pACYC177 containing the *E. coli* CytAB operon overproducing cytochrome *bd*-I. Precultures were grown aerobically in LB medium with ampicillin (50 mg/ml) in a shaking incubator at 37 °C (~175 rpm). Liter flasks of basal glycerol/fumarate minimal medium⁴¹ containing ampicillin (50 mg/ml) were inoculated with 5% of the LB culture, filled to the rim, and closed, creating semi-anaerobic conditions. Cells were allowed to grow at 37 °C in a shaking incubator for 20 h. These starter cultures were used to inoculate (4%) four 25-liter glass vessels with basal glycerol/fumarate medium and ampicillin (5 mg/ml). Cells were grown under hypo-aerobic conditions after nitrogen flushing, while stirring at 30 °C for 65 h.

Purification of Cytochrome bd-I oxidase

After a 25-fold concentration of the cell cultures in a cross-flow filtration system, the cells were harvested by centrifugation (4 °C, 10 min, 9000 g) and washed once with 50 mM Tris-HCl buffer, pH 8. The washed cell pellets were resuspended in the same buffer prior to cell disruption at 1.8 kbar. The resulting suspension was centrifuged (4 °C, 10 min, 3000 g) to remove cell debris. The supernatant was then centrifuged in a Beckman ultracentrifuge (4 °C, 1 h, 100,000 g) to spin down the cell membranes containing the *bd*-I oxidase. Membranes were resuspended in 25 mM MOPS, pH 6.8, 1 mM EDTA and washed once or twice. The enzyme was extracted from the *E. coli* membranes by addition of 1% lauryl maltoside to the solution and incubating while stirring on ice for 15 min. Purification of the membrane-extracted enzyme consisted of a single column chromatography step (Q-Sepharose FastFlow) with 25 mM MOPS buffer, pH 6.8, as the running buffer. Diluted fractions were pooled by activity, concentrated, and stored at 80 °C.

Freeze-quench Experiments

MHQ, EPR, UV-visible experiments, and kinetic simulations were performed as described previously^{38, 39} using the IGOR Pro software from Wavemetrics, Inc. The MHQ setup was modified just before the mixer entry with a stainless steel tubing extension immersed in ethylene glycol at 5 °C to bring the reaction temperature to 1±1 °C. For kinetic experiments, purified enzyme (150 or 300 mM) in 50 mM sodium phosphate buffer, pH 7.8, 5 mM EDTA, 0.05% lauryl maltoside was made anaerobic, reduced with 2 mM sodium dithionite, and subsequently mixed with the same buffer saturated with O₂. EPR spectra were normalized at the intensity of heme *b*₅₉₅ and in separate experiments using an internal CuClO₄ (0.1 mM) standard in the oxygenated buffer before mixing. Data in Fig. 5 represent the average of four independent experiments. UV-visible averaged spectra were corrected for scatter and base line as described previously^{38, 39} and normalized as follows. Normalization is necessary because for the UV-visible experiments, the amounts of cold freeze-quenched powder in the low temperature cuvette is variable. Low temperature reference spectra (not prepared by MHQ) of fully reduced and “as isolated” enzyme (10 mM) were recorded in buffer, and the Soret band maxima relative to 490 nm were determined (1.0 and 0.46, respectively). The major difference in the measured maximal amplitude of the Soret band absorbance is due to the relatively sharp peak of reduced heme *b*₅₅₈, in particular for samples after 100 μs. The relatively broad Soret peaks of the oxidized hemes contribute mainly to the difference 450 – 490 nm, in particular for samples after 100 μs. With these two parameters, the relative intensities of the spectra shown in Fig. 4 were calculated. From these, the fractional amount of reduced heme *b*₅₅₈ was calculated from the spectra in the α-band region. The error in this calculation amounts to ~0.1 heme *b*₅₅₈ per enzyme. For the absorbance at 680 nm, the error was 0.35 per enzyme. The maximal absorbance at 680 nm was taken the same as that of oxidized heme *d* (cf. Ref. 29).

Determination of ROS

Spin trapping assays were performed with 25 mM DEPMPO⁴² in the same buffer as above. The reaction was started by addition of 0.1 mM *bd*-I oxidase or 200 mM dQH₂, both, or both in the presence of either catalase (1 unit) or superoxide dismutase (1 unit). The 200 mM dQH₂ is fully oxidized in 20 s. Superoxide was prepared from solid KO₂ in 1 M NaOH. The DEPMPO superoxide adduct has a half-life time of 17 min⁴². Room temperature EPR spectra were recorded in a 100-ml aqueous sample cell 120 s after addition of the reagents and

subsequently after 240 and 360 s. The spectra in Fig. 7 are the average of these three spectra. At longer reaction times, a background DEPMPO radical developed in the presence of dQH₂. Similar experiments with 400 mM ferrous cytochrome *c* + 0.1 mM *Paracoccus denitrificans* cytochrome *aa*₃ oxidase produced a background signal after 200 s, limiting the detection level of the assay with cytochrome *aa*₃ oxidase to one ROS per 250 turnovers. The Amplex Red hydrogen peroxide/peroxidase assay was performed according to the manufacturer's protocol (Invitrogen). The final assay volume of 80 µl each consisted of 50 µl of the Amplex Red reagent/HRP working solution; to this 30 µl of buffer was added yielding the same final enzyme and reagent concentrations as used for EPR. The formation of resorufin was monitored at 550 nm in an HP Agilent 8453 diode array spectrophotometer in 1-min intervals after manual mixing of the enzymatic solution with the reagent working solution. All assays were performed at room temperature, and a background trace was recorded for each assay. The background reaction with dQH₂ limits the sensitivity of the assay to 1 H₂O₂ per 1000 turnovers of the cytochrome *bd* oxidase. The assay could not be performed successfully with cytochrome *aa*₃ oxidase because of spectral overlap of resorufin and ferrous cytochrome *c*.

Results

Heme d Oxoferryl Porphyrin π -Cation Radical Intermediate (Compound I) Detected by EPR Spectroscopy

To study the mechanism of O–O bond splitting by the cytochrome *bd* oxidase, single turnover experiments were performed at 1 °C to slow down the reaction. After the reaction between reduced enzyme and O₂, intermediates were trapped by means of freeze-quenching at times ≥ 100 µs and analyzed by EPR and low temperature UV-visible spectroscopy.

The EPR spectrum of as-isolated cytochrome *bd* oxidase displays resonances from two high spin heme species, the axial heme *d* ($g \sim 6$) and the rhombic heme *b*₅₉₅ ($g_x \sim 6.2$ and $g_y \sim 5.7$) and a third signal from the low spin heme *b*₅₅₈ ($g_z \sim 3.58$) (cf. Fig. 1)^{24,43}. The reduced enzyme is EPR-silent. After reacting for 100 µs, heme *b*₅₉₅ became fully oxidized (Fig. 1, middle trace), whereas only ~0.1–0.2 heme *d* had converted to the ferric state. The middle trace in Fig. 1 further shows a previously undetected intermediate at 3100–3500 G, which is argued below to be a compound I derivative of heme *d*. The new EPR signal (Fig. 2 and supplemental Fig. S1) consists of three overlapping signals arising from three rhombic $S = 1/2$ spin systems when recorded at 4.2 K. At higher temperatures the line shapes of the three EPR signals change and coalesce at 77 K into a single rhombic signal with g values that are the average of the individual signals (Table 1 and supplemental Fig. S1). At 4.2 K the integrated intensity of the three signals together accounts for 0.75–0.85 spins per enzyme. The unusual temperature dependence of the EPR signals is due to a magnetic dipolar interaction between oxidized heme *b*₅₉₅ and the compound I, a conclusion that will be explained below.

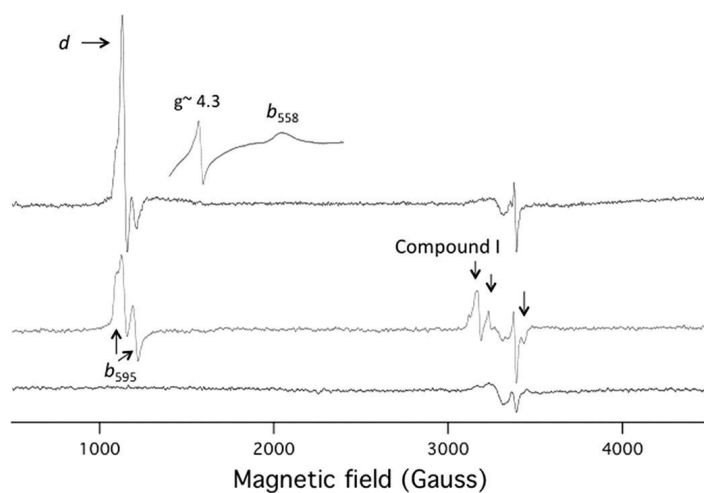


Figure 1: EPR spectra of freeze-quenched samples of cytochrome *bd* oxidase. **Top**, as isolated enzyme (“infinite time”); **middle**, after reaction for 100 μ s with O_2 ; **bottom**, fully reduced enzyme (“zero time”). The (partial) upper spectrum shows the g_z resonance of the low spin heme b_{558} at $g = 3.58$ from a 25-fold concentrated as isolated enzyme solution; the peak at $g = 3.58$ is too weak to be detected in freeze-quenched samples. The peak at $g = 4.3$ is from adventitious iron, the broad peak around 3200 G is from adventitious Cu^{2+} in the cavity, and the sharp signal at 3380 G is due to the freeze-quench procedure. EPR conditions are as follows: Microwave frequency, 9.45 GHz; modulation amplitude, 0.5 millitesla; microwave power, 20 microwatts; temperature, 4.2 K. Full traces are displayed at the same gain.

Table 1
Compound I EPR parameters

Compound I type	g_x	g_y	g_z
Signal at 77 K	2.157	2.112	1.973
Signal 1 at 4.2 K	2.173	2.092	1.973
Signal 2 at 4.2 K	2.158	2.128	1.973
Signal 3 at 4.2 K	2.146	2.131	1.973

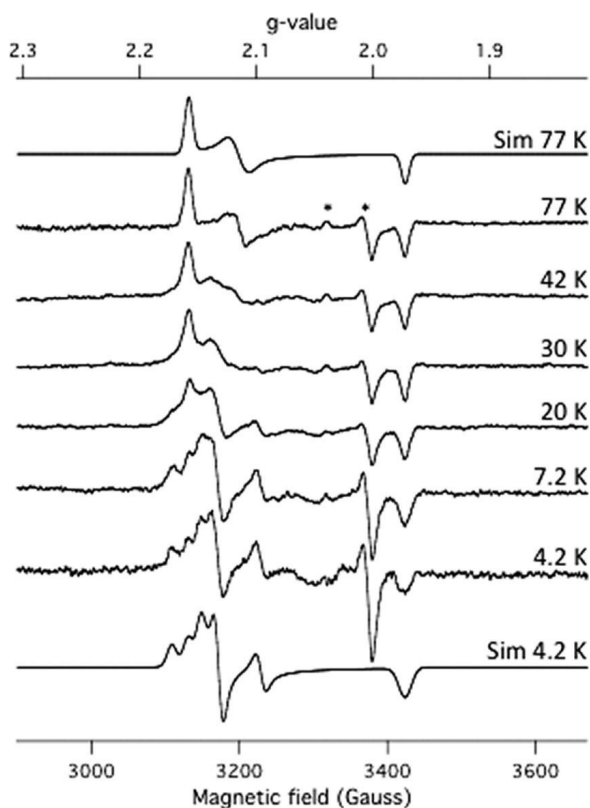


Figure 2: EPR spectra of compound I (after 100 s) at different temperatures between 4.2 and 77 K and simulations. The EPR spectrum recorded at 4.2 K is simulated as a sum of three signals in a ratio of 0.4:0.3:0.3 for signal 1, signal 2, and signal 3, respectively. The intensities of the spectra are corrected for differences in temperature, microwave power (20 microwatt to 5 milliwatts), and gain. The dots indicate the artificial signals due to the freeze-quench procedure.

The magnetic properties of compound I are well understood (supplemental material)^{44, 45}. Briefly, compound I comprises an $S = 1$ heme oxoferryl center ($\text{Fe}^{4+}=\text{O}$) that is magnetically coupled to a $S = 1/2$ porphyrin π -cation radical. The coupling of the two spins yields three Kramer's doublets (*cf.* Fig. 3B) yielding either an $S = 1/2$ or $S = 3/2$ ground state, which depends on the relative magnitudes and signs of the Heisenberg exchange interaction (J) between the $\text{Fe}^{4+}=\text{O}$ and the porphyrin radical and further on the zero-field splitting (D) of the $S = 1$ species. The finding here that the three g values are close to $g = 2$ indicates a total spin of $S = 1/2$ for the ground state of the compound I. The Kramer doublets are separated in energy by an amount Δ ($\sim D$) and J . Because Δ is usually quite small, $20 - 40 \text{ cm}^{-1}$, compound I species follow a two-phonon Orbach relaxation mechanism. The presence of a low-lying first excited state will also result in significant loss of spin intensity at temperatures greater than (*i.e.* above $\sim 30 \text{ K}$). Hence, to validate the assignment as compound I, both the relaxation behavior and the ground state population were determined (Fig. 3). Both these experiments should yield a similar value for Δ ⁴⁶.

The increase of the relaxation rate upon increasing the temperature follows an Orbach relaxation mechanism at $T > 4.2$ K (Fig. 3A) for a first excited state at $\Delta = 36.8 \pm 4.8$ cm^{-1} . The decrease of spin intensity corresponds to the presence of excited states that are 32.2 ± 10.4 cm^{-1} (Δ) and 33.9 ± 11.7 cm^{-1} ($\Delta + J$), respectively, above the ground state (Fig. 3B). The latter two values indicate a small value for J of ~ 2 cm^{-1} or $\Delta < 0.1 J$. Such a small value for J (either negative or positive) relative to Δ (or D) is consistent with g values close to $g = 2$ (Table 1), and in fact is quite similar to those calculated for the isolated $S = 1$ Fe(IV) system for which $J = 0$ ⁴⁷. The value $g_z = 1.973$ determined here is consistent with a calculated value for D (or Δ) of ~ 30 cm^{-1} ⁴⁷ and close to that determined here. The decrease of the ground state spin population rules out that the EPR signal is derived from a ferric heme peroxy center for which the first excited state lies at > 700 cm^{-1} , determined by the strength of the crystal field (supplemental material)⁴⁸. In addition, the g values would be very unusual for low spin heme centers.

The observation that the compound I EPR signal is split into three signals (Figs. 1 and 2 and supplemental Fig. S1) with similar intensities suggests that compound I is coupled to a nearby anisotropic magnet for which at 4.2 K the relaxation is much slower than that of compound I, whereas at higher temperatures the reverse holds. At $T > 60$ K, the relaxation of this magnet is so fast that the splitting averages out resulting at 77 K in a compound I signal with g values that are the average of those at 4.2 K (Table 1). Previous studies have provided evidence for magnetic interactions between ferric heme d and heme b_{595} ^{9, 24, 43}. We therefore propose an anisotropic magnetic dipolar interaction between the heme d -derived compound I and heme b_{595} . At high temperatures, the relaxation of the ferric heme b_{595} is much faster than that of compound I, consistent with the detection of an EPR signal of the latter at 77 K but not of heme b_{595} (see supplemental material). Interestingly, the splitting is much more pronounced in the $g_{x,y}$ resonances than in the g_z peak. The g_z is directed along the $\text{Fe}^{4+}=\text{O}$ bond, perpendicular to the plane of heme d . Because the angle between the heme d and heme b_{595} normals is $\sim 55^\circ$ ^{16, 17}, which is close to the magic angle of 54.7° at which the magnetic dipolar coupling is zero, the small splitting in the g_z resonance is consistent with this angle determined by other methods. We conclude that the new EPR signal is from a heme d oxoferryl porphyrin π -cation radical in dipolar magnetic interaction with heme b_{595} ³⁺.

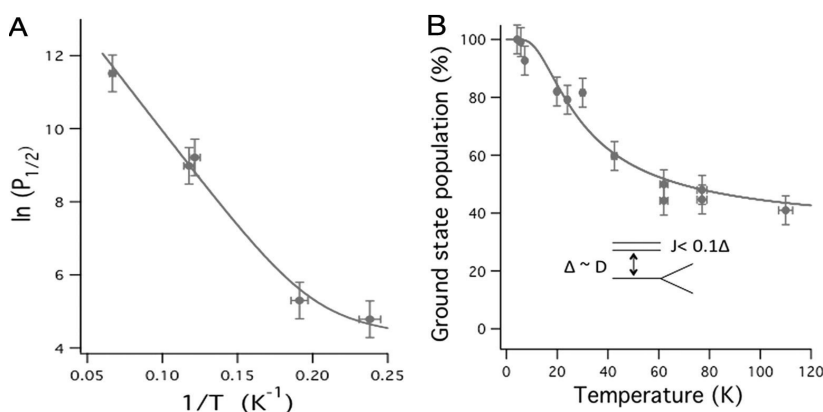


Figure 3: Saturation behavior (A) and ground state population (B) of compound I as a function of temperature. Data in A were fitted to $\ln(P_{1/2}) = \ln(A \cdot T + B \cdot (e^{\Delta/T} - 1)^{-1})$, where $A \cdot T$ represents the direct

process ($A = 22$ microwatts/K) and the second term the Orbach relaxation ($B = 4.2$ megawatts). Ground state population in B was calculated with the equation: $(1 + e^{-\Delta/T} + e^{-(\Delta+J)/T})^{-1}$. Values Δ of and $(\Delta + J)$ are given in the text. The three Kramer's doublets and their energy separations are shown in the lower inset in B .

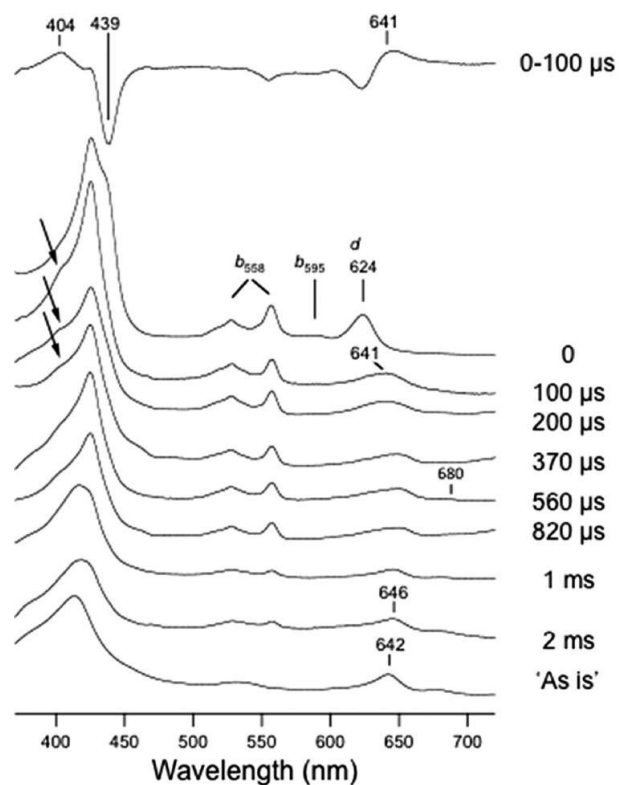


Figure 4: Low temperature absolute UV-visible spectra of reduced cytochrome *bd* oxidase reacted with O_2 for different times. The upper trace is the "time 0" (reduced enzyme) minus 100- μ s difference spectrum, and the lower trace is the spectrum of the as-isolated enzyme. Spectra were normalized in respect to each other as described under "Experimental Procedures." Arrows indicate the absorbance of compound I.

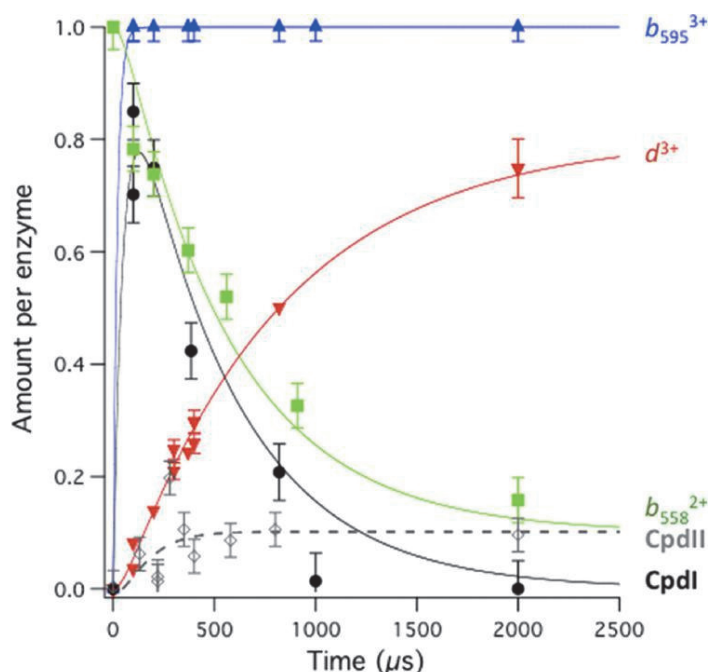


Figure 5: Kinetic traces of the various reaction intermediates determined from the EPR and UV-visible measurements and simulations ($\text{Red}^3 \rightarrow \text{Cpdl} \rightarrow \text{CpdlI} \rightarrow \text{Oxy}^1$ kinetic sequence, see Fig. 6) using the parameters listed in Table 2. Because the system evolves to a quasi-steady state (see text), the traces of b_{558}^{2+} and d^{3+} (Oxy^1) are calculated for a total change of 0.9 and 0.8 per enzyme, respectively. For the same reason the kinetics of CpdlI were calculated by the “approach to steady-state method” employing the relevant equations in Ref. 39 using the rate constants in Table 2. Data for heme b_{595} , heme d , and Cpdl are from EPR (e.g. supplemental Fig. S2) and those for CpdlI and heme b_{558} from the UV-visible spectra in e.g. Fig. 4.

Compound I Species Detected by UV-visible Spectroscopy

Fig. 4 shows low temperature UV-visible spectra of the reaction between cytochrome *bd*-I oxidase and O_2 . After 100 μs , the peak of heme d at 624 nm has shifted to 641 nm and broadened considerably, whereas heme b_{558} has remained largely reduced (75–85%). In agreement with the EPR spectra (Fig. 1), heme b_{595} is completely oxidized after 100 μs indicated by the disappearance of the broad absorbance around 595 nm and the appearance of a negative peak in the Soret region (439 nm) in the “0–100- μs ” difference spectrum⁴⁹. This difference spectrum further indicates the appearance of a broad absorbance at 404 nm. The peak at 404 nm (and that at 641 nm) is ascribed to that of the heme d compound I intermediate. In agreement with this are the blue shifts from ~430 nm for the ferrous state to 404 nm and the low extinction, ~25–30% of the intensity of the Soret band of heme b_{595} , two features also observed for compound I from horseradish peroxidase⁵⁰. The compound I absorbance is also directly visible in the absolute spectra of Fig. 4 as a shoulder at 404 nm on the Soret peaks of hemes b_{595} and b_{558} . This shoulder disappears as the reaction proceeds.

Difference spectra calculated for times 100 μ s did not resolve the 404-nm band as well as after 100 μ s because of spectral interference from hemes b_{558} and d , the latter changing to the ferric state at longer reaction times. In contrast, the intermediate state obtained after 100 μ s is quite pure, *i.e.* full oxidation of heme b_{595} , > 75% change of heme d^{2+} to heme $d^{4+}=O$, < 25% heme d^{3+} , and < 25% change of heme b_{558}^{2+} to b_{558}^{3+} .

Kinetic Analysis

The time-dependent redox changes calculated from UV-visible and EPR spectra are shown in Figs. 4 and 5 and supplemental Fig. S2. The formation of compound I within 100 μ s is followed by the slower oxidation of heme b_{558} (Fig. 4) and by optical changes in the Soret region and around 640 nm because of formation of heme d^{3+} , also observed by an increase of the signal at $g \sim 6$ (supplemental Fig. S2). In the same time window, the EPR signal of compound I disappears (supplemental Fig. S2). The absorbance changes at 680 nm (**F**) are small and difficult to analyze due to sloping base lines. **F** is estimated to accumulate to ~ 0.1 per enzyme and did not show the transient behavior expected for a true intermediate. The lack of this transient and the remaining 15–20% reduction of heme b_{558} after 2 ms are explained by the slight excess of reductant present (sodium dithionite), which renders the oxidation kinetics not pure single turnover; instead, the enzyme reaches a quasi steady state. Here, heme d is $\sim 80\%$ oxidized with the remainder present as **F** and a small amount of heme $d^{2+}-O_2$ represented by the absorbance at 646 nm (*cf.* ^{26–28}). This electronic distribution is in agreement with experiments that show that **F** and Oxy^1 are dominant steady-state species ⁵¹. Note that the 680 nm band is also present in the enzyme as isolated (Fig. 4) ^{26–28} but that heme $d^{2+}-O_2$ is absent in our preparation.

Table 2:

Rate constants at 1 °C for various intermediate steps of the cytochrome *bd* oxidase catalytic cycle

Species	k _{s⁻¹}
b_{595}^{2+} oxidation ^a	20,000 \pm 2000
Compound I decay	1950 \pm 200
b_{558}^{2+} oxidation	1850 \pm 400
Compound II decay	7300 \pm 2500
d^{3+} formation	1250 \pm 100

^a Data include the rate of O_2 binding. Estimated from Ref. 29 and this work.

EPR spectroscopy (supplemental Fig. S2) shows that as compound I disappeared and heme d^{3+} is formed, the line shape of heme b_{595} , in particular the $g \sim 5.7$ derivative-like resonance, shifts by ~ 10 G. The small shift is interpreted as a change in magnetic interaction between heme b_{595} and heme d , as the latter changes from the compound I state to the ferric state. After 2 ms, the EPR spectrum of the high spin heme centers is similar to that of the “as-isolated enzyme.”

The kinetic profiles of the various intermediates determined from the UV-visible and EPR spectra are shown in Fig. 5, and the calculated rate constants are listed in Table 2. The rates of oxygen binding, heme b_{595} oxidation, and compound I formation were too fast to be determined directly in this study, even at the reaction temperature of 1 °C, where these reactions appear completed within 100 μ s. Flow-flash experiments ²⁹ indicate a 10-fold lower

rate of oxidation of heme b_{558} than the preceding reactions suggesting a (combined) rate of $\sim 20,000\text{ s}^{-1}$ for oxygen binding, oxidation of heme b_{595} , and compound I formation (*cf.* Table 2). The accumulation of compound I to 0.75–0.85 per enzyme is consistent with the ~ 10 -fold higher rate of its formation than its rate of decay (Table 2).

Significantly, the rates of compound I decay and oxidation of heme b_{558} are the same, but the formation of heme d^{3+} is slower (Table 2). The similar rates of compound I decay and heme b_{558} oxidation are consistent with the view that electron transfer from heme b_{558} leads to direct reduction of the porphyrin π -cation radical, thus producing the ferryl form of heme d or **F**. In the subsequent reaction **F**, which barely accumulates, is rapidly reduced further, by excess reductant, yielding heme d^{3+} . The rate of compound II reduction is calculated at $\sim 7300\text{ s}^{-1}$ based on the experimental time delay between compound I decay and heme d^{3+} formation and the accumulation to 0.1 per enzyme estimated from the 680 nm absorbance.

Discussion

Catalytic Mechanism

The reduction of O_2 by reduced cytochrome *bd* oxidase will in general not yield clean (pseudo-) first-order traces because the complete reaction needs four electrons, and the enzyme can store only three. In our experiments, the small excess reductant leads to rapid net 4–5 electron transfer leaving some reduced enzyme after 2 ms that is slowly oxidized in a quasi-steady state in which excess reductant and remaining oxygen are exhausted. In the flow-flash experiments, **F** was formed almost stoichiometrically in 47 ms, apparently corresponding to a net three-electron reaction²⁹. In the next step (~ 1.1 ms), **F** was converted to a mixture of oxidized and oxygenated enzyme as observed here. The transient kinetics of **F** in the flow-flash experiments show that it is a true intermediate. The nontransient kinetics of **F** in our experiments might suggest that it is not part of the main catalytic pathway but, for example, in rapid equilibrium with another/unknown intermediate. However, because the reaction proceeds to a quasi-steady state, also a true intermediate may show nontransient kinetics.

The optical and kinetic properties of the intermediate formed after 100 μs with peaks at 404 and 641 nm are the same as those observed for the peroxy intermediate **P** formed after 4.5 μs (peak at 635 nm at 20 °C²⁹). The assignment as a peroxy intermediate by the authors was based solely on UV-visible spectroscopy and on the notion that formation of compound I “is not very likely, because it would require oxidation of a nearby amino acid residue or the porphyrin ring that is energetically unfavorable in the presence of the reduced heme b_{558} in the proximity of the catalytic center”²⁹. Here, we provide both EPR and UV-visible spectroscopic evidence that the intermediate labeled **P** in Ref. 29 is in fact compound I. We therefore propose a new reaction mechanism for the cytochrome *bd* oxidase (Fig. 6). Accordingly, after binding of O_2 to the fully reduced enzyme (Red^3) in which Oxy^3 is formed, the O–O bond is split in a single four-electron reaction producing within 100 μs the compound I intermediate (CpdI or **F**⁺*) without formation of a peroxy state. Oxygen bond breaking is accomplished in an apparently concerted electron transfer reaction from heme b_{595} , heme d (two electrons), and the heme d porphyrin moiety. The obligatory proton donor needed for O–O bond splitting remains unknown. The subsequent internal electron transfer from heme b_{558} (525 μs) converts CpdI into CpdII (or **F**). Rapid electron transfer from dithionite or from endogenous QH_2 (1–2 electrons per enzyme) produces a largely oxidized enzyme after 2 ms and a mixture of some heme b_{558}^{2+} , Oxy^1 , and CpdII. The formation of

kinetically competent compound I and II intermediates by the cytochrome *bd* oxidases resembles the mechanism of plant peroxidases and eukaryotic catalases. The catalytic mechanism of cytochrome *bd* oxidases is similar to that of heme-copper oxidases, which also break the O–O bond in a single four-electron transfer. However, in the heme-copper oxidases, **P_M** rather than CpdI is formed initially, *i.e.* a heme *a*₃ oxoferryl intermediate plus an amino acid radical, most likely a tyrosine radical⁵².

ROS Production

Breaking the O–O bond in a single four-electron transfer represents a mechanism to protect the cell from ROS production during aerobic growth. Possible production of ROS was determined by the EPR spin trapping assay with DEPMPO⁴² and the UV-visible based Amplex Red reagent assay. The sensitivity of the Amplex Red assay is limited by a slow background reaction and the spin trapping method by the DEPMPO-derivative stability, its EPR detection limit, and the dQH₂ solubility of 200 mM limiting the number of turnovers. Both methods indicated that the production of ROS by cytochrome *bd* oxidase was below the detection limit of 1 per 1000 turnovers, *i.e.* less than 0.1 mM O₂^{•−} or H₂O₂ produced per 100 mM O₂ consumed (*cf.* Fig. 7). The production of ROS by purified *P. denitrificans* cytochrome *aa*₃ oxidase was determined at 1 per 250 turnovers, a relatively high value because of the presence of a background signal. However, the production of ROS by the similar mitochondrial cytochrome *aa*₃ oxidase has previously been estimated to be much lower than 1/250 turnovers^{33–35, 53}. In fact ROS production is too low to detect mainly due to the contribution by other respiratory enzymes. *In vivo* ROS production by mitochondria is estimated at 1 per 1000 turnovers of the respiratory chain⁵³ and possibly similar in bacteria⁵⁴. If terminal oxidases indeed produce negligible amounts of ROS, as is generally believed, their contribution should be below 1 per 10,000 turnovers, a value too low to measure directly with current techniques. Because both classes of terminal oxidases break the O–O bond in a single four-electron transfer, significant production of H₂O₂ and OH• is considered unlikely, but production of O₂^{•−} cannot be completely prevented because of the Fe²⁺-O₂ ↔ Fe³⁺-O₂^{•−} equilibrium in the initial oxy-derivative. Resonance Raman spectroscopy on the two classes of terminal oxidases and oxymyoglobin indeed shows considerable superoxide character for the oxy-complexes^{27, 55, 56}. The release of O₂^{•−} by oxymyoglobin is, however, very slow (*t*_{1/2} ~10 h⁵⁷) among others because of its high midpoint potential (~0.1 V)⁵⁸. In the terminal oxidases the midpoint potentials of the hemes are even higher (~0.3 V)^{43, 52}, which would most likely result in even slower release of O₂^{•−}. In addition, the oxy-complexes of the terminal oxidases are rapidly (~< 10 μs) converted to CpdI or to **P_M** yielding a calculated O₂^{•−} production of <1 per 10⁹ turnovers, far below current detection levels and far below that of other respiratory complexes.

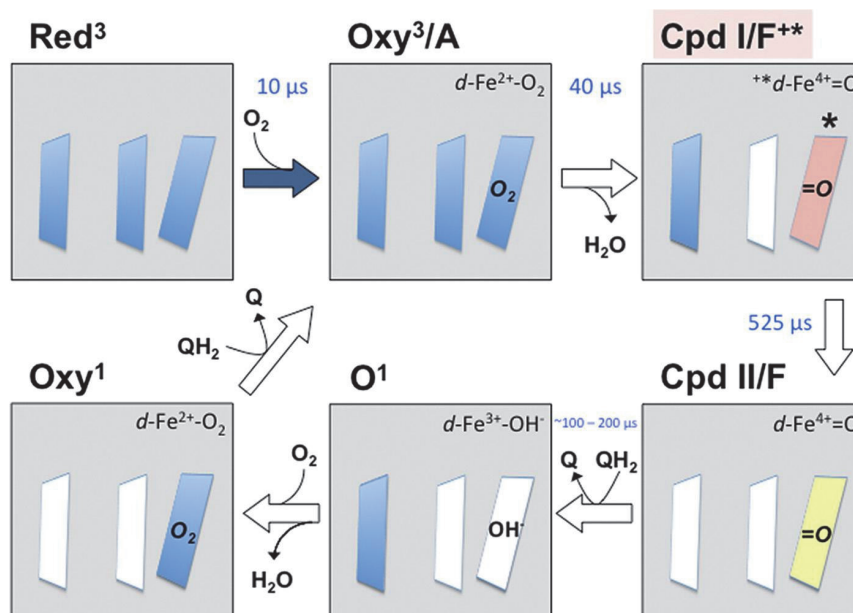


Figure 6: Proposal for the catalytic cycle of cytochrome *bd* oxidase. Half-lives (in microseconds) of the various steps are indicated. Protons needed in some of the reactions are omitted from the figure. The heme normals of heme *d* and heme *b*₅₉₅ make an angle of 55°, suggested here by the nonparallel porphyrin plane of heme *d*, although not drawn at 55°. See text for further explanation of the catalytic mechanism. The superscripts in O¹, Oxy¹, Oxy³, and Red³ refer to the total number of electrons in the heme centers of the enzyme.

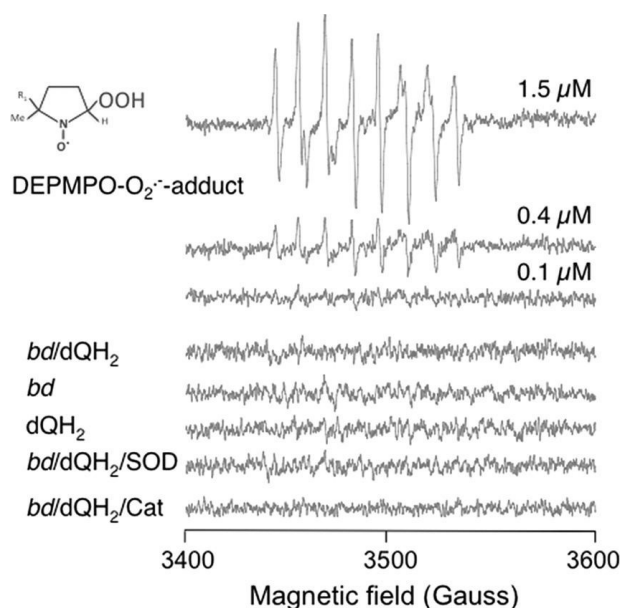


Figure 7: Room temperature EPR spectra of DEPMPPO- $\text{O}_2^{\cdot-}$ adduct (upper three spectra) and of cytochrome *bd* oxidase reacted in various ways to detect possible formation of the DEPMPPO- $\text{O}_2^{\cdot-}$ or other (e.g. OOH^{\cdot}) adducts during the reaction. None are seen in the complete reaction (*bd/dQH₂*), or in the controls with superoxide dismutase (*bd/dQH₂/SOD*), or catalase (*bd/dQH₂/Cat*), or in the presence of only enzyme (*bd*) or substrate (*dQH₂*). The DEPMPPO- $\text{O}_2^{\cdot-}$ adduct at 1.5 μM was prepared as described under “Experimental Procedures.” The traces of 0.4 and 0.1 μM were calculated from the 1.5 μM spectrum by multiplication of 0.27 and 0.067, respectively, and then adding a random noise function with the same noise as the experimental spectrum. The DEPMPPO- $\text{O}_2^{\cdot-}$ detection limit is below $\sim 0.1 \mu\text{M}$, because in this (calculated) spectrum the S/N ratio is $\sim <1$. Microwave frequency, 9.79 GHz, modulation amplitude, 0.1 millitesla, microwave power, 20 milliwatt.

It appears that the cytochrome *bd* oxidases and heme-copper oxidases have evolved independently to minimize if not prevent production of ROS by very rapidly breaking the O–O bond in an apparently concerted single four-electron transfer and protonation reaction. To do so, both classes of terminal oxidases harbor a compact bi-metallic center integrated with a nearby proton donor. This bi-metallic center contains one metal ion able to attain the Fe^{4+} state and an additional redox center, either the porphyrin ring itself, or a nearby amino acid as donor of the fourth electron. In the single heme-containing peroxidases, catalases, and cytochrome P_{450} enzymes, the same natural variation is observed that the porphyrin ring or a nearby amino acid such as Trp or Tyr donates the extra electron to cleave the peroxy O–O bond^{44, 45, 59 – 61}.

References

1. Osborne, J. P., and Gennis, R. B. (1999) Sequence analysis of cytochrome bd oxidase suggests a revised topology for subunit I. *Biochim. Biophys. Acta* 1410, 32–50
2. Schröder, I., and de Vries, S. (2008) in *Archaea: New Models for Prokaryotic Biology* (Blum, P., ed) pp. 1–26, *Caister Academic Press*, Hethersett, Norwich, UK
3. Puustinen, A., Finel, M., Haltia, T., Gennis, R. B., and Wikström, M. (1991) Properties of the two terminal oxidases of *Escherichia coli*. *Biochemistry* 30, 3936–3942
4. Borisov, V. B., Murali, R., Verkhovskaya, M. L., Bloch, D. A., Han, H., Gennis, R. B., and Verkhovsky, M. I. (2011) Aerobic respiratory chain of *Escherichia coli* is not allowed to work in fully uncoupled mode. *Proc. Natl. Acad. Sci. U.S.A.* 108, 17320–17324
5. Baughn, A. D., and Malamy, M. H. (2004) The strict anaerobe *Bacteroides fragilis* grows in and benefits from nanomolar concentrations of oxygen. *Nature* 427, 441–444
6. Mason, M. G., Shepherd, M., Nicholls, P., Dobbin, P. S., Dodsworth, K. S., Poole, R. K., and Cooper, C. E. (2009) Cytochrome bd confers nitric oxide resistance to *Escherichia coli*. *Nat. Chem. Biol.* 5, 94–96
7. Borisov, V. B., Forte, E., Sarti, P., Brunori, M., Konstantinov, A. A., and Giuffrè, A. (2006) Nitric oxide reacts with the ferryl-oxo catalytic intermediate of the CuB-lacking cytochrome bd terminal oxidase. *FEBS Lett.* 580, 4823–4826
8. Borisov, V. B., Belevich, I., Bloch, D. A., Mogi, T., and Verkhovsky, M. I. (2008) Glutamate 107 in subunit I of cytochrome bd from *Escherichia coli* is part of a transmembrane intraprotein pathway conducting protons from the cytoplasm to the heme b595/heme d active site. *Biochemistry* 47, 7907–7914
9. Jünemann, S. (1997) Cytochrome bd terminal oxidase. *Biochim. Biophys. Acta* 1321, 107–127
10. Kaysser, T. M., Ghaim, J. B., Georgiou, C., and Gennis, R. B. (1995) Methionine 393 is an axial ligand of the heme b558 component of the cytochrome bd ubiquinol oxidase from *Escherichia coli*. *Biochemistry* 34, 13491–13501
11. Mogi, T. (2009) Probing the heme d-binding site in cytochrome bd quinol oxidase by site-directed mutagenesis. *J. Biochem.* 145, 763–770
12. Mogi, T., Endou, S., Akimoto, S., Morimoto-Tadokoro, M., and Miyoshi, H. (2006) Glutamates 99 and 107 in transmembrane helix III of subunit I of cytochrome bd are critical for binding of the heme b595-d binuclear center and enzyme activity. *Biochemistry* 45, 15785–15792
13. Sun, J., Kahlow, M. A., Kaysser, T. M., Osborne, J. P., Hill, J. J., Rohlf, R. J., Hille, R., Gennis, R. B., and Loehr, T. M. (1996) Resonance Raman spectroscopic identification of a histidine ligand of b595 and the nature of the ligation of chlorine d in the fully reduced *Escherichia coli* cytochrome bd oxidase. *Biochemistry* 35, 2403–2412
14. Tsubaki, M., Uno, T., Hori, H., Mogi, T., Nishimura, Y., and Anraku, Y. (1993) Cytochrome d axial ligand of the bd-type terminal quinol oxidase from *Escherichia coli*. *FEBS Lett.* 335, 13–17
15. Yang, K., Zhang, J., Vakkasoglu, A. S., Hielscher, R., Osborne, J. P., Hemp, J., Miyoshi, H., Hellwig, P., and Gennis, R. B. (2007) Glutamate 107 in subunit I of the cytochrome bd quinol oxidase from *Escherichia coli* is protonated and near the heme d/heme b595 binuclear center. *Biochemistry* 46, 3270–3278
16. Ingledew, W. J., Rothery, R. A., Gennis, R. B., and Salerno, J. C. (1992) The orientation of the three hemes of the “in situ” ubiquinol oxidase, cytochrome bd, of *Escherichia coli*. *Biochem. J.* 282, 255–259
17. Borisov, V. B., Liebl, U., Rappaport, F., Martin, J. L., Zhang, J., Gennis, R. B., Konstantinov, A. A., and Vos, M. H. (2002) Interactions between heme d and heme b595 in quinol oxidase bd from *Escherichia coli*. A photoselection study using femtosecond spectroscopy. *Biochemistry* 41, 1654–1662
18. Yang, F. D., Yu, L., Yu, C. A., Lorence, R. M., and Gennis, R. B. (1986) Use of an azido-ubiquinone derivative to identify subunit I as the ubiquinol-binding site of the cytochrome d terminal oxidase complex of *Escherichia coli*. *J. Biol. Chem.* 261, 14987–14990
19. Zhang, J., Hellwig, P., Osborne, J. P., Huang, H. W., Moënne-Loccoz, P., Konstantinov, A. A., and Gennis, R. B. (2001) Site-directed mutation of the highly conserved region near the Q-loop

- of the cytochrome bd quinol oxidase from *Escherichia coli* specifically perturbs heme b595. *Biochemistry* 40, 8548–8556
20. Hastings, S. F., Kaysser, T. M., Jiang, F., Salerno, J. C., Gennis, R. B., and Ingledew, W. J. (1998) Identification of a stable semiquinone intermediate in the purified and membrane-bound ubiquinol oxidase-cytochrome bd from *Escherichia coli*. *Eur. J. Biochem.* 255, 317–323
 21. Arutyunyan, A. M., Borisov, V. B., Novoderezhkin, V. I., Ghaim, J., Zhang, J., Gennis, R. B., and Konstantinov, A. A. (2008) Strong excitonic interactions in the oxygen-reducing site of bd-type oxidase. The Fe-to-Fe distance between hemes d and b595 is 10 Å. *Biochemistry* 47, 1752–1759
 22. Hata-Tanaka, A., Matsuura, K., Itoh, S., and Anraku, Y. (1987) Electron flow and heme-heme interaction between cytochromes b-558, b-595, and d in a terminal oxidase of *Escherichia coli*. *Biochim. Biophys. Acta* 893, 289–295
 23. Hill, J. J., Alben, J. O., and Gennis, R. B. (1993) Spectroscopic evidence for a heme-heme binuclear center in the cytochrome bd ubiquinol oxidase from *Escherichia coli*. *Proc. Natl. Acad. Sci. U.S.A.* 90, 5863–5867
 24. Jünemann, S., and Wrigglesworth, J. M. (1995) Cytochrome bd oxidase from *Azotobacter vinelandii*. Purification and quantitation of ligand binding to the oxygen reduction site. *J. Biol. Chem.* 270, 16213–16220
 25. Rappaport, F., Zhang, J., Vos, M. H., Gennis, R. B., and Borisov, V. B. (2010) Heme-heme and heme-ligand interactions in the di-heme oxygen-reducing site of cytochrome bd from *Escherichia coli* revealed by nanosecond absorption spectroscopy. *Biochim. Biophys. Acta* 1797, 1657–1664
 26. Kahlow, M. A., Zuberi, T. M., Gennis, R. B., and Loehr, T. M. (1991) Identification of a ferryl intermediate of *Escherichia coli* cytochrome d terminal oxidase by resonance Raman spectroscopy. *Biochemistry* 30, 11485–11489
 27. Poole, R. K., Baines, B. S., Hubbard, J. A. M., Hughes, M. N., and Campbell, N. J. (1982) Resonance Raman spectroscopy of an oxygenated intermediate species of cytochrome oxidase d from *Escherichia coli*. *FEBS Lett.* 150, 147–150
 28. Sun, J., Osborne, J. P., Kahlow, M. A., Kaysser, T. M., Hill, J. J., Gennis, R. B., and Loehr, T. M. (1995) Resonance Raman studies of *Escherichia coli* cytochrome bd oxidase. Selective enhancement of the three heme chromophores of the “as-isolated” enzyme and characterization of the cyanide adduct. *Biochemistry* 34, 12144–12151
 29. Belevich, I., Borisov, V. B., and Verkhovsky, M. I. (2007) Discovery of the true peroxy intermediate in the catalytic cycle of terminal oxidases by real time measurement. *J. Biol. Chem.* 282, 28514–28519
 30. Hill, B. C., Hill, J. J., and Gennis, R. B. (1994) The room temperature reaction of carbon monoxide and oxygen with the cytochrome bd quinol oxidase from *Escherichia coli*. *Biochemistry* 33, 15110–15115
 31. Yang, K., Borisov, V. B., Konstantinov, A. A., and Gennis, R. B. (2008) The fully oxidized form of the cytochrome bd quinol oxidase from *E. coli* does not participate in the catalytic cycle: direct evidence from rapid kinetics studies. *FEBS Lett.* 582, 3705–3709
 32. Babcock, G. T., and Wikström, M. (1992) Oxygen activation and the conservation of energy in cell respiration. *Nature* 356, 301–309
 33. Boveris, A., and Chance, B. (1973) The mitochondrial generation of hydrogen peroxide. General properties and effect of hyperbaric oxygen. *Biochem. J.* 134, 707–716
 34. Hinkle, P. C., Butow, R. A., Racker, E., and Chance, B. (1967) Partial resolution of the enzymes catalyzing oxidative phosphorylation. XV. Reverse electron transfer in the flavin-cytochrome b region of the respiratory chain of beef heart submitochondrial particles. *J. Biol. Chem.* 242, 5169–5173
 35. Cadenas, E., Boveris, A., Ragan, C. I., and Stoppani, A. O. (1977) Production of superoxide radicals and hydrogen peroxide by NADH-ubiquinone reductase and ubiquinol-cytochrome c reductase from beef-heart mitochondria. *Arch. Biochem. Biophys.* 180, 248–257
 36. Dröse, S., and Brandt, U. (2008) The mechanism of mitochondrial superoxide production by the cytochrome bc₁ complex. *J. Biol. Chem.* 283, 21649–21654

37. Kussmaul, L., and Hirst, J. (2006) The mechanism of superoxide production by NADH:ubiquinone oxidoreductase (complex I) from bovine heart mitochondria. *Proc. Natl. Acad. Sci. U.S.A.* 103, 7607–7612
38. Cherepanov, A. V., and De Vries, S. (2004) Microsecond freeze-hyper-quenching. Development of a new ultrafast micro-mixing and sampling technology and application to enzyme catalysis. *Biochim. Biophys. Acta* 1656, 1–31
39. Wiertz, F. G., Richter, O. M., Ludwig, B., and de Vries, S. (2007) Kinetic resolution of a tryptophan-radical intermediate in the reaction cycle of *Paracoccus denitrificans* cytochrome c oxidase. *J. Biol. Chem.* 282, 31580–31591
40. Bekker, M., de Vries, S., Ter Beek, A., Hellingwerf, K. J., and de Mattos, M. J. (2009) Respiration of *Escherichia coli* can be fully uncoupled via the nonelectrogenic terminal cytochrome bd-II oxidase. *J. Bacteriol.* 191, 5510–5517
41. Spencer, M. E., and Guest, J. R. (1974) Proteins of the inner membrane of *Escherichia coli*. Changes in composition associated with anaerobic growth and fumarate reductase amber mutation. *J. Bacteriol.* 117, 954–959
42. Frejaville, C., Karoui, H., Tuccio, B., Le Moigne, F., Culcasi, M., Pietri, S., Lauricella, R., and Tordo, P. (1995) 5-(Diethoxyphosphoryl)-5-methyl-1-pyrroline N-oxide. A new efficient phosphorylated nitrene for the in vitro and in vivo spin trapping of oxygen-centered radicals. *J. Med. Chem.* 38, 258–265
43. Meinhardt, S. W., Gennis, R. B., and Ohnishi, T. (1989) EPR studies of the cytochrome-d complex of *Escherichia coli*. *Biochim. Biophys. Acta* 975, 175–184
44. Fujii, H., Yoshimura, T., and Kamada, H. (1996) ESR studies of A(1u) and A(2u) oxoiron(IV) porphyrin p-cation radical complexes. Spin coupling between ferryl Iron and A(1u)/A(2u) orbitals. *Inorg. Chem.* 35, 2373–2377
45. Houseman, A. L., Doan, P. E., Goodin, D. B., and Hoffman, B. M. (1993) Comprehensive explanation of the anomalous EPR spectra of wild-type and mutant cytochrome c peroxidase compound ES. *Biochemistry* 32, 4430–4443
46. Mandon, D., Weiss, R., Jayaraj, K., Gold, A., Turner, J., Bill, E., and Trautwein, A. X. (1992) Models for peroxidase compound I: generation and spectroscopic characterization of new oxoferryl porphyrin p cation radical species. *Inorg. Chem.* 31, 4404–4409
47. Oosterhuis, W. T., and Lang, G. (1973) Magnetic properties of the t_{42g} configuration in low symmetry crystal fields. *J. Chem. Phys.* 58, 4757–4765
48. Zoppellaro, G., Bren, K. L., Ensign, A. A., Harbitz, E., Kaur, R., Hersleth, H.P., Ryde, U., Hederstedt, L., and Andersson, K. K. (2009) Review. Studies of ferric heme proteins with highly anisotropic/highly axial low spin (S 1/2) electron paramagnetic resonance signals with bis-histidine and histidine-methionine axial iron coordination. *Biopolymers* 91, 1064–1082
49. Vos, M. H., Borisov, V. B., Liebl, U., Martin, J. L., and Konstantinov, A. A. (2000) Femtosecond resolution of ligand-heme interactions in the high affinity quinol oxidase bd. A di-heme active site? *Proc. Natl. Acad. Sci. U.S.A.* 97, 1554–1559
50. Hewson, W. D., and Hager, L. P. (1979) Oxidation of horseradish peroxidase compound II to compound I. *J. Biol. Chem.* 254, 3182–3186
51. Borisov, V. B., Forte, E., Sarti, P., and Giuffrè, A. (2011) Catalytic intermediates of cytochrome bd terminal oxidase at steady state. Ferryl and oxy-ferrous species dominate. *Biochim. Biophys. Acta* 1807, 503–509
52. Kaila, V. R., Verkhovsky, M. I., and Wikström, M. (2010) Proton-coupled electron transfer in cytochrome oxidase. *Chem. Rev.* 110, 7062–7081
53. Murphy, M. P. (2009) How mitochondria produce reactive oxygen species. *Biochem. J.* 417, 1–13
54. Korshunov, S., and Imlay, J. A. (2006) Detection and quantification of superoxide formed within the periplasm of *Escherichia coli*. *J. Bacteriol.* 188, 6326–6334
55. Han, S. W., Ching, Y. C., and Rousseau, D. L. (1990) Primary intermediate in the reaction of oxygen with fully reduced cytochrome c oxidase. *Proc. Natl. Acad. Sci. U.S.A.* 87, 2491–2495
56. Tsubaki, M., and Yu, N. T. (1981) Resonance Raman investigation of di-oxygen bonding in oxycobalt myoglobin and oxycobalt hemoglobin. Structural implication of splittings of the bound O–O stretching vibration. *Proc. Natl. Acad. Sci. U.S.A.* 78, 3581–3585

57. Goto, T., and Shikama, K. (1974) Autoxidation of native oxymyoglobin from bovine heart muscle. *Arch. Biochem. Biophys.* 163, 476 – 481
58. Hildebrand, D. P., Lim, K. T., Rosell, F. I., Twitchett, M. B., Wan, L., and Mauk, A. G. (1998) Spectroscopic and functional studies of a novel quad-ruple myoglobin variant with increased peroxidase activity. *J. Inorg. Biochem.* 70, 11–16
59. Ivancich, A., Dorlet, P., Goodin, D. B., and Un, S. (2001) Multifrequency high field EPR study of the tryptophanyl and tyrosyl radical intermediates in wild-type and the W191G mutant of cytochrome c peroxidase. *J. Am. Chem. Soc.* 123, 5050 –5058
60. Rittle, J., and Green, M. T. (2010) Cytochrome P450 compound I. Capture, characterization, and C–H bond activation kinetics. *Science* 330, 933–937
61. Schünemann, V., Lendzian, F., Jung, C., Contzen, J., Barra, A. L., Sligar, S.G., and Trautwein, A. X. (2004) Tyrosine radical formation in the reaction of wild type and mutant cytochrome P450cam with peroxy acids. A multifrequency EPR study of intermediates on the millisecond time scale. *J. Biol. Chem.* 279, 10919 –10930

Supplemental data

- A: EPR spectra of Compound I and spectral simulations
- B: Background theory to the EPR spectroscopy of Compound I
- C: EPR spectra of hemes and Compound I during the reaction between cytochrome *bd* oxidase and O₂
- D: References

A: EPR spectra of Compound I and spectral simulations

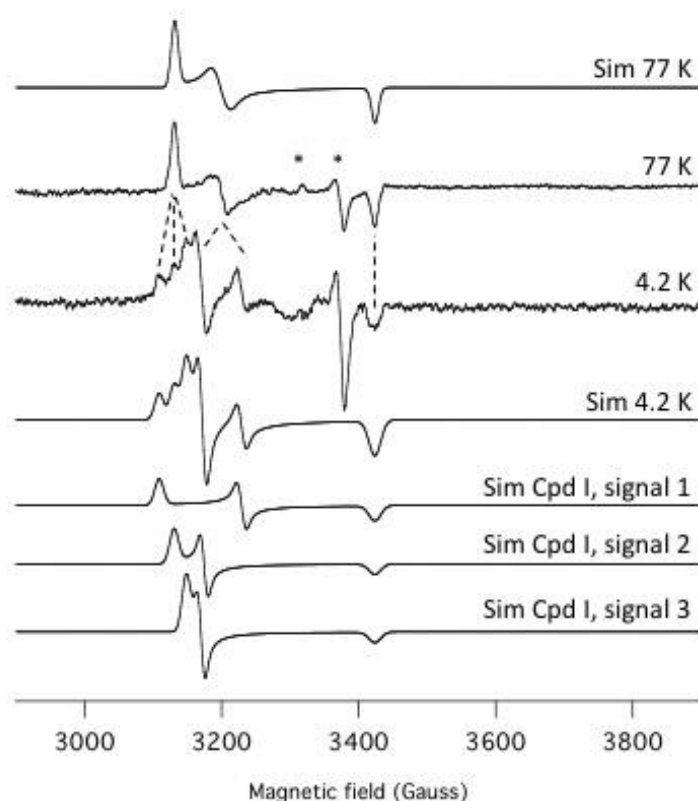


Figure S1: EPR spectra at 4.2 K and 77 K and their respective simulations. The EPR spectrum recorded at 4.2 K is simulated as a sum of three signals in a ratio of 0.4/0.3/0.3 for signal 1, signal 2 and signal 3, respectively. The dotted lines indicate the coalescence of the g_x , g_y and g_z resonances. The g_z resonance only appears to sharpen at 77 K, rather than shift; however, at 4.2 K these (three) g_z resonances might still be at slightly different positions that cannot be resolved owing to the relatively large line width. The g -values used for the simulation at 77 K and of the three signals at 4.2 K are listed in Table 1. The intensities of the spectra are corrected for differences in temperature, microwave power and gain. The dots indicate the artificial signals due to the freeze-quench procedure. EPR conditions: Microwave frequency, 9.45 GHz, modulation amplitude, 0.5 mT, microwave power, 20 μ W (4.2 K) and 5 mW (77K).

B: Background theory to the EPR spectroscopy of Compound I

The magnetic properties of Compound I have been analyzed previously in many reports¹⁻¹¹ and are summarized here. Compound I consists of a $S = 1$ heme Fe(IV) center, which is magnetically coupled to a $S = 1/2$ porphyrin π -cation radical. The complete spin Hamiltonian for this system with a rhombic Fe(IV) center is given by the spin Hamiltonian (Eqn. 1):

$$\hat{H}_{CpdI} = D \left[\hat{S}_z^2 - \frac{1}{3} S(S+1) \right] + \frac{E}{D} \left(\hat{S}_x^2 - \hat{S}_y^2 \right) + \mu_B \bar{S} \bar{g} \bar{B} + \mu_B \bar{S}' \bar{g}' \bar{B} + \bar{S} \bar{J} \bar{S}'$$

The spin Hamiltonian contains the axial (D) and rhombic (E) zero-field splitting parameters of the $S=1$ Fe(IV) species, the two Zeeman terms described by an anisotropic g -tensor of the individual $S = 1$ and $S' = 1/2$ components, and the Heisenberg exchange term (J), that couples the two individual spins S and S' to $S_{eff} = 1/2$ or $3/2$ for the Compound I system. The Heisenberg exchange term contains both the isotropic (J_i) and anisotropic (J_a) contributions to the exchange. The traceless anisotropic J_a -tensor accounts for the dipole-dipole interaction between the two spins.

By a combination of EPR and Mössbauer spectroscopy it is in principle possible to determine the values of the various spin Hamilton parameters D , E , g_x, g_y and g_z of Fe(IV), the g -values of the porphyrin π -cation radical and of the components of the J -tensor. In practice, however, assumptions have to be made about the g -values of the individual spin centers, because measurements are performed in general on the total coupled Compound I system. Hence, the three g -values of the porphyrin π -cation radical are usually set to the isotropic value $g = 2$, whereas the g_x - and g_y -values of the Fe(IV) center ($2.15 - 2.25$ for $D \sim 15 - 30 \text{ cm}^{-1}$) and g_z ($1.95 - 2$) are taken from a perturbation theory calculation¹².

The coupling between a $S=1$ and $S = 1/2$ spin system in Compound I results in the formation of three Kramers doublets (*cf.* Figure 3), the ground state producing the typical Compound I EPR spectra. To first approximation the energy differences between the two lower Kramers doublets are given by Δ (close in magnitude to D) and between the two upper levels by J . The total effective spin of the ground state of the coupled system is either $S = 1/2$ or $3/2$ depending on the relative magnitudes and signs of J and Δ (or D). For $S = 3/2$ the g_x - and g_y -values are expected around $g = 4$, for $S = 1/2$ the g -values are close to $g = 2$ ^{3, 5, 6, 9, 10}, in particular when $J \ll \Delta$ as is the case for the Compound I species of the cytochrome *bd* oxidase. For any Compound I system the g_z -value is always close to $g = 2$.

Since in practice values for Δ of Compound I are $20 - 40 \text{ cm}^{-1}$ ^{3, 5, 6, 9, 10} the separation between the ground state and the first excited state provides a route for a rapid and strongly temperature dependent two-phonon Orbach relaxation mechanism in addition to the so-called direct relaxation process. The direct relaxation process is relatively slow and contributes mainly up to temperatures of $1 - 2 \text{ K}$. The total relaxation rate is given by $1/T_1 \sim P_{1/2} = A.T + B.(e^{\Delta/T} - 1)^{-1}$ where $A.T$ represents the direct process and the second term the Orbach relaxation^{3, 5, 6, 9, 10}; A ($\mu\text{W/K}$) and B (W) are fitting parameters. The presence of a low lying first excited state will also result in significant loss of spin intensity in case EPR spectroscopy is performed at temperatures greater than Δ (*i.e.* above approximately 30 K). The loss of spin intensity is described by: $(1 + e^{-\Delta/T} + e^{-(\Delta+J)/T})^{-1}$. In the high temperature limit only one-third is present in the ground state. Hence, to validate the assignment of the new EPR signal(s) as from Compound I, both the relaxation behavior and the ground state population were determined (Figure 3). Both these experiments should yield a similar value for Δ , born out by experiment (*cf.* Figure 3).

Note that for low spin heme ferric peroxy compounds for which the peroxy group might be bound either in a side-on or end-on manner, $g_{x,y} \sim 4 / g_z \sim 2$ or between $g \sim 2.3 - 1.9$ are found^{13, 14}, respectively. However, in these systems, the relaxation follows a T^7 -

⁹ dependent Raman mechanism, but more importantly, the lowest excited state is $\sim 700 \text{ cm}^{-1}$ above the ground state, the separation determined by the strength of the crystal field^{13, 14}. As a consequence, the spin population of the ground state for low-spin heme centers should within experimental error remain the same between 4.2K and 110K, contrast to observation. Hence, the EPR signal observed in Figures 1, 2 and S1 is due to Compound I.

In contrast to Compound I EPR spectra availing in the literature, that of cytochrome *bd* oxidase appears to consist of three overlapping species in approximately the same amounts (Figures 1, 2 and S1) at temperatures below $\sim 77\text{K}$. The three signals coalesce into a single signal at 77K with g-values that are the average of the three species. The splitting into three signals suggests that at low temperature Compound I is coupled to a nearby relatively slowly relaxing anisotropic magnet. While with increasing temperatures the relaxation rates of Compound I and the nearby magnet will both increase, that of the latter determines the spectral features at high temperatures, *i.e.* its relaxation is now so much faster that the anisotropy is averaged out. This nearby magnet is heme b_{595}^{3+} . There is ample EPR evidence in the literature^(15,16) and *cf.* Figure S2) for magnetic interactions between heme *d* and heme b_{595} , such as changes in lineshape as a function of their redox states, although the precise nature of the interaction has not been analyzed qualitatively or quantitatively.

At temperatures above Δ the relaxation rate of Compound I increases more or less linear with T, whereas for heme b_{595}^{3+} this is according to T^{7-9} . In other words, a cross-over of relaxation rates is expected above $T > \Delta$ in which heme b_{595}^{3+} will relax much faster than Compound I. This is indeed seen in Figure 2. That heme b_{595}^{3+} relaxes much faster than Compound I is also clear from the finding that the latter is detectable by EPR at 77K, whereas the heme b_{595}^{3+} EPR signal starts to broaden at $T > 10\text{-}15 \text{ K}$ and cannot be observed at $T > 60\text{K}$ ¹⁷.

Although the precise distance between heme b_{595}^{3+} and heme *d* are presently unknown, it has been estimated at 10 \AA ¹⁸ and hence direct orbital overlap between the two hemes seems unlikely. In order to account for the magnetic interaction between heme *d* and heme b_{595}^{3+} it is therefore reasonable to ignore contributions from additional Zeeman and exchange interactions in the Hamiltonian, but only add a magnetic dipolar coupling term. This leads to the following full spin Hamiltonian of the system (Eqn. 2):

$$\hat{H}_{CpdI-b_{595}} = D \left[\hat{S}_z^2 - \frac{1}{3} S(S+1) + \frac{E}{D} (\hat{S}_x^2 - \hat{S}_y^2) \right] + \mu_B \bar{S} \bar{g} \bar{B} + \bar{S} \bar{J} \bar{S}' + \mu_B \bar{S}' \bar{g}' \bar{B}' + \bar{S}_{CpdI} M_{dip} \bar{S}_{b_{595}}$$

where M_{dip} is given by (Eqn. 3):

$$M_{dip} = \mu_B^2 \left(\frac{(\bar{g}_{CpdI} \bar{S}_{CpdI})(\bar{g}_{b_{595}} \bar{S}_{b_{595}})}{r^3} - 3 \frac{(\bar{r} \bar{g}_{CpdI} \bar{S}_{CpdI})(\bar{r} \bar{g}_{b_{595}} \bar{S}_{b_{595}})}{r^5} \right)$$

Herein $\bar{S}_{CpdI} = 1/2$ and the spin of heme b_{595} may be described by an effective spin $\bar{S}_{b_{595}} = 1/2$ with $g_{x,y} = 3$. $\bar{g}_{b_{595}}$

In addition, calculation of r leads to the well-known result that the magnetic dipolar coupling term is proportional to $(3\cos^2\theta_n - 1)$ in which θ_n is the angle between the magnetic moments of Compound I and heme b_{595} along their respective x, y or z-directions. In case the angle is close to the magic angle of 54.7° the dipolar contribution to the spin Hamiltonian vanishes.

This is seen as the relatively small splitting in the g_z -resonance of Compound I from the cytochrome *bd* oxidase (Figs. 2 and S1).

*C: EPR spectra of hemes and Compound I during the reaction between cytochrome *bd* oxidase and O_2*

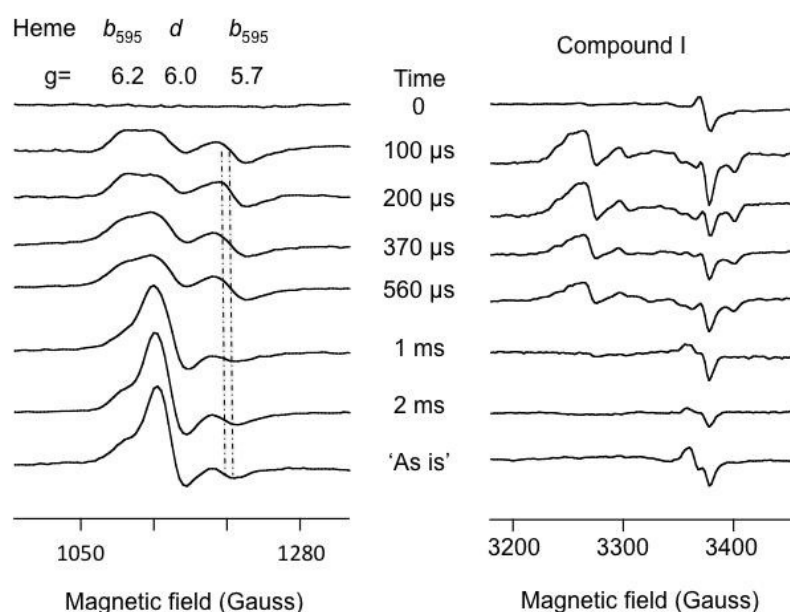


Figure S2: EPR spectra of cytochrome *bd* oxidase freeze-quenched after various times after reaction with O_2 . Left panel, the resonances of the high-spin hemes. The shift of ~ 10 Gauss in the g_y resonance of heme b_{595} (left panel) as the reaction proceeds is indicated by the two vertical lines. Right panel, Compound I. All spectra show a radical-like signal (see also Fig. S1) at approximately 3380 Gauss owing to the freeze-quench procedure. The additional signal just to the left of this radical (1ms, 2ms and 'As is') is unknown. Microwave frequency, 9.45 GHz, modulation amplitude, 1.0 mT, microwave power, 2.0 mW, temperature, 10 K.

D: References

1. Hewson, W. D., and Hager, L. P. (1979) *J. Biol. Chem.* 254, 3182-3186.
2. Hoffman, B. M., Roberts, J. E., Brown, T. G., Kang, C. H., and Margoliash, E. (1979) *Proc. Natl. Acad. Sci. U.S.A.* 76, 6132-6136.
3. Schulz, C. E., Devaney, P. W., Winkler, H., Debrunner, P. G., Doan, N., Chiang, R., Rutter, R., and Hager, L. P. (1979) *FEBS Lett.* 103, 102-105.
4. Hoffman, B. M., Roberts, J. E., Kang, C. H., and Margoliash, E. (1981) *J. Biol. Chem.* 256, 6556-6564.
5. Rutter, R., and Hager, L. P. (1982) *J. Biol. Chem.* 257, 7958-7961.
6. Schulz, C. E., Rutter, R., Sage, J. T., Debrunner, P. G., and Hager, L. P. (1984) *Biochemistry* 23, 4743-4754.

7. Mandon, D., Weiss, R., Jayaraj, K., Gold, A., Turner, J., Bill, E., and Trautwein, A. X. (1992) *Inorg. Chem.* 31, 4404-4409.
8. Benecky, M. J., Frew, J. E., Scowen, N., Jones, P., and Hoffman, B. M. (1993) *Biochemistry* 32, 11929-11933.
9. Houseman, A. L., Doan, P. E., Goodin, D. B., and Hoffman, B. M. (1993) *Biochemistry* 32, 4430-4443.
10. Fujii, H., Yoshimura, T., and Kamada, H. (1996) *Inorg. Chem.* 35, 2373-2377.
11. Ivancich, A., Dorlet, P., Goodin, D. B., and Un, S. (2001) *J. Am. Chem. Soc.* 123, 5050-5058.
12. Oosterhuis, W. T., and Lang, G. (1973) *The Journal of Chemical Physics* 58, 4757-4765.
13. Salerno, J. C., Frey, C., McMillan, K., Williams, R. F., Masters, B. S., and Griffith, O. W. (1995) *J. Biol. Chem.* 270, 27423-27428.
14. Zoppellaro, G., Bren, K. L., Ensign, A. A., Harbitz, E., Kaur, R., Hersleth, H. P., Ryde, U., Hederstedt, L., and Andersson, K. K. (2009) *Biopolymers* 91, 1064-1082.
15. Ingledew, W. J., Rothery, R. A., Gennis, R. B., and Salerno, J. C. (1992) *Biochem. J.* 282, 255-259.
16. Junemann, S. (1997) *Biochim. Biophys. Acta* 1321, 107-127.
17. Meinhardt, S. W., Gennis, R. B., and Ohnishi, T. (1989) *Biochim. Biophys. Acta* 975, 175-184.
18. Arutyunyan, A. M., Borisov, V. B., Novoderezhkin, V. I., Ghaim, J., Zhang, J., Gennis, R. B., and Konstantinov, A. A. (2008) *Biochemistry* 47, 1752-1759.

Chapter VI

Conclusions and outlook

Fundamental biochemical research is of crucial importance for a complete and detailed understanding of what drives enzyme activity and how enzyme kinetic properties are optimized towards survival of the host organism. Since enzymes are too small to be observed with the naked eye and enzymatic catalysis of chemical reactions occurs in micro- to milliseconds, advanced analytical tools are required to gain insight in the mechanisms by which enzymes function.

Spectral kinetic analysis provides a world of information about redox-active metallo-enzymes, such as bacterial cytochrome *aa*₃, *ba*₃ and *bd*-I oxidase, but a high time resolution and submillisecond deadtime of the detection method is essential for observation of the individual reaction steps of a single enzymatic turnover. Using the microsecond freeze-hyperquenching setup (MHQ), with its four-jet tangential stainless steel micromixer and the ability to spray mixtures of enzymes and substrates directly onto the inner wall of a cylinder pre-cooled with liquid nitrogen, it was possible to freeze-quench enzymatic reactions at reaction times from 74 microseconds up to 25 milliseconds.

Microsecond kinetic analysis was performed on a quinol oxidase (cytochrome *bdI* oxidase from *Escherichia coli*), a Type A cytochrome *c* oxidase (cytochrome *aa*₃ oxidase from *Paracoccus denitrificans*) and a Type B cytochrome *c* oxidase (cytochrome *ba*₃ oxidase from *Thermus thermophilus*). Stopped-flow UV-vis spectroscopy in the millisecond-to-second time range was combined with microsecond freeze hyperquenching and low temperature UV-vis and EPR spectroscopy in the micro- to millisecond time range to obtain a full overview of catalytic turnover of the enzymes. Although the three bacterial oxidases from three different host organisms vary considerably in terms of 3D structure, identity of the redox-active groups and bio-energetic efficiency, the underlying mechanisms of these enzymes for the reduction of oxygen to water turned out not to be so different.

In order to further increase the understanding of enzymatic oxygen reduction in respiration and to better define the similarities and differences between the main types of cytochrome *c* and quinol oxidases it is crucial to extend the list of examples with pre-steady state microsecond kinetic analysis of other respiratory oxidoreductases. In addition, computerized modeling of biomolecules has become a powerful tool over the past years for predicting and understanding enzyme function and the thermodynamics involved in catalysis and proton transfer. The obvious next step is therefore making the connection between the *experimental* models based on spectral information with the *calculated* models that are built on the 3D structure of the enzyme. As in a perfect symbiosis, modeling can provide input for smart design of lab experiments and aid interpretation of the results, while the microsecond spectral data obtained on micro-to-millisecond reaction samples provides a means of testing hypotheses that originate from the *in silico* models.

Curriculum vitae

Angela Paulus werd geboren op 27 oktober 1982 in Zevenhuizen (Zuid-Holland). In 2001 behaalde ze haar VWO diploma aan het Comenius college te Capelle aan den IJssel, waarna ze direct begon aan de studie Life Science & Technology, een samenwerking tussen de Technische Universiteit Delft en de Universiteit Leiden. Haar afstudeerstage werd uitgevoerd bij de sectie Enzymologie (tegenwoordig BOC) binnen de afdeling Biotechnologie van de TU Delft onder begeleiding van professor S. De Vries†. Dit afstudeeronderzoek, waarmee zij haar masteropleiding *cum laude* afrondde in de richting Cell diagnostics, maakte deel uit van het promotieonderzoek waaraan ze in mei 2006 begon.

Haar promotieonderzoek bij de Sectie Enzymology aan de Technische Universiteit Delft verliep onder begeleiding van promotor professor S. de Vries. De resultaten van haar promotieonderzoek zijn in dit proefschrift beschreven. Inmiddels richt zij zich op de ontwikkeling van enzymen voor industriële toepassingen in haar werk bij Royal DSM, waar ze werkzaam is als wetenschapper in de sectie Analytische Biochemie.

List of publications

- Paulus A, Rossius SG, Dijk M, de Vries S. Oxoferryl-porphyrin radical catalytic intermediate in cytochrome *bd* oxidases protects cells from formation of reactive oxygen species *J Biol Chem*. 2012 Mar 16;287(12):8830-8.
- Paulus A, Werner C, Ludwig B, de Vries S. The cytochrome *ba*₃ oxidase from *Thermus thermophilus* does not generate a tryptophan radical during turnover: Implications for the mechanism of proton pumping *Biochim Biophys Acta*. 2015 Oct;1847(10):1093-100.
- Paulus A, de Vries S. Energy conversion and conservation by cytochrome oxidases *Copper-Oxygen Chemistry*, John Wiley & Sons, Inc., Hoboken, NJ, USA, 2011, 107-129

Dankwoord

Het dankwoord is misschien wel het moeilijkste deel van een proefschrift om te schrijven, in de eerste plaats niet omdat het zo lastig is om 'dankjewel' te zeggen, maar om de woorden te vinden die de boodschap het beste overbrengen. Daarnaast valt het niet mee om iedereen te noemen die een bijdrage heeft gehad aan de totstandkoming van een proefschrift, want zoals er een dorp nodig is om een kind op te voeden, is ook een promotieonderzoek niet iets wat je helemaal in je eentje doet. Ik wil daarom iedereen die ik gedurende mijn promotietijd heb gekend bedanken voor hun inzichten, hun samenwerking en hun steun, hun vertrouwen en hun koffieklets, hun oprechtheid en enthousiasme. Ik heb mij binnen de sectie Enzymologie en de afdeling Biotechnologie 5 jaar lang elke dag welkom gevoeld en het doet me deugd nog met enige regelmaat oud-collega's te ontmoeten als nieuwe collega's, en te merken dat sommige dingen niet veranderen.

Twee personen die ik wel specifiek zal bedanken zijn mijn promotoren, Simon en Fred. Een twee-eenheid zoals die van jullie kom je zelden tegen. Ik ben dankbaar dat ik van jullie beiden heb mogen leren tijdens en na mijn werkzaamheden bij de sectie Enzymologie.

Simon heeft mij de waarde van opportunisme laten zien en hij had een aanstekelijk doorzettingsvermogen, waardoor opgeven ook voor mij nooit een optie was. Simon heeft mij gekend in goede, maar ook in slechte tijden. Hij was altijd bereid om te luisteren en desgevraagd te adviseren, als wetenschapper, maar vooral als mens. Hij wist wanneer hij mij met rust moest laten en wanneer hij mij moest uitdagen. Natuurlijk botste het soms ook, met name wanneer wij beiden vasthielden aan onze eigen overtuiging en de feiten geen uitsluitsel boden, maar wederzijds respect overheerste altijd. Ik had het Simon van harte gegund om getuige te zijn van mijn laatste optreden ter verkrijging van de graad van doctor, evenzeer hij het mij gunde om een proefschrift af te leveren om trots op te zijn.

Na het afscheid van Simon heeft Fred de rol van promotor overgenomen. Fred, je hebt mij (en in zekere zin ook Simon) hiermee een enorme dienst bewezen. Ik begrijp waarom je deze taak op je hebt genomen, maar het kan niet makkelijk zijn geweest. Ik ben je bijzonder dankbaar dat je mij de mogelijkheid hebt gegeven om mijn proefschrift af te ronden binnen de sectie Enzymologie (of tegenwoordig, BOC) in Delft. Gedurende de 5 jaar dat ik op het lab te vinden was hadden we eigenlijk niet veel contact, maar dat de wereld klein is bleek maar weer eens toen wij elkaar in een consortium met o.a. de TU en DSM tegenkwamen. Ik kan je droge humor altijd erg waarderen en heb bewondering voor de manier waarop je rust weet uit te stralen, ongeacht de situatie. Ik dank je voor de moeite die je hebt genomen om je te verdiepen in de hoofdstukken van mijn proefschrift en voor de opmerkingen die het proefschrift beter hebben gemaakt.

Erik, ik heb je plechtig beloofd je niet te bedanken in mijn proefschrift, dus bij dezen. ;-)

Tobias en Daniël, Grote en Kleine Boef, jullie zijn nog te jong om te bevatten waar al die heisa nou om is, maar ik ben trots dat ik het ooit aan jullie zal mogen uitleggen.

